Supplementary Information

Nicotinic Acid-Catalyzed Synthesis of Novel Benzothiazoles and Benzimidazoles from Carbohydrate-Derived Furfurals: Structural, Computational, and Antimicrobial Studies

Prajwal Naik C [a], Saikat Dutta [a*], Chethan B. S. [b], Chethan Prathap K. N. [c], Lokanath N. K. [d], B.C. Revanasiddappa [e], Nitha Naveen Dsouza [e]

[a] *Department of Chemistry, National Institute of Technology Karnataka (NITK), Surathkal, Mangalore-575025, Karnataka, India.*
[b] *Department of Physics, Sri Siddhartha Institute of Technology, SSAHE, Tumakuru-572105, Karnataka, India.*
[c] *Department of Physics, University College of Science, Tumkur University, Tumakuru-572103, Karnataka, India.*
[d] *Department of Studies in Physics, University of Mysore, Manasagangotri, Mysuru-570006, Karnataka, India.*
[e] *Department of Pharmaceutical Chemistry, NGSM Institute of Pharmaceutical Sciences (A Constituent College of Nitte Deemed to be University), Paneer, Deralakatte, Mangalore-575018, Karnataka, India*

* *Corresponding author. E-mail: sdutta@nitk.edu.in*

Table of Contents

1. General Information

1.1 Materials

Furfural (99%), mesitylene (99%), nicotinic acid (99%), formic acid (99%), tetrahydrofuran (99.5%), succinic acid (99%), and levulinic acid (98%) were obtained from Spectrochem Pvt. Ltd. 5-Methylfurfural (99%) was purchased from Sigma-Aldrich. The compounds 5-(chloromethyl)furfural, 5-(hydroxymethyl)furfural, 5-(acetoxymethyl)furfural, 5-(ethoxymethyl)furfural,5-(benzyloxymethyl)furfural,4-methoxy(benzyloxymethyl)furfural, 4-chloro-(benzyloxymethyl)furfural, 4-nitro-(benzyloxymethyl)furfural, and 5-(mesitylmethyl)furfural were synthesized and purified according to procedures reported in the literature.[1,2] Glacial acetic acid (>99%) and 1,4-dioxane (>99%) were procured from Molychem India LLP. 2-Aminobenzenethiol (>97%) and lactic acid (>85%) were obtained from TCI Chemicals Pvt. Ltd. O-Phenylenediamine (98%), oxalic acid (99%), and toluene (99%) were purchased from Loba Chemie Pvt. Ltd. HPLC-grade water was obtained from Spectrochem. Methanol and ethanol were provided by Nirani Sugar Limited. Petroleum ether (60–80 °C, 99%) and dimethyl sulfoxide (DMSO, 99%) were purchased from Himedia Laboratories, Mumbai. Thin-layer chromatography (TLC) plates, pre-coated with silica gel on aluminum sheets (TLC Silica Gel 60 F_{254}) and HPLC-grade acetonitrile were supplied by Merck India Pvt. Ltd.

1.2 Instruments

The synthesized compounds were characterized using various spectroscopic and analytical techniques. Fourier-transform infrared (FTIR) spectra were recorded on a Bruker Alpha II spectrometer equipped with an attenuated total reflectance (ATR) accessory, employing a zinc selenide (ZnSe) crystal. Samples were prepared by dissolving the compounds in chloroform, and a thin film was formed by evaporating a drop of the solution on the ATR surface. Each spectrum was collected as an average of 24 scans at a rate of 4 scans per second, over the spectral range of 500-4000 cm^{-1}. Nuclear magnetic resonance (NMR) spectra were recorded in a Bruker NanoBay® NMR spectrometer operating at 400 MHz for ^{1}H and 100 MHz for ^{13}C nuclei. Chemical shifts (δ) are reported in parts per million (ppm) relative to tetramethylsilane (TMS) as an internal reference. Melting points of the synthesized compounds were measured using a Stuart SMP3 digital melting point apparatus. High-resolution mass spectra (HRMS) were recorded on a Xevo QToF mass spectrometer (Waters).

1.3 Single-crystal X-ray diffraction studies

Defect-free single crystals of the selected compounds were chosen for X-ray diffraction analysis. Intensity data were collected using a Rigaku XtaLAB mini diffractometer equipped with MoKα radiation (λ = 0.7103 Å). Data collection was performed with a scan width of 0.5°, an exposure time of 3 s, and a sample-to-detector distance of 50 mm. The collected diffracted X-ray intensity data were processed using CrystalClear software. Crystal structures were solved by the direct method with SHELXS and refined with SHELXL using full-matrix least-squares minimization.[3] All non-hydrogen atoms were refined anisotropically, while hydrogen atoms were positioned geometrically using the appropriate riding model. Geometrical calculations were performed using PLATON software.[4] ORTEP and packing diagrams were generated using Mercury 4.2.0 software.[5]

1.4 Hirshfeld surface analysis

To visualize, understand, and quantify the intermolecular interactions of the compounds in the crystalline environment, the Hirshfeld surface analysis was performed. The intermolecular interactions were quantified using the 2D fingerprint plot analysis. The 2D fingerprint plot (d_i (nearest interior) vs d_e (nearest exterior)) reveals various types of intermolecular interactions. The Hirshfeld surface and 2D fingerprint plot analyses were performed using CrystalExplorer.[6] Furthermore, other surface plots, such as d_{norm}, shape index, and curvedness, provide additional information about the crystal structures.

1.5 Density Functional Theory Studies

To examine the electronic properties of the synthesized compounds, Density Functional Theory (DFT) was employed. The geometries of both compounds were optimized using the B3LYP functional with the 6-311+G(d,p) basis set in ethanol solvent phase using IEFPCM (Integral Equation Formalism Polarizable Continuum Model). Using the optimized geometries, the frontier molecular orbitals (HOMO and LUMO), their respective energy gaps, and related global and local reactivity descriptors were calculated using Koopmans' approximation. Molecular electrostatic potential (MEP) maps were generated to analyze charge distribution and reactive regions within the molecules. All quantum chemical calculations were performed with Gaussian 16 software, and the results were visualized using GaussView 5.0.[7,8]

2. Optimization of Reaction Conditions

The benzothiazole derivative **4b** was initially synthesized by condensing MF with 2-aminobenzenethiol in a 1:1 molar ratio, using anhydrous absolute ethanol as the solvent. The reaction mixture was stirred magnetically under reflux, and the progress was monitored by

thin-layer chromatography (TLC) to observe the disappearance of MF and the formation of the corresponding aldimine intermediate. In the absence of a catalyst, the reaction proceeded very slowly, producing only the intermediate after 24 h, with no formation of the target product. The slow kinetics and poor conversion of MF at ambient temperature indicated that thermal or catalytic activation was necessary for cyclization. Increasing the temperature to 60 °C resulted in only trace amounts of **4b** after 12 h, whereas raising it to 80 °C increased the yield to 18%. However, incomplete conversion and partial decomposition of MF were observed under these conditions, highlighting the need for catalytic assistance. To improve reaction efficiency, a series of biogenic carboxylic acids was tested as catalysts under identical conditions. When the reaction was conducted under reflux in the presence of nicotinic acid (25 mol%), the yield of **4b** increased significantly, reaching 91% isolated yield. The effects of different biorenewable acids on product formation are summarized in Table S1. Among the tested catalysts, oxalic acid (entry 9) and citric acid (entry 10) also yielded the desired benzothiazole derivative in excellent amounts (>80%). Notably, nicotinic acid showed the highest catalytic efficiency, yielding the product at 91% under optimized conditions. No apparent correlation was found between acid strength (pKa) and catalytic performance. For example, 2,5-furandicarboxylic acid yielded only 68% product, likely due to its limited solubility in ethanol. In contrast, acetic acid (entry 2), formic acid (entry 3), lactic acid (entry 4), succinic acid (entry 5), and levulinic acid (entry 6) gave moderate yields (~70%) within 4.5 h of reflux. Therefore, nicotinic acid was identified as the most effective and sustainable catalyst, providing the desired product in a 91% yield within 4 h. Subsequently, further optimization of the reaction conditions was carried out using nicotinic acid as the catalyst. Reaction parameters, such as reaction temperature, solvent type, catalyst loading, and duration were systematically studied. Temperature was found to play a key role owing to its substantial impact on the reaction rate, selectivity, and the stability of reactants and products.

Table S1: Synthesis of benzothiazole **4b** from MF using various biogenic acids as catalysts

Entry	Catalyst	Reaction time (h)	Catalyst (mol%)	Yield (%)
1	No catalyst	24	-	18
2	Acetic acid	4	25	70
3	Formic acid	4	25	74
4	Lactic acid	4.5	25	78
5	Succinic acid	4	25	76
6	Levulinic acid	4	25	72
7	Furan-2,5-dicarboxylic acid	8	25	68

8	Nicotinic acid	4	25	**91**
9	Oxalic acid	5	25	82
10	Citric acid	4	25	86

Reaction conditions: MF (0.250 g, 2.27 mmol) and 2-aminobenzenethiol (0.284 g, 2.27 mmol), absolute ethanol (10 mL), reflux.

2.1 Effect of Reaction Temperature and Catalyst Loading

The influence of temperature on the formation of 2-(5-methylfuran-2-yl)benzo[*d*]thiazole (**4b**) was examined using nicotinic acid (25 mol%) as the catalyst. When the reaction was carried out at room temperature (RT), only a trace amount of **4b** was detected even after extending the reaction duration to 24 h Figure S1. The poor yield can be attributed to sluggish reaction kinetics and incomplete conversion of MF under these mild conditions. Upon a moderate increase in temperature to 40 °C, the reaction proceeded at a faster rate, affording **4b** in 20% yield within 12 h. A further increase to 60 °C slightly improved the yield to 46% under the same duration, suggesting that the activation barrier for cyclization was still not fully overcome. The yield of **4b** increased significantly to 91% when the reaction was conducted under reflux for 4 h, confirming that higher temperature substantially accelerates the condensation-cyclization process. Therefore, reflux was identified as the optimal temperature condition for the synthesis of benzothiazole derivatives from SFLs.

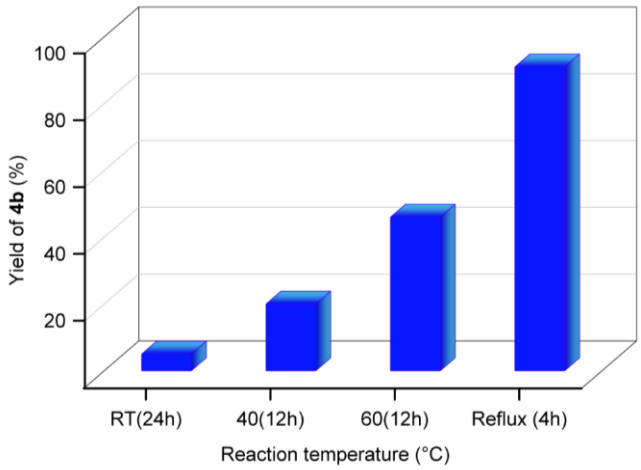

Figure S1. The effect of reaction temperature on the isolated yield of benzothiazole **4b**. *Reaction conditions: MF (0.250 g, 2.27 mmol), 2-aminobenzenethiol (0.284 g, 2.27 mmol), nicotinic acid (25 mol%), ethanol (10 mL).*

The influence of reaction time on the yield of compound **4b** was studied under the optimized reaction conditions. The reaction progress was monitored at regular intervals, and the corresponding isolated yields were measured. As shown in Figure S2(a), the yield of **4b** increased steadily with reaction time and the maximum yield of 91% after 4 h of reflux.

Extending the reaction duration to 5 h did not afford any further increment in yield. Marginal decrease in **4b** yield observed beyond 4 h may be due to partial decomposition caused by prolonged heating.

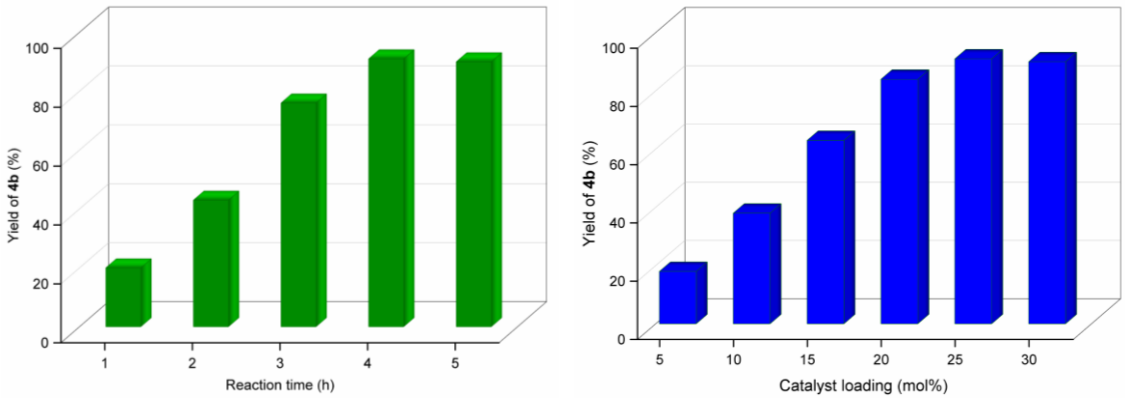

Figure S2. Optimization studies for the isolated yield of **4b**: (a) effect of reaction duration (left) and effect of catalyst loading (right) on the isolated yield. *Reaction conditions: MF (0.250 g, 2.27 mmol), 2-aminobenzenethiol (0.284 g, 2.27 mmol), ethanol (10 mL), reflux; nicotinic acid.*

The effect of catalyst loading on product yield was then investigated under the optimized temperature. When the reaction was carried out without a catalyst, only trace amounts of **4b** were obtained. When the catalyst loading increased to 5 mol%, then 18% of **4b** was obtained after 10 h. When the nicotinic acid loading was at 10 mol%, only 38% of **4b** was obtained after 10 h, indicating incomplete conversion due to insufficient catalytic activation. Increasing the catalyst concentration to 15 mol% improved the yield to 63%, while 20 mol% afforded 84% of **4b**. The maximum yield of 91% was achieved with 25 mol% catalyst within 4 h, demonstrating the importance of adequate acid-site availability in promoting the reaction Figure S2(b). Further increasing the catalyst loading to 30 mol% did not enhance the yield, suggesting that the active sites were already saturated under these conditions. Overall, these results highlight the cooperative role of temperature and catalyst concentration in driving the efficient formation of benzothiazole derivatives from biomass-derived aldehydes.

2.2 Solvent Screening

The effect of solvent on the formation of compound **4b** was systematically examined as shown in Table S2, while maintaining the optimized reaction temperature and nicotinic acid loading. Initially, an organic solvent-free reaction was performed under the same conditions, yielding 76% of **4b** after 10 h. Subsequently, various solvents, including 1,4-dioxane, toluene, water, THF, acetonitrile, methanol, and ethanol, were screened to assess their impact on reaction rate, product selectivity and yield. 1,4-Dioxane and toluene gave only 24% and 36% yields of **4b**, respectively, possibly due to the limited solubility of reactants in these solvents.

The aqueous medium afforded a moderate 64% yield of **4b** after 8 h, due to the incomplete conversion of MF and its partial decomposition at elevated temperatures. THF improved the yield of **4b** to 76% after 10 h, whereas the yield reached 84% after 5 h in acetonitrile. Methanol as a solvent resulted in a 74% yield of **4b** after 6 h, and ethanol achieved the highest yield of 91% within 4 h. The superior performance of ethanol is attributed to its moderate polarity and protic nature, which enhances solubility and facilitates effective proton transfer during the catalytic cycle.

Table S2. Synthesis of benzothiazoles **4b** from MF using various solvents.

Entry	Solvent effect	Reaction time (h)	Yield (%)
1	No solvent	10	76%
2	1,4-Dioxane	14	24%
3	Toluene	14	36%
4	Water	8	64%
5	THF	10	76%
6	Acetonitrile	5	84%
7	Methanol	6	74%
8	Ethanol	4	**91%**

Reaction conditions: MF (0.250 g, 2.27 mmol), 2-Aminobenzenethiol (0.284 g, 2.27 mmol), catalyst (25 mol.%), reflux.

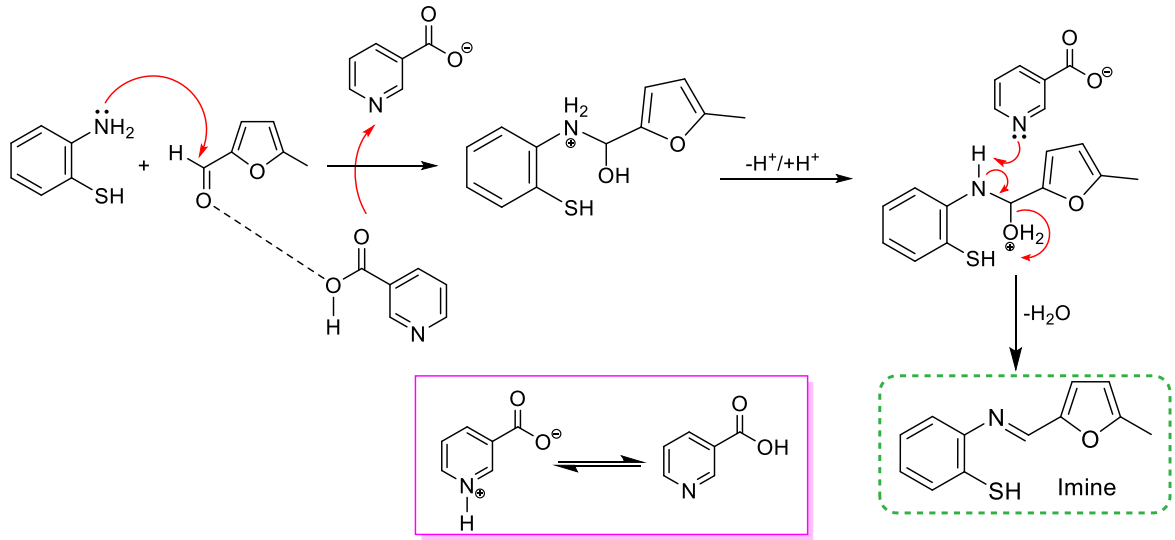

Scheme S1. Proposed mechanism for proton exchange and organocatalytic involvement during imine formation.

3. Structural analysis of compound 4g and 4d

3.1 Structural analysis

The structural analysis of both compounds revealed that compound **4g** crystallized in the *P*-1 space group, whereas compound **4d** crystallized in $Pca2_1$. The structural refinement parameters for compounds **4g** and **4d** are provided in Table S3. Both novel compounds share a common structural backbone, a thiazole moiety. The dihedral angles between the thiazole moiety and the substituents are 80.50° and 72.27° for compounds **4g** and **4d**, respectively Figure S3. The molecules exhibit antiperiplanar conformations at the reactant linkage, with torsion angles of 178.94° (C12-O2-C13-C14) and 177.06° (C12A-O2A-C13A-C14A) for compounds **4g** and **4d**, respectively. Due to the compounds' conformations, various intra- and intermolecular interactions were observed, resulting in the formation of synthons of various sizes. The interactions of compounds **4g** and **4d** are shown in Table S4. The C12–H12A···O3, C19–H19···O2, and C15–H15···O3 intramolecular interactions resulted in the formation of S(5) synthons, while the C20–H20B···H18 resulted in the formation of S(6) synthon in compound **4g** Figure S4. In compound **4d**, the C12B–H12C···O3B interaction resulted in the formation of an S(5) synthon Figure S5. In compound **4g**, the C9–H9···N1 and C20–H20C···O4 intermolecular interaction resulted in the formation of an infinite chain along the *ac* and *bc* planes, respectively. These intermolecular interactions form $R_2^2(6)$ supramolecular synthon, as shown in Figure S6. Conversely, in compound **4d**, the C2B–H2B···N1 intermolecular interaction creates an infinite chain along the *ac* plane, along with the formation of an $R_2^1(5)$ supramolecular synthon, as shown in Figure S7. In addition to these inter- and intramolecular interactions, the compounds also exhibited π···π/Cg···Cg interactions, which significantly stabilize the crystal structure. Details of these interactions are provided in Table S5.

Table S3. Structural refinement table of compounds **4g** and **4d**.

Parameters	**Compound 4g**	**Compound 4d**
CCDC number	2505860	2505858
Empirical formula	$C_{20}H_{15}NO_4S$	$C_{28}H_{22}N_2O_6S_2$
Formula weight	365.39	546.59
Temperature (K)	293(2)	293(2)
Radiation	MoKα	
Wavelength (Å)	0.71073	

Crystal system	Triclinic	Orthorhombic
space group	*P*-1	*P*ca2$_1$
a (Å)	5.3983(12)	11.1510(4)
b (Å)	8.0437(17)	5.3509(3)
c (Å)	20.154(3)	43.3193(17)
α (°)	100.73(2)	90
β (°)	92.23(2)	90
γ (°)	96.548(18)	90
Volume (Å^3)	852.6(3)	2584.8(2)
Z	2	4
Density(calculated) Mg m^{-3}	1.423	1.405
Absorption coefficient mm^{-1}	0.216	0.253
F_{000}	380.0	1136.0
Crystal size (mm)	0.24 x 0.21 x 0.20	0.22 x 0.21 x 0.19
2θ range for data collection	4.122 to 57.274	3.76 to 56.154
h	-6 ≤ h ≤ 7	-14 ≤ h ≤ 13
k	-10 ≤ k ≤ 10	-7 ≤ k ≤ 6
l	-26 ≤ l ≤ 26	-56 ≤ l ≤ 54
Reflections collected	11354	19205
Independent reflections	3895	4936
Data / restraints / parameters	3895 / 0 / 237	4936 / 1 / 349
Goodness-of-fit	1.059	1.042
*R*1, *wR2* [I > 2σ(I)]	0.0929, 0.2589	0.0538, 0.1084
*R*1, *wR2* [all data]	0.1673, 0.3572	0.0817, 0.1213
Residual (eÅ^{-3})	0.54 / -0.74	0.35 / -0.28

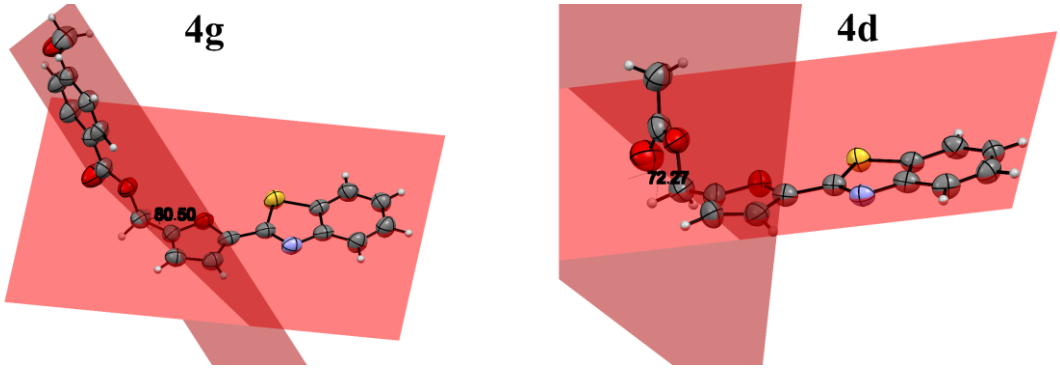

Figure S3. The dihedral angles of compounds **4g** and **4d**, illustrating their non-planarity.

Table S4. The inter- and intramolecular interactions of the compounds **4g** and **4d**.

Type	D–H···A	D–H (Å)	H···A (Å)	D–H···A (Å)	D–H···A (°)
Compound 4g					
Intra	C12–H12A···O3	0.970	2.460	2.630	89.10
Intra	C15–H15···O3	0.931	2.584	2.866	98.02
Intra	C19–H19···O2	0.930	2.469	2.776	99.34
Inter	C20–H20C···O4	0.960	2.636	3.409	137.91
Inter	C9–H9···N1	0.930	2.734	3.630	161.79
Compound 4d					
Intra	C12–H12B···O3B	0.970	2.412	2.639	92.60
Inter	C2B–H2B···N1B	0.930	2.681	3.419	136.84

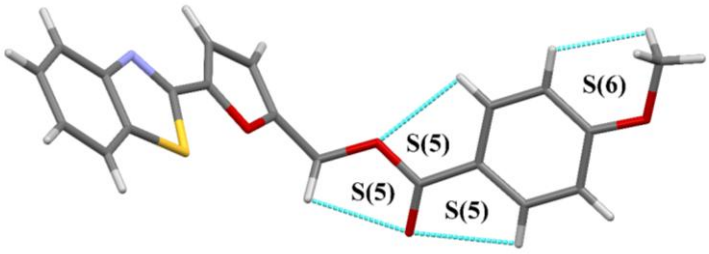

Figure S4. Formation of a synthon due to the intramolecular interactions in compound **4g**.

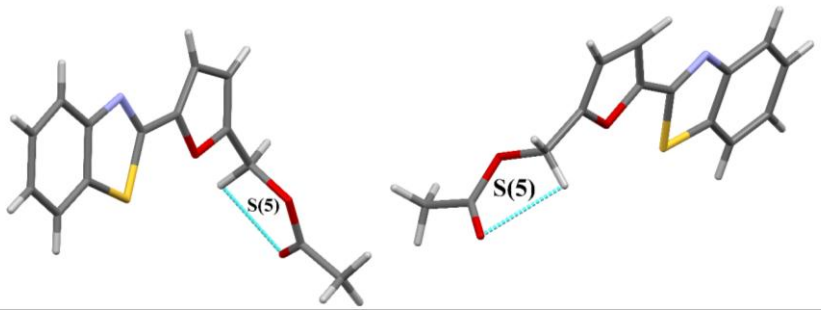

Figure S5. Formation of a synthon due to the intramolecular interaction in compound **4d**.

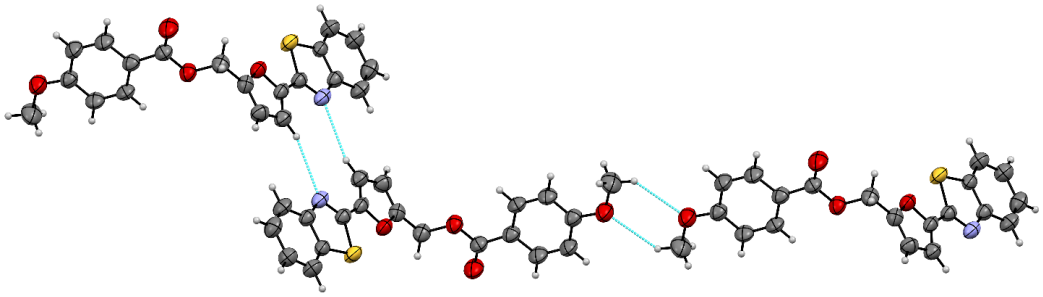

Figure S6. Formation of supramolecular synthon due to the intermolecular interactions exhibited by compound **4g**.

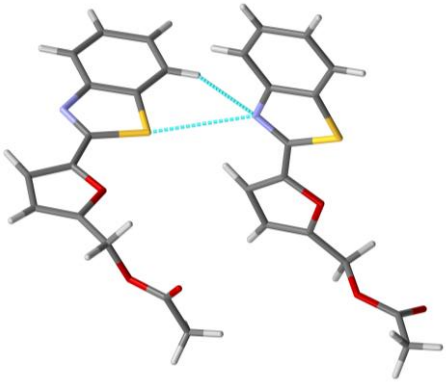

Figure S7. Formation of supramolecular synthon due to the intermolecular interactions exhibited by compound **4d**.

Table S5. Cg···Cg interactions of the compound **4g** and **4d**.

Cg(I)	Cg(J)	Cg(I)···Cg(J) (Å)	α (°)	β (°)	γ (°)	Cg(I) perp (Å)	Cg(J) perp (Å)	Slippage
Compound 4g								
Cg2	Cg3	3.923 (3)	2.8 (3)	25.7	26.2	3.520 (2)	3.535 (2)	1.702
Cg2	Cg5	3.895 (3)	3.4 (2)	26.9	25.5	3.515 (2)	3.474 (1)	1.761
Cg2	Cg5	4.251 (3)	3.4 (2)	31.3	32.0	-3.603 (2)	-3.6330 (1)	2.206
Cg(2): O1/C8/C9/C10/C11, Cg(3): C1/C2/C3/C4/C5/C6, Cg(5): S1/C4/C3/C2/C1/C6/C5/N1								
Compound 4d								
Cg1	Cg2	3.664 (4)	1.1 (3)	1.8	2.3	3.662 (2)	-3.663 (3)	0.113
Cg2	Cg4	3.823 (3)	0.8 (3)	16.9	16.8	-3.660 (3)	3.6581 (1)	1.110
Cg5	Cg6	3.654 (4)	1.4 (3)	1.9	2.7	-3.650 (2)	3.652 (3)	0.122
Cg1: S1A/C5A/C4A/N1A/C7A, Cg2: O1A/C8A/C9A/C10A/C11A, Cg4:S1A/C5A/C1A/C2A/C3A/C4A/N1A, Cg(5):S1B/C3B/C4B/N1B/C7B, Cg(6): O1B/C8B/C9B/C10B/C11B								

3.2 Hirshfeld surface analysis

The intermolecular interactions and the relative contribution of atoms towards the stability of the crystal structures are studied using Hirshfeld surface analysis. The 2D fingerprint plots provide the percentage contribution of specific contact types, which further provides insights into stability and molecular configuration. The d_{norm}-mapped Hirshfeld surface is plotted over the range -1.1969 to 1.1969 Å for compound **4g**, and for compound **4d**, the range is -0.0910 to 1.2883 Å. Large circular depressions indicated by the red color on the d_{norm} plot denote intermolecular hydrogen bond interactions, as shown in the structural analysis. In contrast, the red and blue-green triangles and the flat surfaces on the shape index and curvedness plots reveal Cg.Cg···Cg interactions, as shown in Figure S8 and Figure S9 for compounds **4g** and **4d**, respectively. The percentage contributions of the contacts for compounds **4g** and **4d** are provided in Table S6.

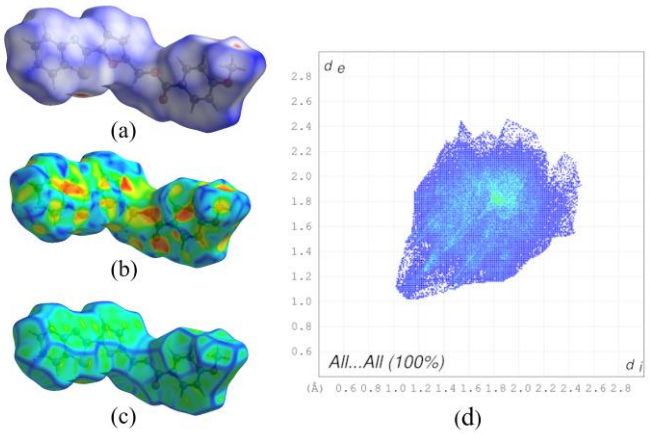

Figure S8. The d_{norm}, shape index, curvedness, and 2D fingerprint plot of the compound **4g**.

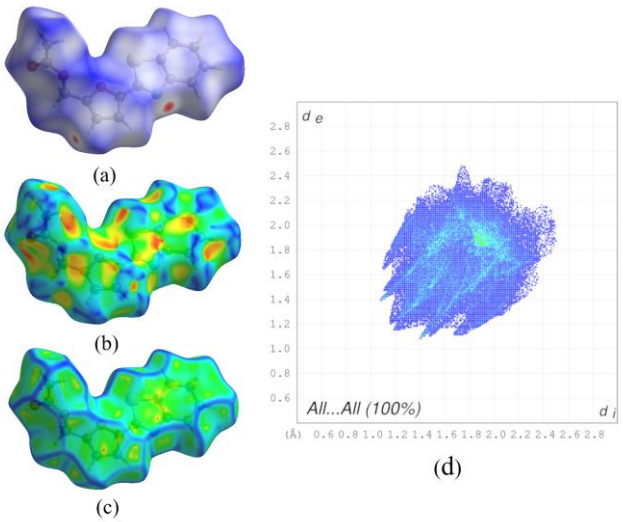

Figure S9. The d_{norm}, shape index, curvedness, and 2D fingerprint plot of the compound **4d**.

Table S6. Percentage contribution of the various contact types to the stability of the crystal structure.

Contact types	Compound **4d**	Compound **4g**
H···H	38.3	38
C···H	13.7	21.3
H···O	21.5	18.6
C···C	6.5	4.4
H···S	8.3	4
C···O	2.1	3.7
H···N	3.6	3.5
C···S	1.2	2.5

Table S7. Physicochemical properties of the synthesized novel compounds.

Parameters	**Compound 4g**	**Compound 4d**
Molecular properties		
Molecular weight	365.41	273.31
LogP	4.9219	3.6194
Number of rotatable bonds	5	3
Number of acceptors	6	5
Number of donors	0	0
Surface area	153.365	113.194
Absorption		
Water solubility (log mol/L)	-4.331	-3.41
Caco-2 permeability (log Papp in 10^{-6} cm/s)	1.166	1.396
Intestinal absorption (% absorbed)	95.474	94.915
Skin permeability (log Kp)	-2.733	-2.433
P-glycoprotein substrate	No	No
P-glycoprotein I inhibitor	Yes	No
P-glycoprotein II inhibitor	Yes	No
Distribution		
VDss (human) (log L/kg)	0.142	-0.105

Fraction unbound (human) (Fu)	0.197	0.226
BBB permeability (log BB)	-0.125	0.176
CNS permeability (log PS)	-1.956	-2.812
MetabolismMetabol		
CYP2D6 substrate	No	No
CYP3A4 substrate	Yes	Yes
CYP1A2 inhibitior	Yes	Yes
CYP2C19 inhibitior	Yes	Yes
CYP2C9 inhibitior	Yes	No
CYP2D6 inhibitior	No	No
CYP3A4 inhibitior	Yes	No
Excretion		
Total Clearance (log ml/min/kg)	0.18	0.194
Renal OCT2 substrate	No	No
Toxicity		
AMES toxicity	No	Yes
Max. tolerated dose (human) (log mg/kg/day)	0.613	-0.011
hERG I inhibitor	No	No
hERG II inhibitor	Yes	No
Oral Rat Acute Toxicity (LD50) (mol/kg)	2.477	2.428
Oral Rat Chronic Toxicity (LOAEL) (log mg/kg_bw/day)	1.225	0.548
Hepatotoxicity	Yes	Yes
Skin Sensitisation	No	No
T.Pyriformis toxicity (log ug/L)	0.319	0.634
Minnow toxicity (log mM)	-2.561	-0.814

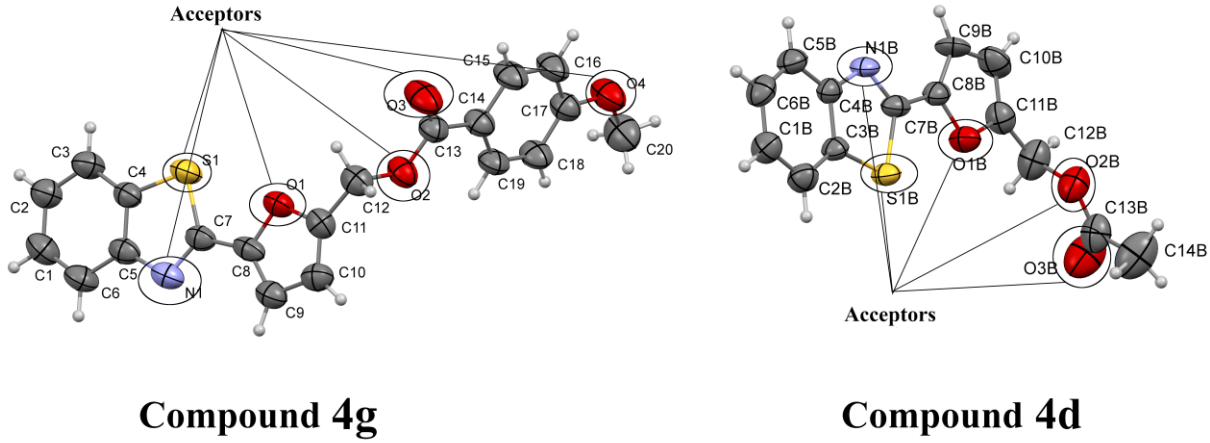

Compound 4g **Compound 4d**

Figure S10. The acceptor sites of compounds **4g** and **4d** are highlighted.

4. Characterization of synthesized compounds

2-(furan-2-yl)benzo[d]thiazole (**4a**):

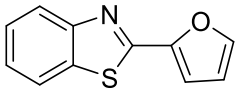

4a

Pale yellow; 0.460 g, 88 %; Melting Point: 103-104 °C; ^{1}H-NMR ($CDCl_3$, 400 MHz) δ (ppm): 7.98 (d, 1H, Ar-**H**, *J* = 8 Hz), 7.82 (d, 1H, Ar-**H**, *J* = 8 Hz), 7.53 (d, 1H, Ar-**H**, *J* = 1.6 Hz), 7.43-7.30 (m, 2H, Ar-**H**), 7.12 (d, 1H, furyl-C**H,** *J* = 3.2 Hz), 6.53-6.51 (m, 1H, furyl-C**H**); ^{13}C-NMR ($CDCl_3$, 100 MHz) δ (ppm): 157.5, 153.7, 148.7, 144.6, 134.2, 126.4, 125.1, 123.1, 121.5, 112.5, 111.4; FTIR (cm^{-1}): 3123, 3061, 1556, 1245, 1151, 1012.[9]

2-(5-methylfuran-2-yl)benzo[d]thiazole (**4b**):

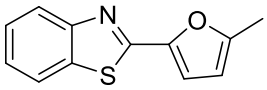

4b

Yellow solid; 0.443 g, 91%; Melting Point: 107-108 °C; ^{1}H-NMR ($CDCl_3$, 400 MHz) δ (ppm): 7.96 (d, 1H, Ar-**H**, *J* = 8 Hz), 7.78 (d, 1H, Ar-**H**, *J* = 8 Hz), 7.40-7.36 (m, 1H, Ar-**H**), 7.28-7.24 (m, 1H, Ar-**H**), 6.99 (d, 1H, furyl-C**H**, *J* = 3.6 Hz), 6.10 (d, 1H, furyl-C**H**, *J* = 3.6 Hz), 2.35 (s, 3H, -C**H**$_3$); ^{13}C-NMR ($CDCl_3$, 100 MHz) δ (ppm): 157.7, 155.4, 153.7, 147.0, 134.0, 126.3, 124.8, 122.8, 121.4, 113.0, 108.8, 13.9; FTIR (cm^{-1}): 2952, 2921, 1608, 1545, 1433, 1014.[10]

(5-(benzo[d]thiazol-2-yl)furan-2-yl)methanol (**4c**):

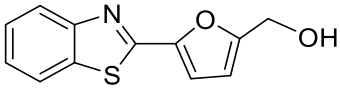

4c

Pale brown solid; 0.329 g, 72 %; Melting point: 166-167 °C; ^{1}H-NMR (DMSO-d_6, 400 MHz) δ (ppm): 8.14 (d, 1H, Ar-**H**, *J* = 7.6 Hz), 8.01 (d, 1H, Ar-**H**, *J* = 8.4 Hz), 7.56-7.52 (m, 1H, Ar-**H**), 7.46-7.42 (m, 1H, Ar-**H**), 7.30 (d, 1H, furyl-C**H**, *J* = 3.2 Hz), 6.60 (d, 1H, furyl-C**H**, *J* = 3.2 Hz), 5.50 (s, 1H, -O**H**), 4.52 (s, 2H, -C**H**$_2$); ^{13}C-NMR (DMSO-d_6, 100 MHz) δ (ppm): 158.7, 156.7, 153.3, 147.0, 133.6, 126.7, 125.3, 122.5, 122.3, 112.8, 110.0, 55.6; FTIR (cm^{-1}): 3212, 2957, 2918, 1602, 1543, 1024.[9]

(5-(benzo[d]thiazol-2-yl)furan-2-yl)methyl acetate (**4d**):

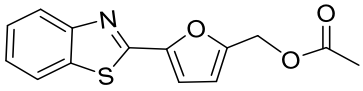

4d

Light brown solid; 0.314 g, 78%; Melting Point: 131-132 °C; ^{1}H-NMR (DMSO-d_6, 400 MHz) δ (ppm): 8.16 (d, 1H, Ar-**H**, *J* = 8 Hz), 8.04 (d, 1H, Ar-**H**, *J* = 8 Hz), 7.57-7.53 (m, 1H, Ar-**H**), 7.48-7.44 (m, 1H, Ar-**H**), 7.34 (d, 1H, furyl-C**H**, *J* = 3.6 Hz), 6.82 (d, 1H, furyl-C**H**, *J* = 3.6 Hz), 5.17 (s, 2H, -C**H**$_2$), 2.09 (s, 3H, -C**H**$_3$); ^{13}C-NMR (DMSO-d_6, 100 MHz) δ (ppm): 169.9, 156.3, 153.2, 152.3, 148.1, 133.7, 126.8, 125.5, 122.7, 122.4, 113.6, 112.8, 57.3, 20.5; FTIR (cm^{-1}): 1731, 1551, 1373, 1263, 1206, 1016. HRMS (ESI) calculated for $C_{14}H_{11}NO_3S$ $[M+H]^+$ 274.0532, found 274.0549.

(5-(benzo[d]thiazol-2-yl)furan-2-yl)methyl benzoate (**4e**):

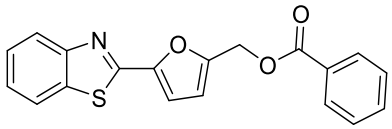

4e

Light yellow solid; 0.308 g, 85%; Melting Point 105-106 °C; ^{1}H-NMR ($CDCl_3$, 400 MHz) δ (ppm): 7.97-7.93 (m, 3H, Ar-**H**), 7.78 (d, 1H, Ar-**H**, *J* = 8 Hz), 7.46-7.42 (m, 1H, Ar-**H**), 7.40-7.24 (m, 4H, Ar-**H**), 7.05 (d, 1H, furyl-C**H**, *J* = 3.2 Hz), 6.57 (d, 1H, furyl-C**H**, *J* = 3.2 Hz), 5.30 (s, 2H, -C**H**$_2$); ^{13}C-NMR ($CDCl_3$, 100 MHz,) δ (ppm): 166.1, 157.1, 153.6, 151.9, 148.9, 134.2, 133.2, 129.7, 129.5, 128.3, 126.5, 125.3, 123.1, 121.5, 113.4, 112.3, 58.3. FTIR (cm^{-1}): 1718, 1603, 1455, 1264, 1214, 1093. HRMS (ESI) calculated for $C_{19}H_{13}NO_3S$ $[M+H]^+$ 336.0689, found 336.0702.

(5-(benzo[d]thiazol-2-yl)furan-2-yl)methyl 4-chlorobenzoate (**4f**):

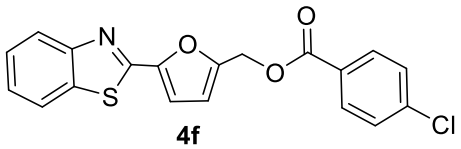

4f

White solid; 0.301 g, 86%; Melting point: 144-146 °C; ^{1}H-NMR ($CDCl_3$, 400 MHz) δ (ppm): 8.08 (d, 1H, Ar-**H**, *J* = 8 Hz), 8.02 (d, 2H, Ar-**H**, *J* = 8.4 Hz), 7.90 (d, 1H, Ar-**H**, *J* = 8 Hz), 7.52-7.48 (m, 1H, Ar-**H**), 7.42-7.38 (m, 3H, Ar-**H**), 7.17 (d, 1H, furyl-C**H**, *J* = 3.6 Hz), 6.7 (d, 1H, furyl-C**H**, *J* = 3.6 Hz), 5.40 (s, 2H, -C**H**$_2$); ^{13}C-NMR ($CDCl_3$, 100 MHz,) δ (ppm): 165.3, 157.1, 153.6, 151.6, 149.1, 139.7, 134.2, 131.2, 128.7, 128.1, 126.6, 125.4, 123.2, 121.6, 113.6, 112.4, 58.5; FTIR (cm^{-1}): 1719, 1594, 1550, 1261, 1090, 1015. HRMS (ESI) calculated for $C_{19}H_{12}ClNO_3S$ $[M+H]^+$ 370.0290, found 370.0299.

(5-(benzo[d]thiazol-2-yl)furan-2-yl)methyl 4-methoxybenzoate (**4g**):

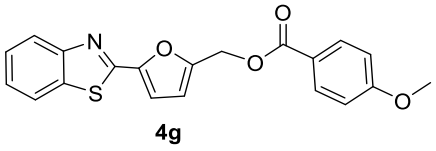

4g

White solid; 0.308 g, 88%; Melting point: 119-120 °C; ^{1}H-NMR ($CDCl_3$, 400 MHz) δ (ppm): 8.08-8.06 (d, 1H, Ar-**H**, *J* = 8 Hz), 8.04-8.02 (m, 2H, Ar-**H**), 7.90 (d, 1H, Ar-**H**, *J* = 8 Hz), 7.51-7.48 (m, 1H, Ar-**H**), 7.41-7.37 (m, 1H, Ar-**H**), 7.19 (d, 1H, furyl-C**H**, *J* = 3.6 Hz), 6.92-6.90 (m, 2H, Ar-**H**), 6.68 (d, 1H, furyl-C**H**, *J* = 3.6 Hz), 5.38 (s, 2H, -C**H₂**), 3.85 (s, 3H, -C**H₃**); ^{13}C-NMR ($CDCl_3$, 100 MHz,) δ (ppm): 165.8, 163.6, 157.2, 153.2, 152.4, 148.6, 134.0, 131.8, 126.6, 125.4, 123.0, 121.9, 121.5, 113.6, 113.2, 112.8, 58.0, 55.4; FTIR (cm^{-1}): 2958, 2930, 1710, 1604, 1249, 1089. HRMS (ESI) calculated for $C_{20}H_{15}NO_4S$ $[M+H]^+$ 366.0795, found 366.0802.

2-(5-(2,4,6-trimethylbenzyl)furan-2-yl)benzo[d]thiazole (**4h**):

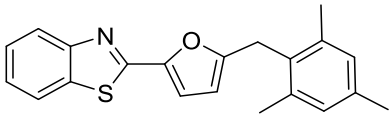

4h

Pale brown solid; 0.301 g, 82%; Melting point: 112-113 °C; ^{1}H-($CDCl_3$, 400 MHz) δ (ppm): 8.04 (d, 1H, Ar-**H**, *J* = 8 Hz), 7.88 (d, 1H, Ar-**H**, *J* = 8 Hz), 7.49-7.45 (m, 1H, Ar-**H**), 7.38-7.33 (m, 1H, Ar-**H**), 7.05 (d, 1H, furyl-C**H**, *J* = 3.6 Hz), 6.90 (s, 2H, Ar-**H**), 5.90 (d, 1H, furyl-C**H**, *J* = 3.6 Hz), 4.08 (s, 2H, -C**H₂**), 2.33 (s, 6H, -C**H₃**), 2.3 (s, 3H, -C**H₃**); ^{13}C-NMR ($CDCl_3$, 100 MHz,) δ (ppm): 157.7, 157.5, 153.7, 147.3, 136.8, 136.3, 134.0, 130.3, 129.0, 126.3, 124.8, 122.8, 121.4, 112.7, 108.6, 28.4, 20.8, 19.9; FTIR (cm^{-1}): 2947, 2919, 1608, 1483, 1433, 1011. HRMS (ESI) calculated for $C_{21}H_{19}NOS$ $[M+H]^+$ 334.1260, found 334.1269.

2-(furan-2-yl)-1-(furan-2-ylmethyl)-1H-benzo[d]imidazole (**5a**):

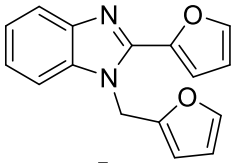

5a

Pale brown solid; 0.312 g, 64%; Melting Point: 96-98 °C; ^{1}H-($CDCl_3$, 400 MHz) δ (ppm): 7.79 (m, 1H, Ar-**H**), 7.64 (s, 1H, furyl-C**H**), 7.50-7.48 (m, 1H, Ar-**H**), 7.32-7.31 (m, 3H, Ar-**H**), 7.22 (d, 1H, furyl-C**H**, *J* = 3.6 Hz), 6.61-6.59 (dd, 1H, furyl-C**H**, J_1 = 1.6 Hz, J_2 = 1.6 Hz), 6.28-6.27 (dd, 1H, furyl-C**H**, J_1 = 1.6 Hz, J_2 = 1.6 Hz), 6.23 (d, 1H, furyl-C**H**, *J* = 3.6 Hz), 5.63 (s, 2H, -C**H₂**); ^{13}C-NMR ($CDCl_3$, 100 MHz,) δ (ppm): 149.5, 145.3, 143.9, 143.8, 142.9, 142.6, 135.4, 123.1, 122.8, 119.7, 112.8, 112.0, 110.4, 109.9, 108.3, 41.6; FTIR (cm^{-1}): 3147, 3118, 1608, 1510, 1149, 1010.[11]

2-(furan-2-yl)-1H-benzo[d]imidazole(**6a**)**:**

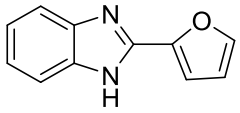

6a

Light yellow solid; 0.105 g, 31 %; Melting Point: 292-294 °C; ^{1}H-NMR (DMSO-d_6, 400 MHz) δ (ppm): 12.90 (br s, 1H, -N**H**), 7.93 (s, 1H, furyl-C**H**), 7.55 (s, 2H, Ar-**H**), 7.20-7.18 (m, 3H), 6.73-6.72 (m, 1H, furyl-C**H**); ^{13}C-NMR (DMSO-d_6, 100 MHz) δ (ppm): 144.9, 144.0, 143.1, 122.1, 121.3, 118.1, 111.8, 110.8, 109.9, 39.5; FTIR (cm^{-1}): 2958, 2919, 1738, 1519, 1413, 1115.[12]

2-(5-methylfuran-2-yl)-1-((5-methylfuran-2-yl)methyl)-1H-benzo[d]imidazole (**5b**):

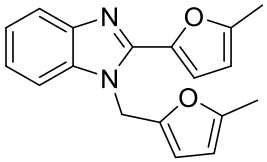

5b

Light yellow solid; 0.351 g, 66%; Melting Point: 94-96 °C; ^{1}H-($CDCl_3$, 400 MHz) δ (ppm): 7.78-7.76 (m, 1H, Ar-**H**), 7.49-7.47 (m, 1H, Ar-**H**), 7.28-7.26 (m, 2H, Ar-**H**), 7.07 (d, 1H, furyl-C**H**, *J* = 3.2 Hz), 6.19 (d, 1H, furyl-C**H**, *J* = 3.2 Hz), 6.12 (d, 1H, furyl-C**H**, *J* = 3.2 Hz), 5.86 (d, 1H, furyl-C**H**, *J* = 3.2 Hz), 5.51 (s, 2H, -C**H₂**), 2.45 (s, 3H, -C**H₃**), 2.21 (s, 3H, -C**H₃**); ^{13}C-NMR ($CDCl_3$, 100 MHz,) δ (ppm): 154.4, 152.3, 147.6, 144.3, 143.3, 142.9, 135.5, 122.8, 122.6, 119.5, 113.8, 109.9, 109.1, 108.1, 106.3, 41.7, 13.8, 13.4; FTIR (cm^{-1}): 2950, 2923, 1612, 1285, 1212, 1020.[13]

2-(5-methylfuran-2-yl)-1H-benzo[d]imidazole) (**6b**):

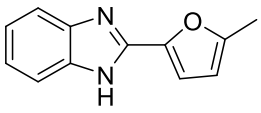

6b

Light yellow solid; 0.113 g, 33%; Melting point: 266-268 °C; ^{1}H-NMR (DMSO-d_6, 400 MHz) δ (ppm): 12.78 (br s, 1H, -N**H**), 7.57-7.46 (m, 2H, Ar-**H)**, 7.18 (dd, 2H, Ar-**H**, J_1= 2.8 Hz, J_2= 2.8 Hz), 7.07 (d, 1H, furyl-C**H**, *J* = 3.6 Hz), 6.34 (d, 1H, furyl-C**H**, *J* = 3.6 Hz), 2.41 (s, 3H, -C**H₃**); ^{13}C-NMR (DMSO-d_6, 100 MHz) δ (ppm): 153.7, 144.0, 143.8, 143.7, 122.3, 121.6, 118.5, 111.5, 111.2, 108.5, 13.4; FTIR (cm^{-1}): 2955, 2925, 1733, 1631, 1444, 1019.[13]

2-(5-(ethoxymethyl)furan-2-yl)-1-((5-(ethoxymethyl)furan-2-yl)methyl)-1H-benzo[d]imidazole(**5c**):

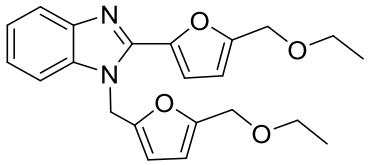

5c

Brown solid; 0.429 g, 61%; Melting Point: 108-110 °C; ^{1}H-($CDCl_3$, 400 MHz) δ (ppm): 7.81-7.78 (m, 1H, Ar-**H**), 7.56-7.54 (m, 1H, Ar-**H**), 7.32-7.30 (m, 2H, Ar-**H**), 7.23 (d, 1H, furyl-C**H**, *J* = 3.2 Hz), 6.52 (d, 1H, furyl-C**H**, *J* = 3.2 Hz), 6.28 (d, 1H, furyl-C**H**, *J* = 3.2 Hz), 6.20 (d, 1H, furyl-C**H**, *J* = 3.2 Hz), 5.64 (s, 2H, -C**H₂**), 4.57 (s, 2H, -C**H₂**), 4.34 (s, 2H, -C**H₂**), 3.61-3.55 (m, 2H, -C**H₂**), 3.50-3.45 (m, 2H, -C**H₂**), 1.26-1.22 (m, 3H, -C**H₃**), 1.19-1.16 (m, 3H, -C**H₃**); ^{13}C-NMR ($CDCl_3$, 100 MHz) δ (ppm): 154.2, 152.3, 149.4, 144.5, 143.3, 135.2, 123.5, 123.2, 119.3, 114.2, 111.3, 110.1, 109.9, 109.4, 65.9, 65.7, 64.5, 64.4, 41.9, 15.1, 15.0; FTIR (cm^{-1}): 2955, 2920, 1733, 1610, 1459, 1348. HRMS (ESI) calculated for $C_{22}H_{24}N_2O_4$ $[M+H]^+$ 381.1809, found 381.1829.

2-(5-(ethoxymethyl)furan-2-yl)-1H-benzo[d]imidazole) (**6c**):

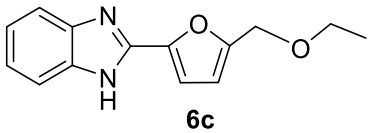

6c

Light brown solid; 0.107 g, 24%; Melting Point: 125-126 °C; ^{1}H-NMR (DMSO-d_6, 400 MHz) δ (ppm): 12.92 (br s, 1H, -N**H**), 7.59-7.57 (m, 2H, Ar-**H**), 7.25-7.23 (m, 2H, Ar-**H**), 7.21 (d, 1H, furyl-C**H**, *J* = 3.6 Hz), 6.70 (d, 1H, furyl-C**H**, *J* = 3.6 Hz), 4.51 (s, 2H, -C**H₂**), 3.56-3.51 (m, 2H, -C**H₂**), 1.17-1.13 (s, 3H, -C**H₃**); ^{13}C-NMR (DMSO-d_6, 100 MHz) δ (ppm): 154.5, 145.0, 143.4, 123.2, 112.3, 65.5, 64.1, 15.4; FTIR (cm^{-1}): 2958, 2923, 1729, 1675, 1206, 1092.[14]

(5-((2-(5-(acetoxymethyl)furan-2-yl)-1H-benzo[d]imidazol-1-yl)methyl)furan-2-yl)methyl acetate (**5d**):

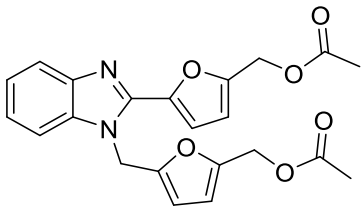

5d

Light brown solid; 0.468 g, 62%; Melting Point: 112-114 °C; ^{1}H-($CDCl_3$, 400 MHz) δ (ppm): 7.69-7.67 (m, 1H, Ar-**H**), 7.43-7.41 (m, 1H, Ar-**H**), 7.21-7.19 (m, 2H, Ar-**H**), 7.09 (d, 1H, furyl-C**H**, *J* = 3.6 Hz), 6.51 (d, 1H, furyl-C**H**, *J* = 3.6 Hz), 6.51 (d, 1H, furyl-C**H**, *J* = 3.6

Hz), 6.20 (d, 1H, furyl-C**H**, *J* = 3.2 Hz), 6.15 (d, 1H, furyl-C**H**, *J* = 3.2 Hz), 5.50 (s, 2H, -C**H₂**), 5.08 (s, 2H, -C**H₂**), 4.86 (s, 2H, -C**H₂**), 1.99 (s, 3H, -C**H₃**), 1.93 (s, 3H, -C**H₃**); ^{13}C-NMR ($CDCl_3$, 100 MHz) δ (ppm): 170.3, 170.3, 151.1, 150.0, 149.5, 145.2, 143.1, 142.4, 135.2, 123.3, 122.9, 119.5, 113.6, 112.6, 111.3, 109.9, 109.2, 57.6, 41.5, 20.6, 20.5; FTIR (cm^{-1}): 2956, 2921, 1738, 1611, 1220, 1157, 1018. HRMS (ESI) calculated for $C_{22}H_{20}N_2O_6$ $[M+H]^+$ 409.1394, found 409.1402.

(5-(1H-benzo[d]imidazol-2-yl)furan-2-yl)methyl acetate (**6d**):

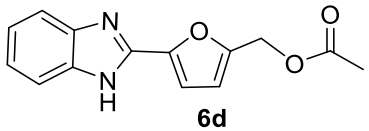

6d

Brown solid; 0.132 g, 28%; Melting Point: 123-124 °C; ^{1}H-NMR (DMSO-d_6, 400 MHz) δ (ppm): 13.01 (br s, 1H, -N**H**), 8.12 (s, 2H, Ar-**H**), 7.51 (s, 1H, furyl-C**H**), 7.17 - 7.13 (m, 2H, Ar-**H**), 6.73 (d, 1H, furyl-C**H**, *J* = 3.6 Hz), 5.11 (s, 2H, -C**H₂**), 2.46-2.45 (m, 2H, -C**H₂**), 2.04 (s, 3H, -C**H₃**); ^{13}C-NMR (DMSO-d_6, 100 MHz) δ (ppm): 169.4, 162.6, 150.2, 145.3, 142.6, 121.8, 112.5, 112.5, 110.6, 56.9, 20.0.; FTIR (cm^{-1}): 2956, 2922, 1741, 1631, 1374, 1231. HRMS (ESI) calculated for $C_{14}H_{13}N_2O_3$ $[M+H]^+$: 257.0921, found 257.0930.

(5-((2-(5-((benzoyloxy)methyl)furan-2-yl)-1H-benzo[d]imidazol-1-yl)methyl)furan-2-yl)methyl benzoate (**5e**):

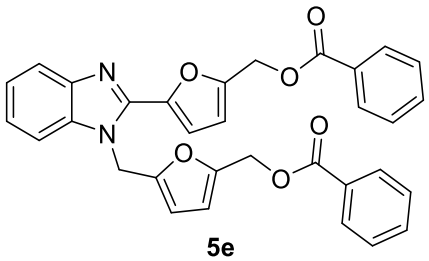

5e

Pale brown solid; 0.532 g, 54%; Melting Point: 157-158 °C; ^{1}H-($CDCl_3$, 400 MHz) δ (ppm): 8.34 (d, 2H, Ar-**H**, *J* = 7.6 Hz), 8.27 (d, 2H, Ar-**H**, *J* = 7.6 Hz), 8.10-8.07 (m, 1H, Ar-**H**), 7.85-7.81 (m, 3H, Ar-**H**), 7.72-7.66 (m, 4H, Ar-**H**), 7.59-7.57 (m, 2H, Ar-**H**), 7.51 (d, 1H, furyl-C**H**, *J* = 3.2 Hz), 6.97 (d, 1H, furyl-C**H**, *J* = 3.2 Hz), 6.58 (d, 1H, furyl-C**H**, *J* = 3.2 Hz), 6.55 (d, 1H, furyl-C**H**, *J* = 3.2 Hz), 5.93 (s, 2H, -C**H₂**), 5.72 (s, 2H, -C**H₂**), 5.46 (s, 2H, -C**H₂**); ^{13}C-NMR ($CDCl_3$, 100 MHz,) δ (ppm): 166.0, 151.1, 150.2, 149.6, 145.7, 143.2, 142.7, 135.4, 133.2, 133.0, 129.6, 129.6, 129.5, 128.3, 128.2, 123.4, 123.0, 119.7, 113.6, 112.9, 111.4, 109.9, 109.4, 58.2, 41.6; FTIR (cm^{-1}): 2959, 2926, 1715, 1602, 1484, 1020. HRMS (ESI) calculated for $C_{32}H_{24}N_2O_6$ $[M+H]^+$ 533.1707, found 533.1729.

(5-(1H-benzo[d]imidazol-2-yl)furan-2-yl)methyl benzoate (**6e**):

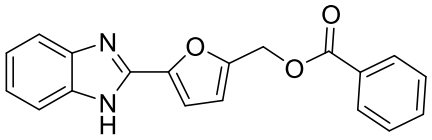

6e

Light brown solid; 0.131 g, 22%; Melting Point: 192-194 °C; ^{1}H-NMR (DMSO-d_6, 400 MHz) δ (ppm): 13.07 (br s, 1H, -N**H**), 8.0-7.98 (m, 2H, Ar-**H**), 7.69-7.65 (m, 2H, Ar-**H**), 7.55-7.51 (m, 4H, Ar-**H**), 7.24 (d, 1H, furyl-C**H**, J = 3.6 Hz), 7.21-7.12 (m, 2H, Ar-**H**), 6.87 (d, 1H, furyl-C**H**, J = 3.6 Hz), 5.44 (s, 2H, -C**H₂**); ^{13}C-NMR (DMSO-d_6, 100 MHz) δ (ppm): 165.4, 150.7, 146.1, 143.2, 133.7, 129.3, 129.2, 128.9, 113.5, 111.4, 58.3; FTIR (cm^{-1}): 2956, 1718, 1599, 1263, 1096, 1020. HRMS (ESI) calculated for $C_{19}H_{14}N_2O_3$ $[M+H]^+$: 319.1077, found: 319.1092.

(5-((2-(5-(((4-nitrobenzoyl)oxy)methyl)furan-2-yl)-1H-benzo[d]imidazol-1-yl)methyl)furan-2-yl)methyl 4-nitrobenzoate (**5f**):

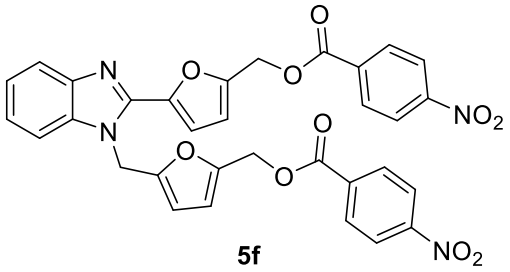

5f

Light yellow solid; 0.714 g, 62%; Melting Point: 121-122 °C; ^{1}H-($CDCl_3$, 400 MHz) δ (ppm): 8.21-8.12 (m, 6H, Ar-**H**), 8.05-8.02 (m, 2H, Ar-**H**), 7.74-7.72 (m, 1H, Ar-**H**), 7.47-7.45 (m, 1H, Ar-**H**), 7.25-7.22 (m, 2H, Ar-**H**), 7.19 (d, 1H, furyl-C**H**, J = 3.2 Hz), 6.66 (d, 1H, furyl-C**H**, J = 3.2 Hz), 6.29 (d, 1H, furyl-C**H**, J = 3.2 Hz), 6.22 (d, 1H, furyl-C**H**, J = 3.2 Hz), 5.59 (s, 2H, -C**H₂**), 5.41 (s, 2H, -C**H₂**), 5.15 (s, 2H, -C**H₂**); ^{13}C-NMR ($CDCl_3$, 100 MHz,) δ (ppm): 164.2, 164.1, 150.7, 150.6, 150.5, 150.4, 149.1, 145.6, 143.1, 142.3, 135.2, 134.9, 134.8, 130.9, 130.8, 123.7, 123.5, 123.4, 123.3, 119.7, 113.9, 113.6, 112.1, 110.0, 109.6, 59.0, 58.9, 41.7; FTIR (cm^{-1}): 2957, 2924, 1724, 1605, 1526, 1263. HRMS (ESI) calculated for $C_{32}H_{22}N_4O_{10}$ $[M+H]^+$ 623.1409, found 623.1429.

(5-(1H-benzo[d]imidazol-2-yl)furan-2-yl)methyl 4-nitrobenzoate (**6f**):

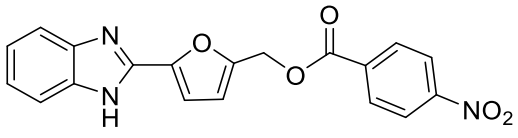

6f

Light yellow solid; 0.215 g, 32%; Melting Point: 110-112 °C; ^{1}H-NMR (DMSO-d_6, 400 MHz) δ (ppm): 12.96 (br s, 1H, -N**H**), 8.33-8.31 (m, 2H, Ar-**H**), 8.20-8.16 (m, 2H, Ar-**H**), 7.56-7.54 (m, 2H, Ar-**H**), 7.23 (d, 1H, furyl-C**H**, *J* = 3.6 Hz), 7.21-7.18 (m, 2H, Ar-**H**), 6.90 (d, 1H, furyl-C**H**, *J* = 3.6 Hz), 5.49 (s, 2H, -C**H$_2$**); ^{13}C-NMR (DMSO-d_6, 100 MHz) δ (ppm): 164.0, 150.4, 150.3, 146.3, 143.2, 134.6, 130.9, 124.0, 122.5, 113.9, 111.4, 59.1; FTIR (cm^{-1}): 2956, 2921, 1726, 1605, 1526, 1266, 1097. HRMS (ESI) calculated for $C_{19}H_{13}N_3O_5$ $[M+H]^+$ 364.0928, found 364.0940.

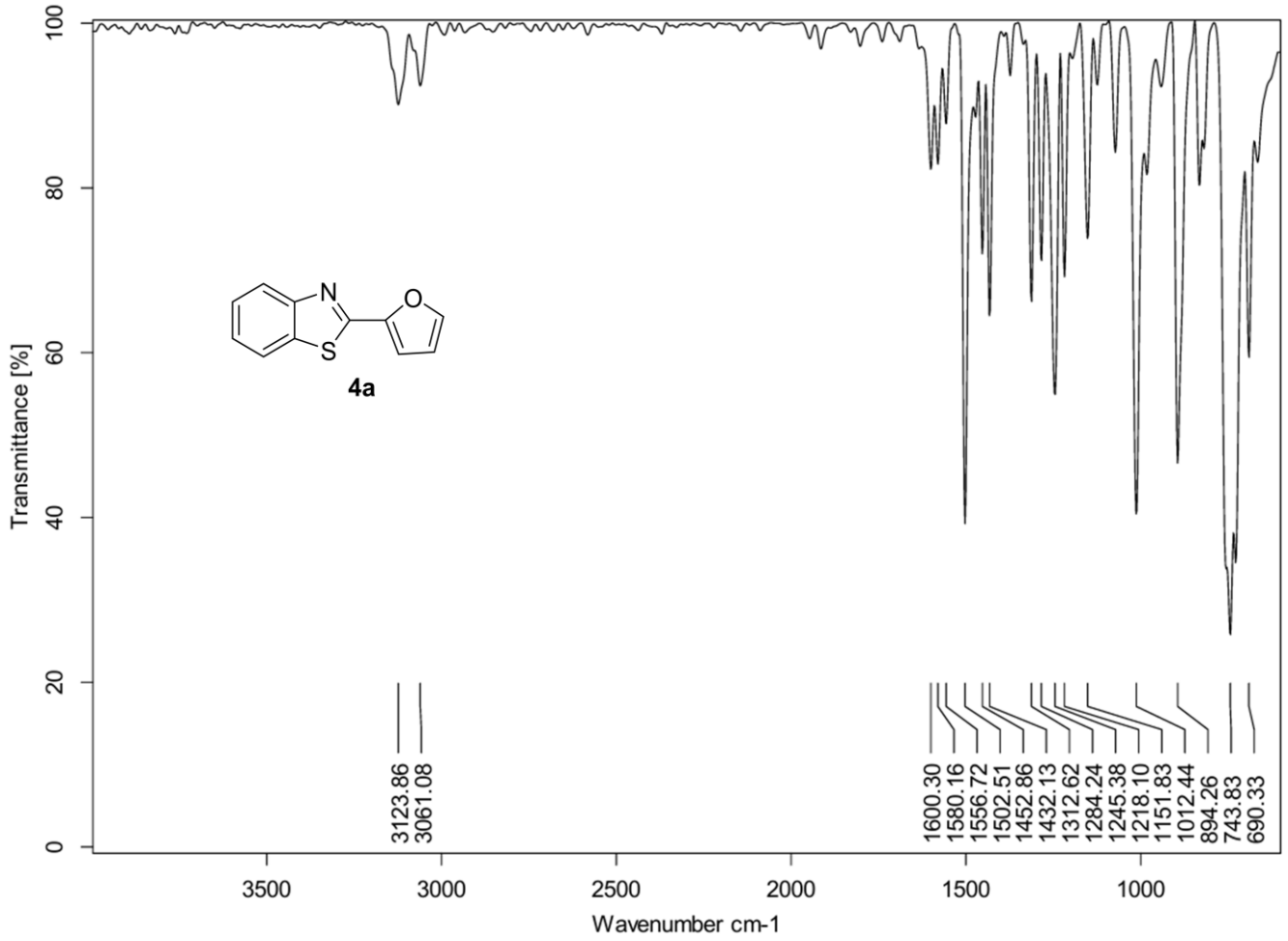

Figure S11. The FTIR spectrum of **4a**.

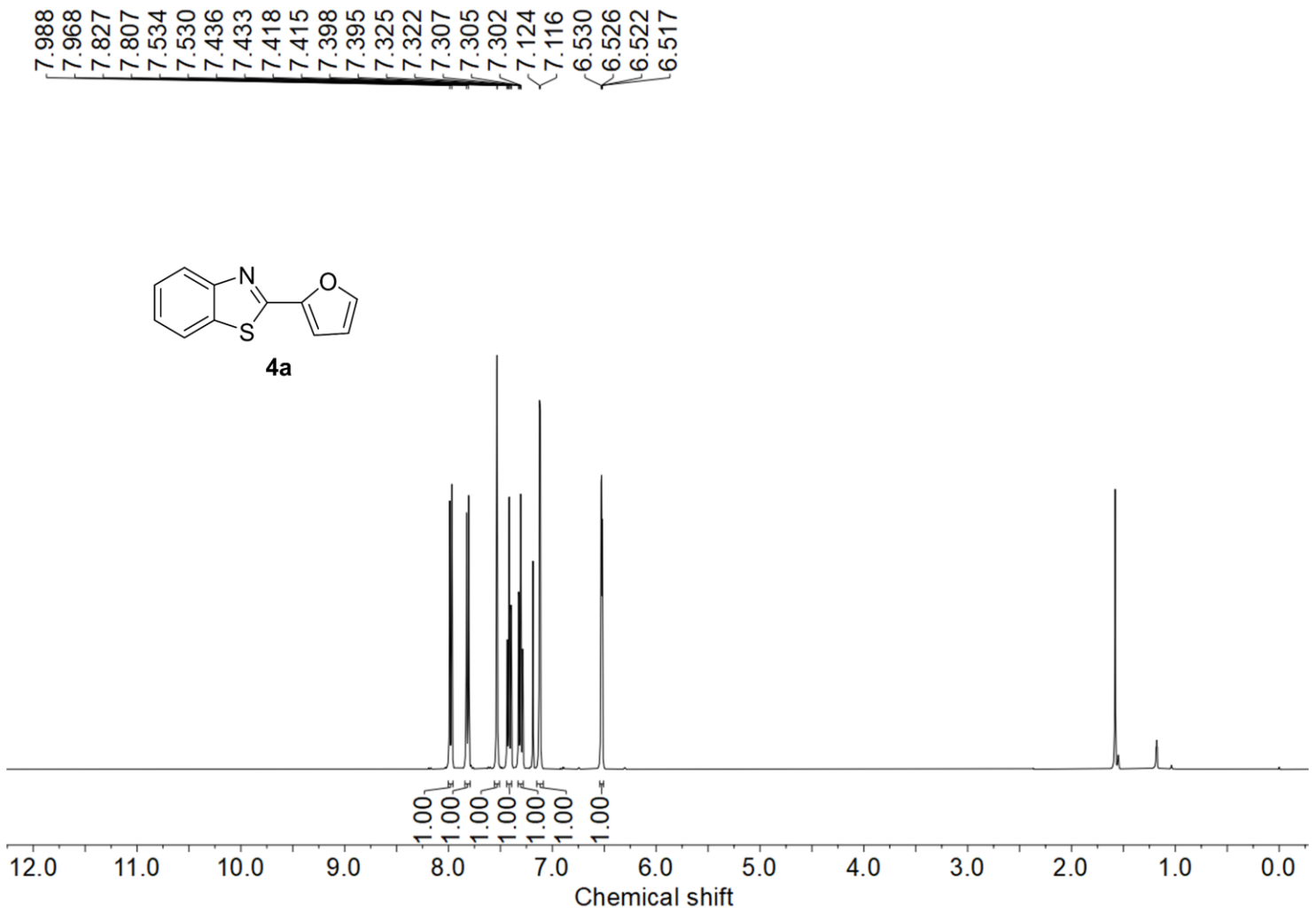

Figure S12. The ^{1}H-NMR spectrum of **4a**.

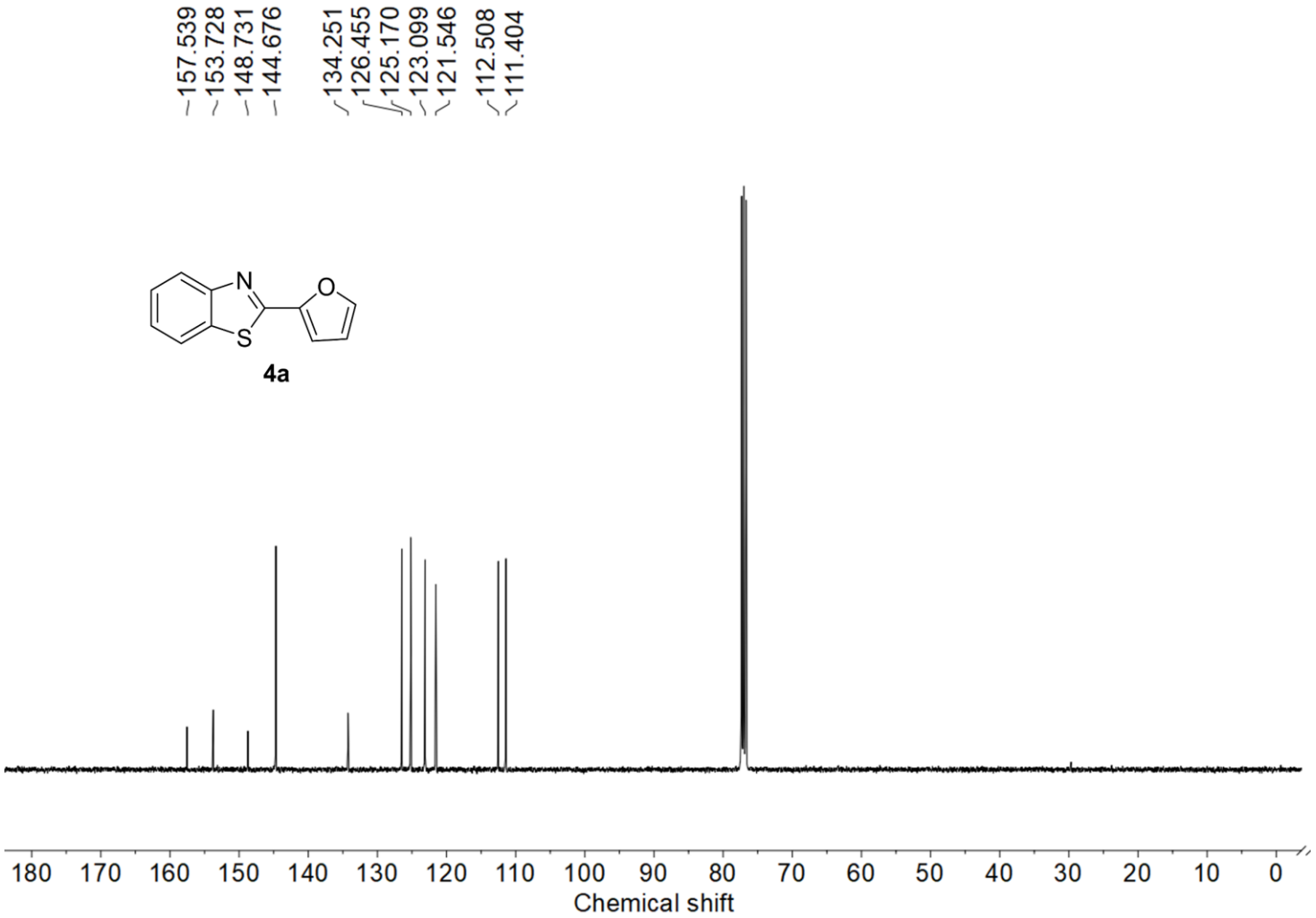

Figure S13. The ^{13}C-NMR spectrum of **4a**.

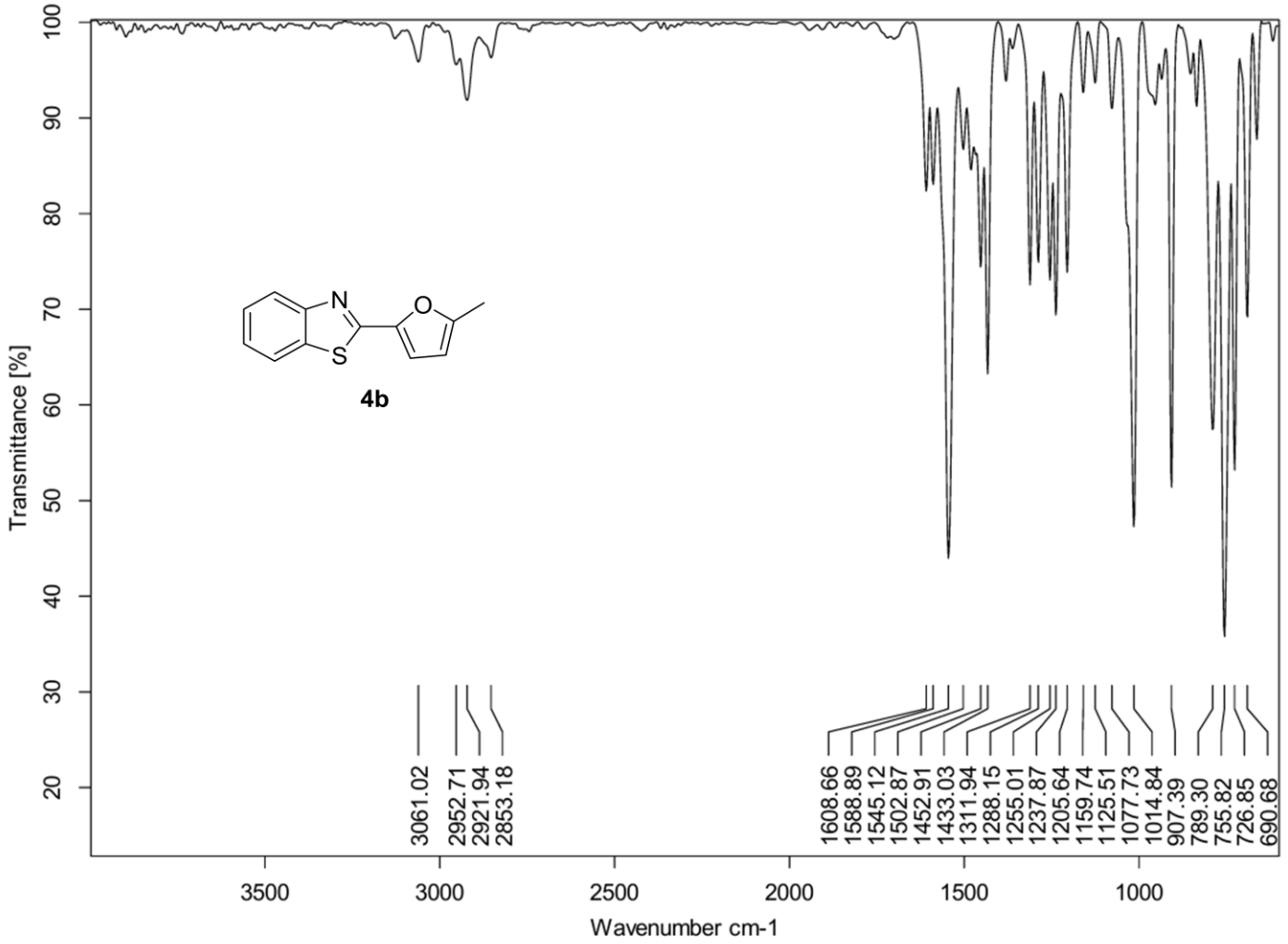

Figure S14. The FTIR spectrum of **4b**.

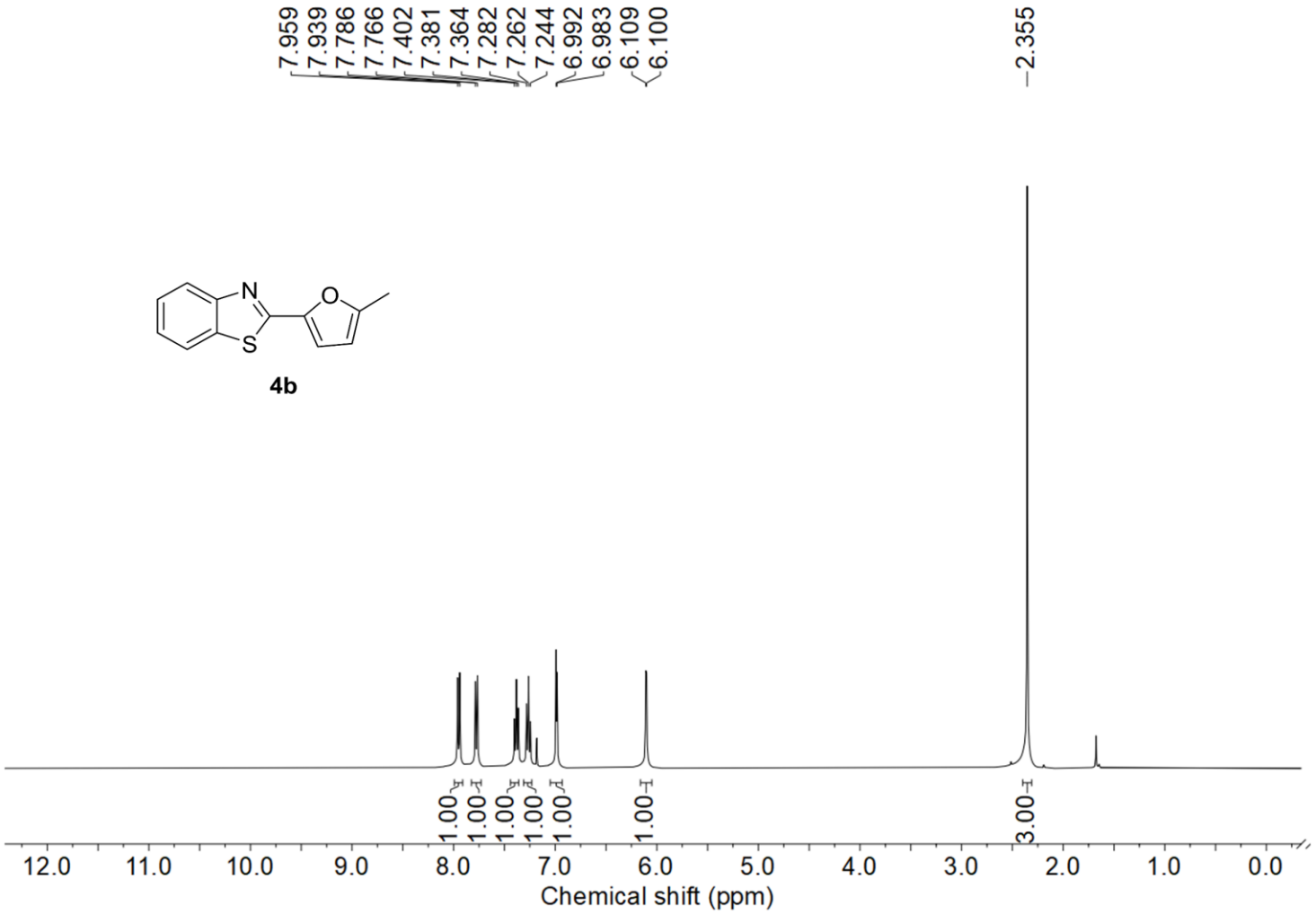

Figure S15. The ^{1}H-NMR spectrum of **4b**.

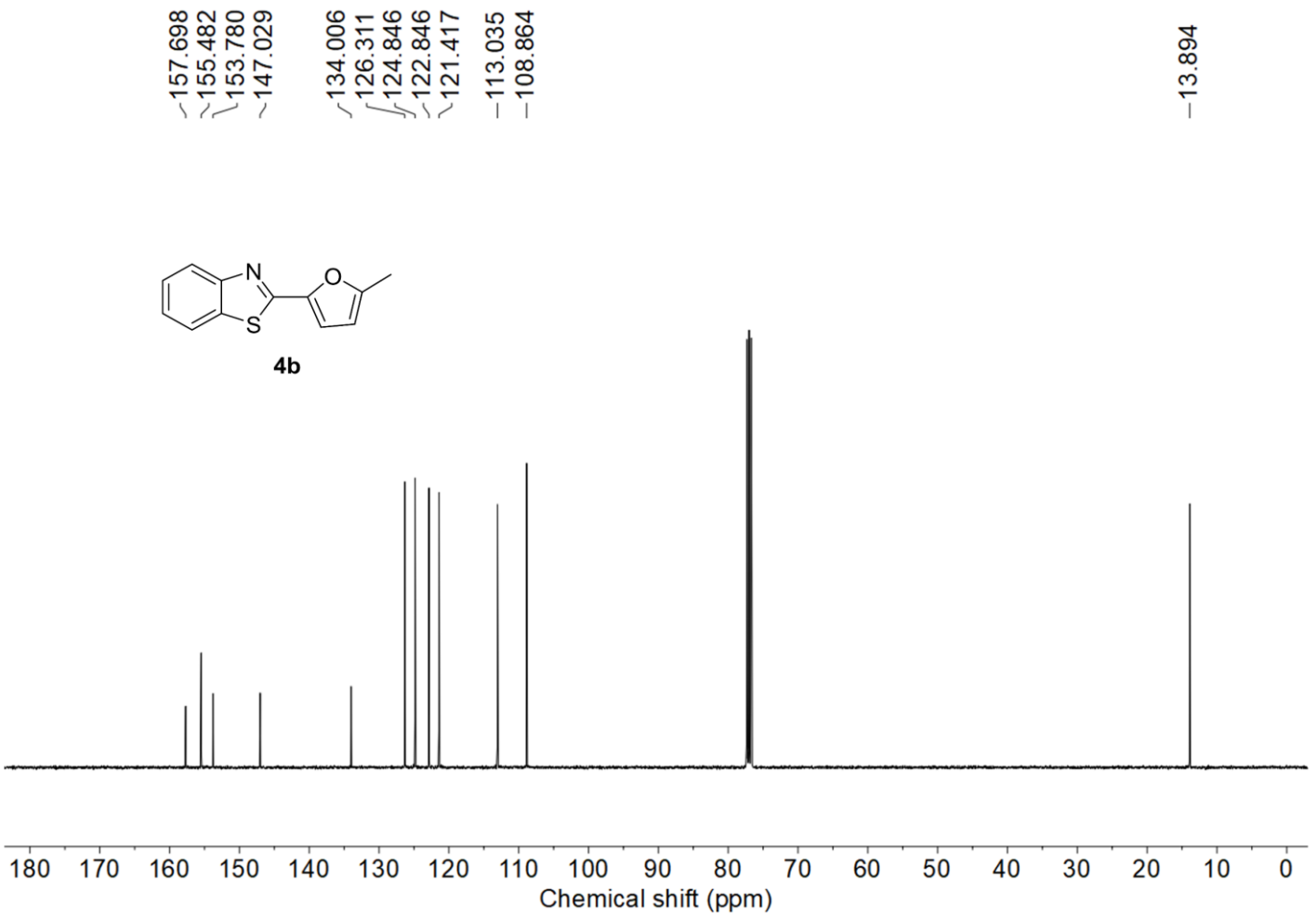

Figure S16. The ^{13}C-NMR spectrum of **4b.**

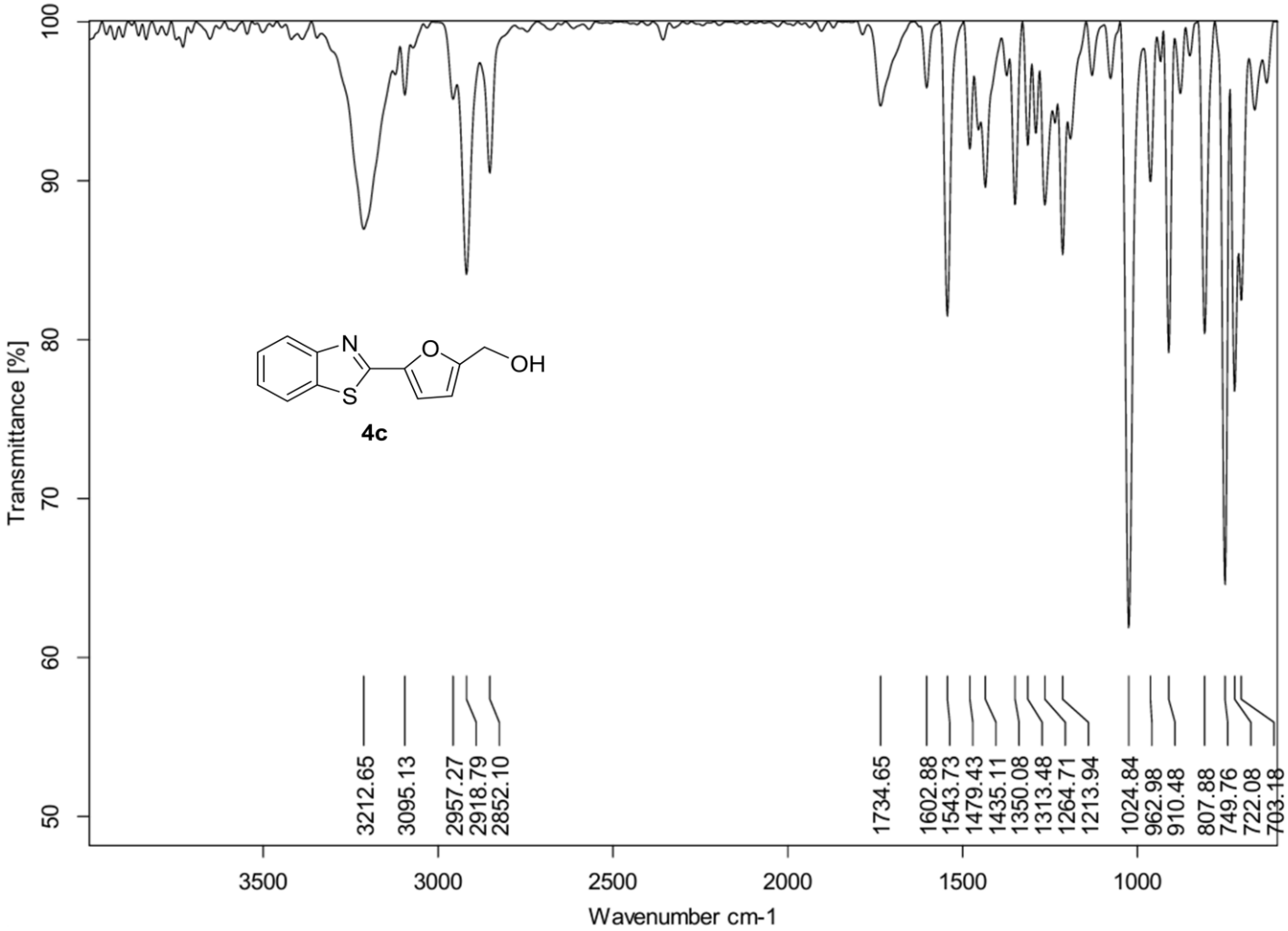

Figure S17. The FTIR spectrum of **4c**.

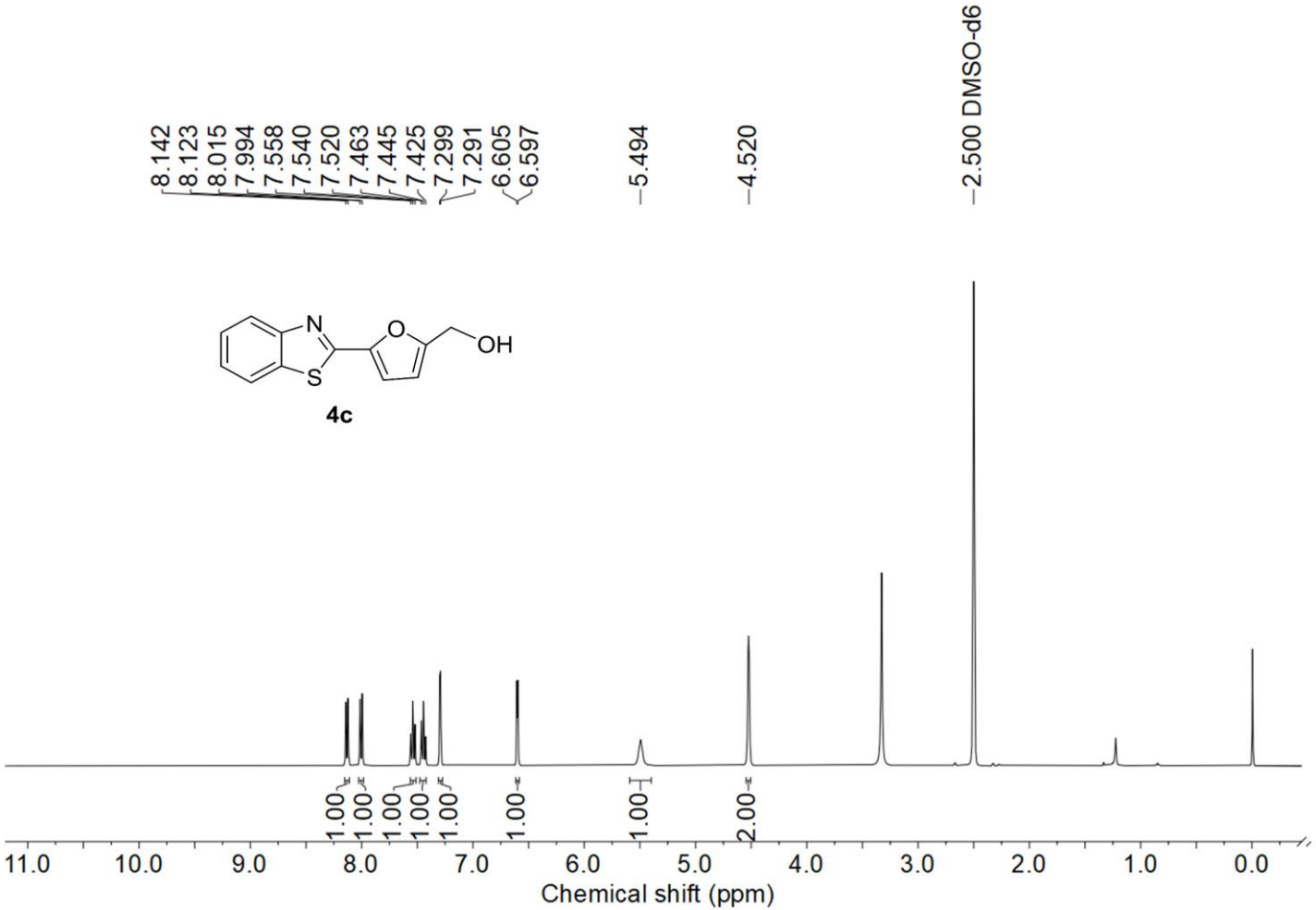

Figure S18. The ^{1}H-NMR spectrum of **4c**.

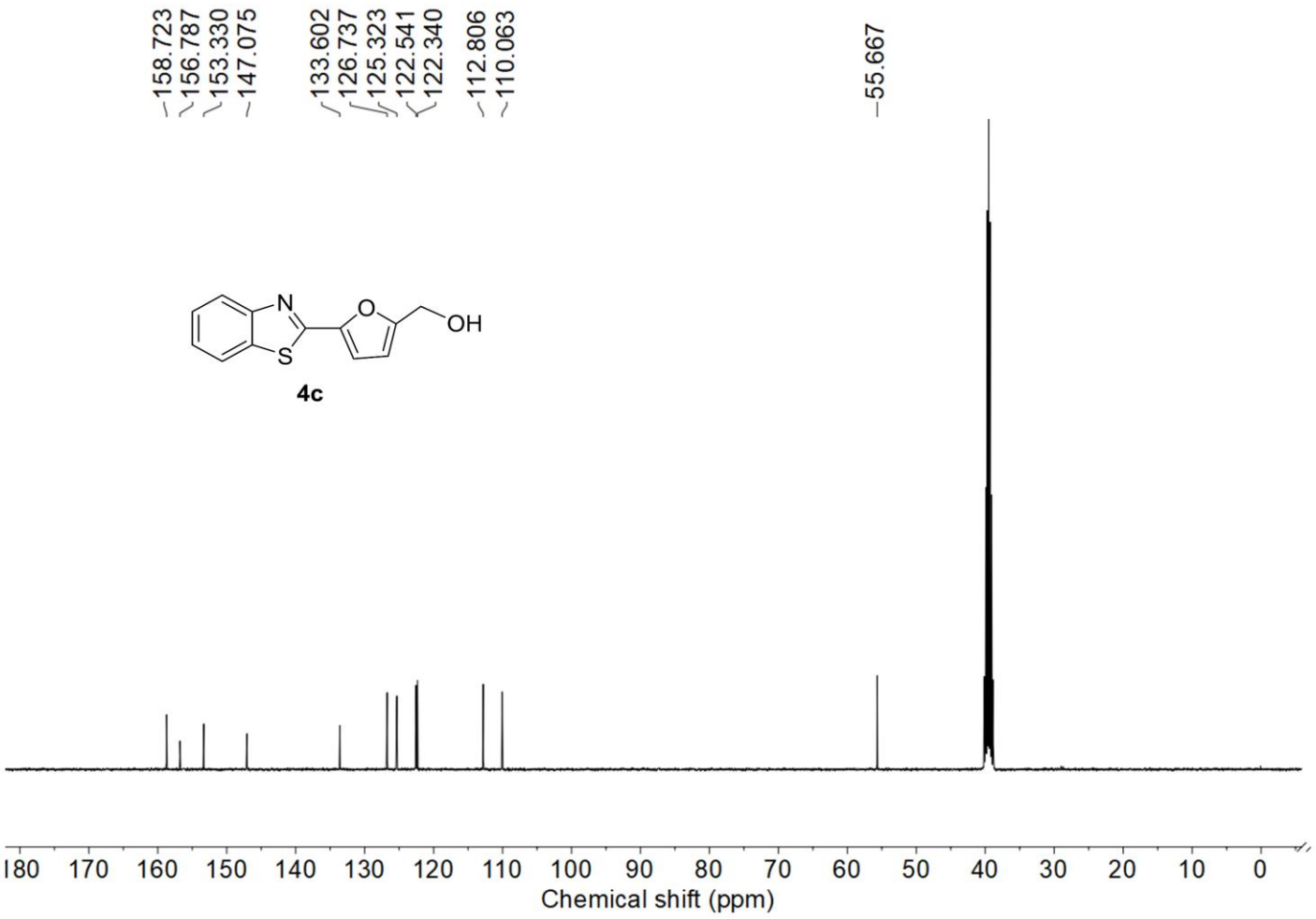

Figure S19. The ^{13}C-NMR spectrum of **4c.**

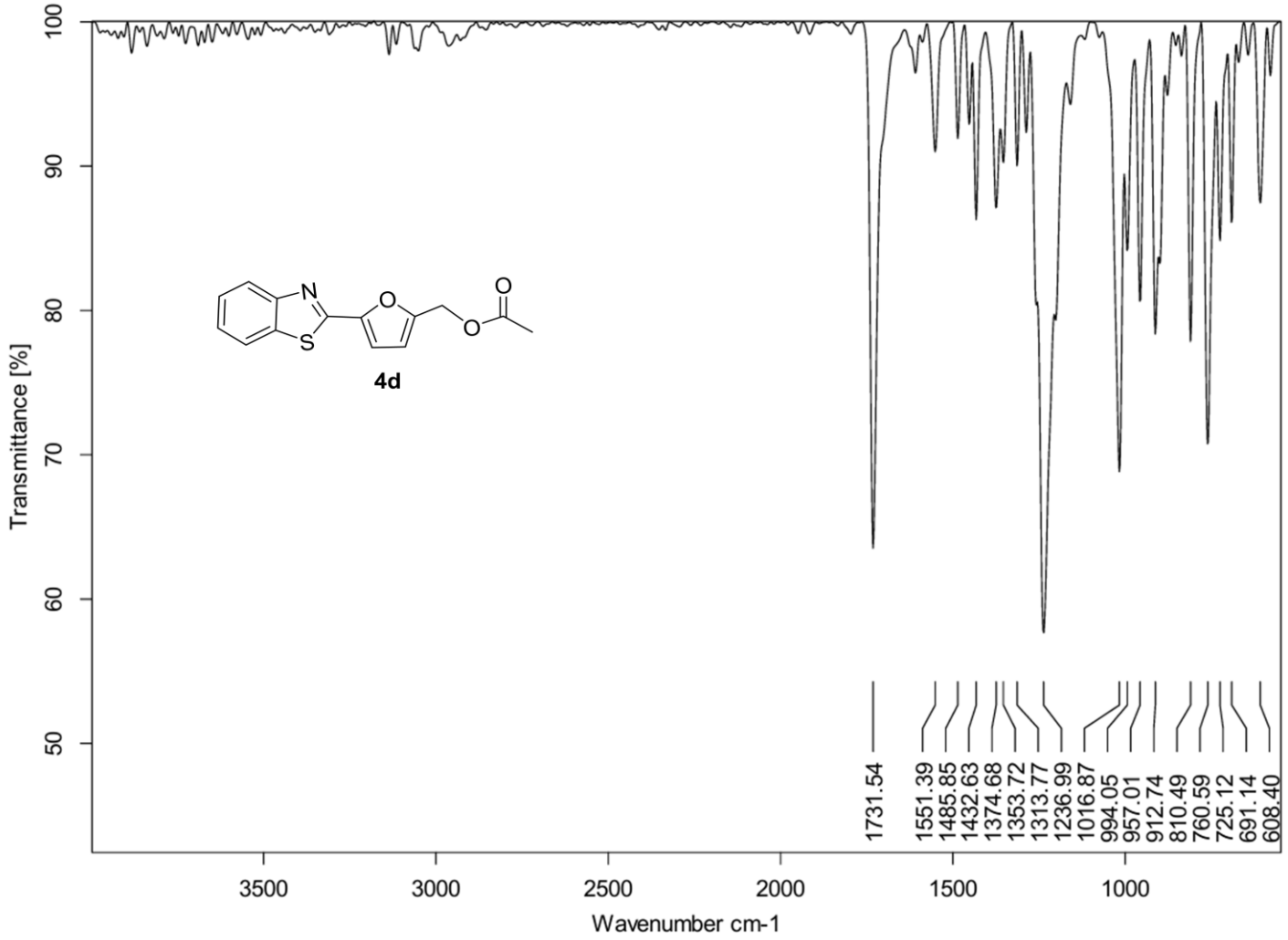

Figure S20. The FTIR spectrum of **4d**.

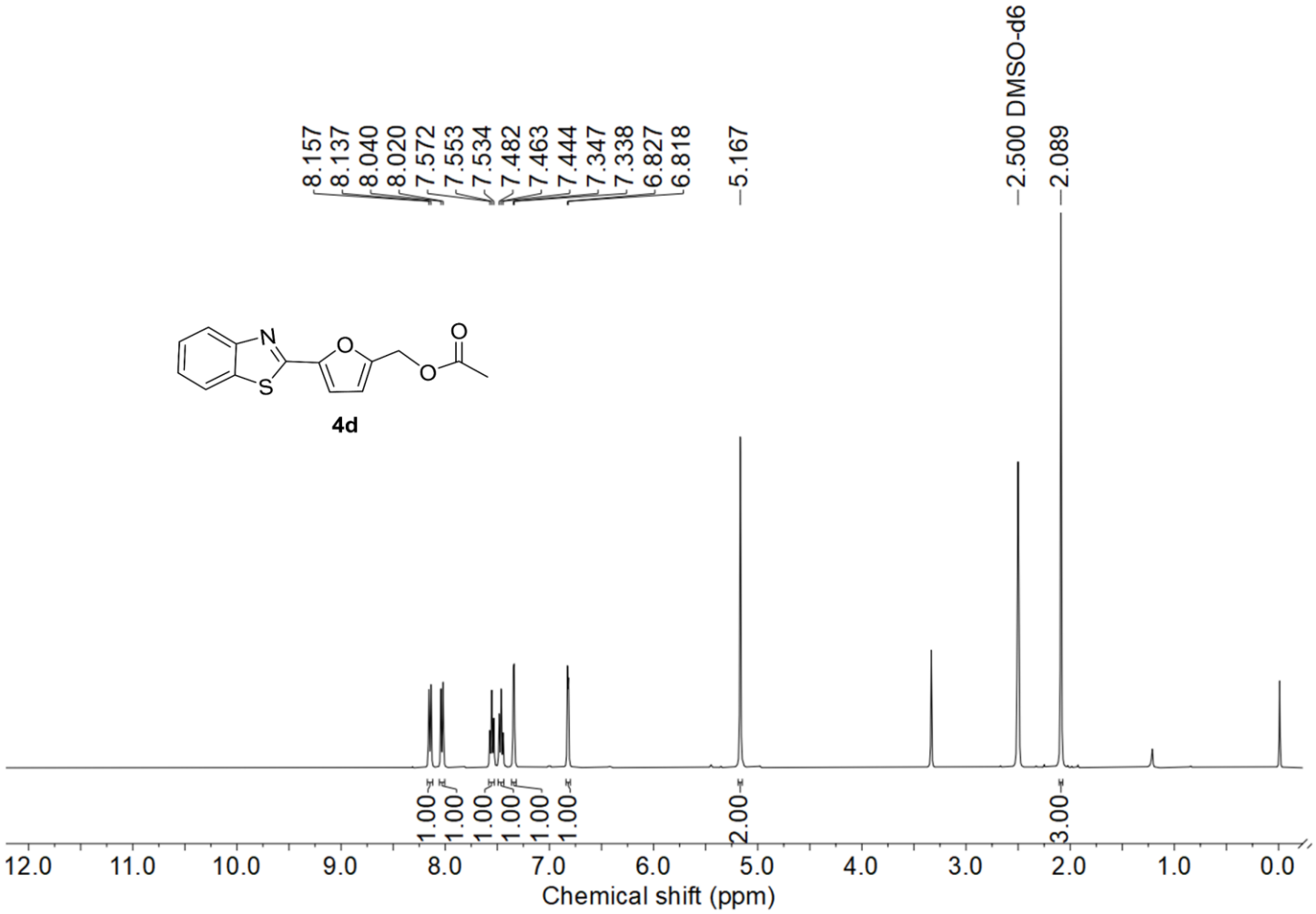

Figure S21. The ^{1}H-NMR spectrum of **4d**.

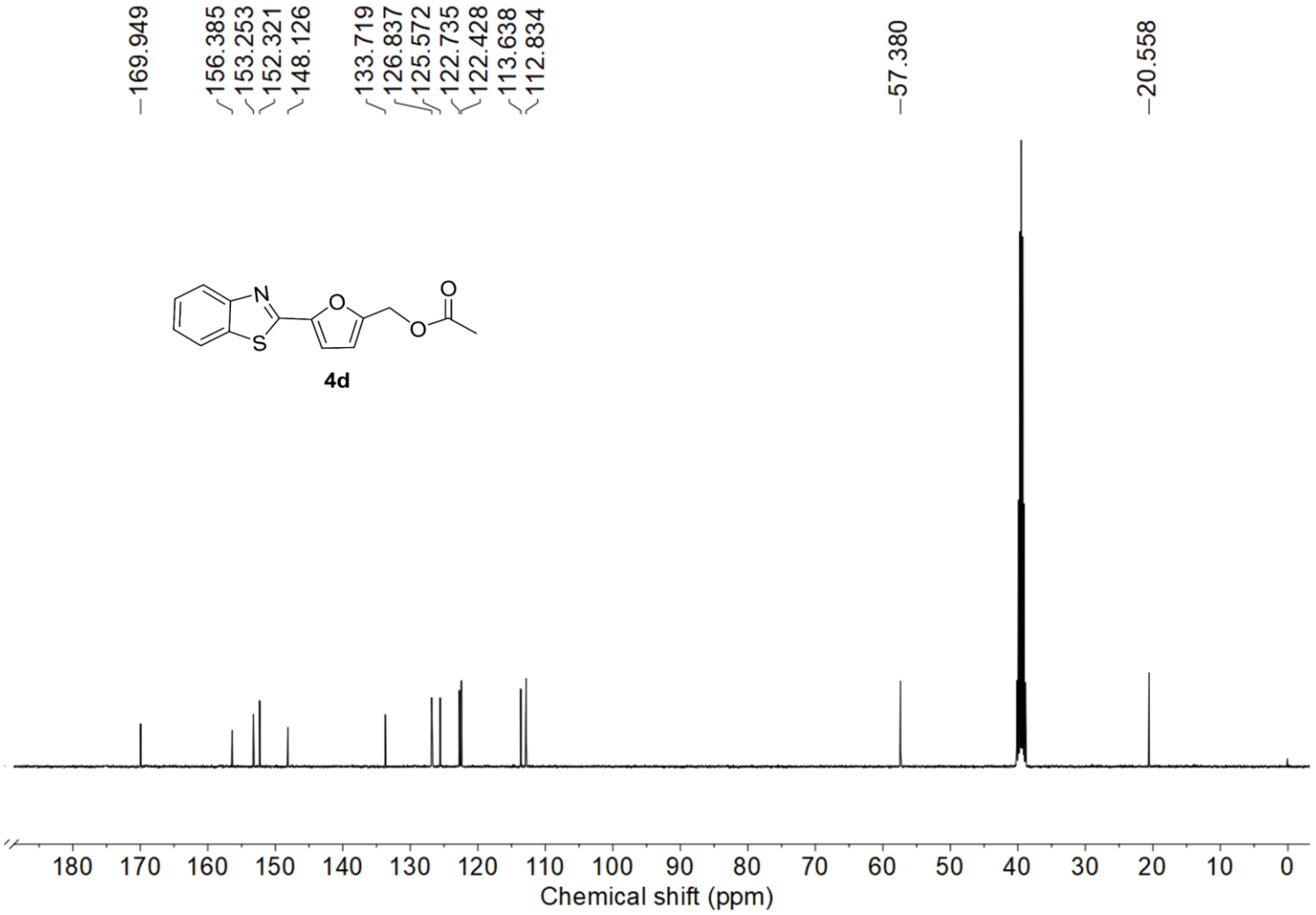

Figure S22. The ^{13}C-NMR spectrum of **4d**.

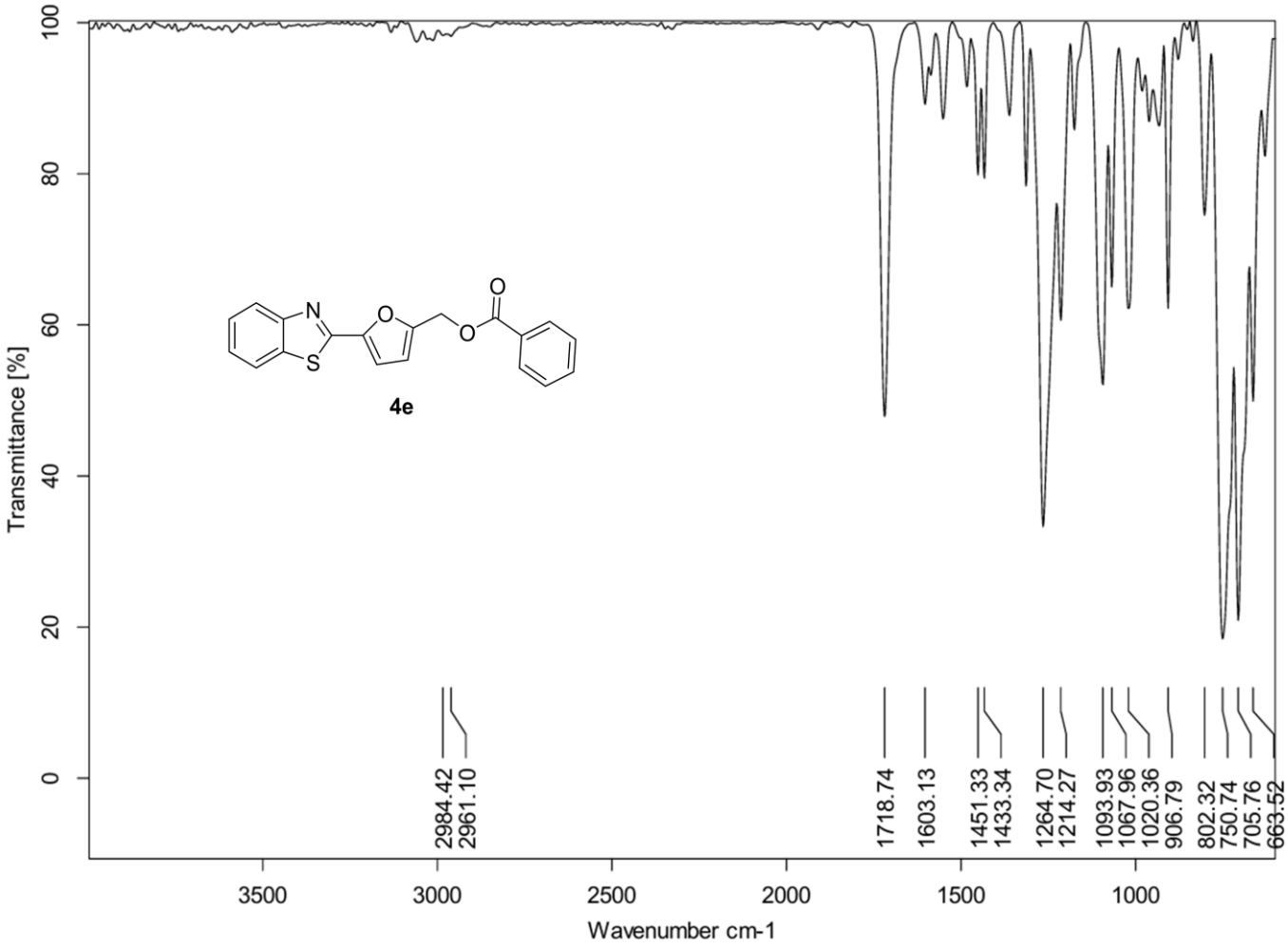

Figure S23. The FTIR spectrum **4e**.

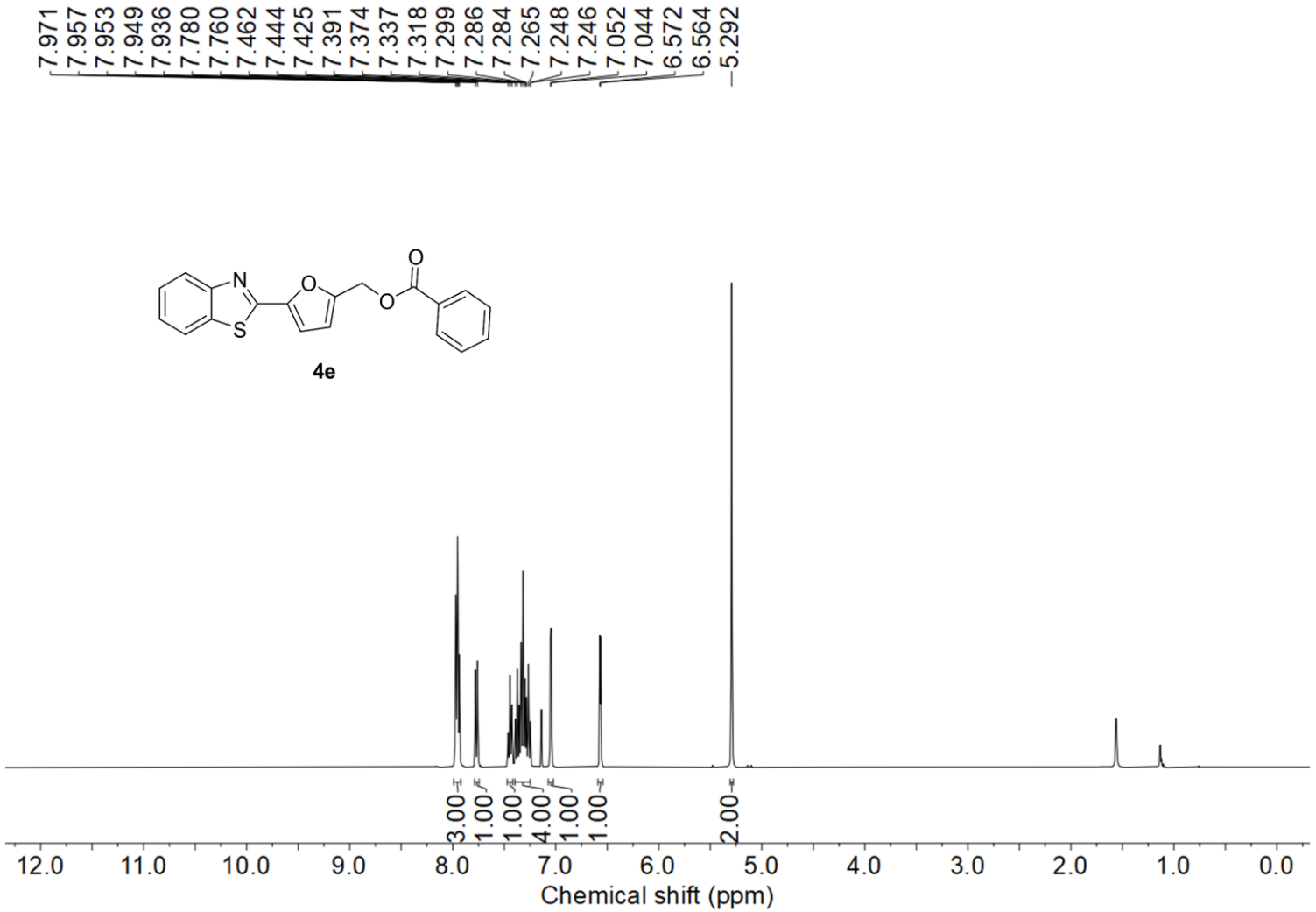

Figure S24. The ^{1}H-NMR spectrum **4e**.

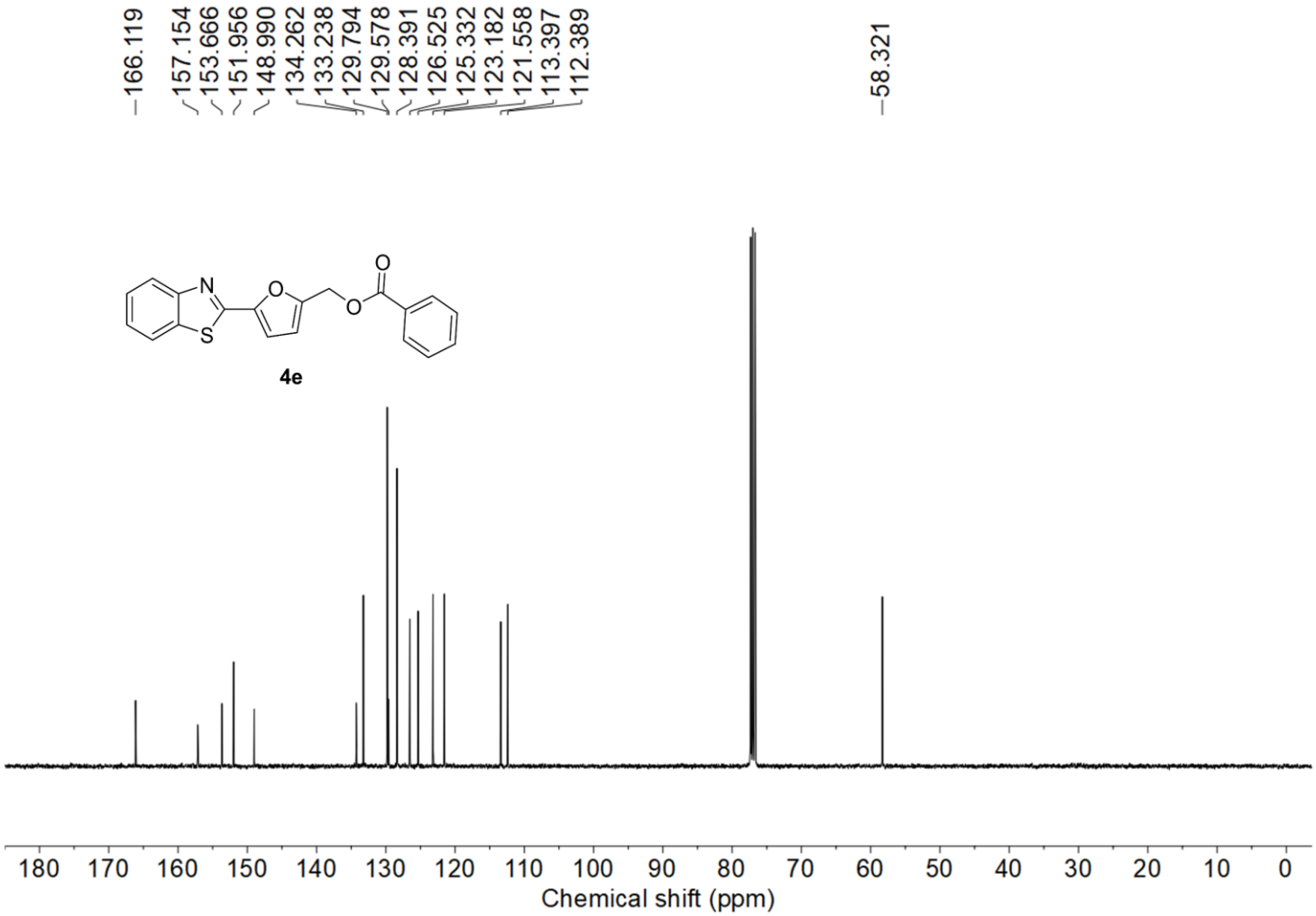

Figure S25. The ^{13}C-NMR spectrum **4e**.

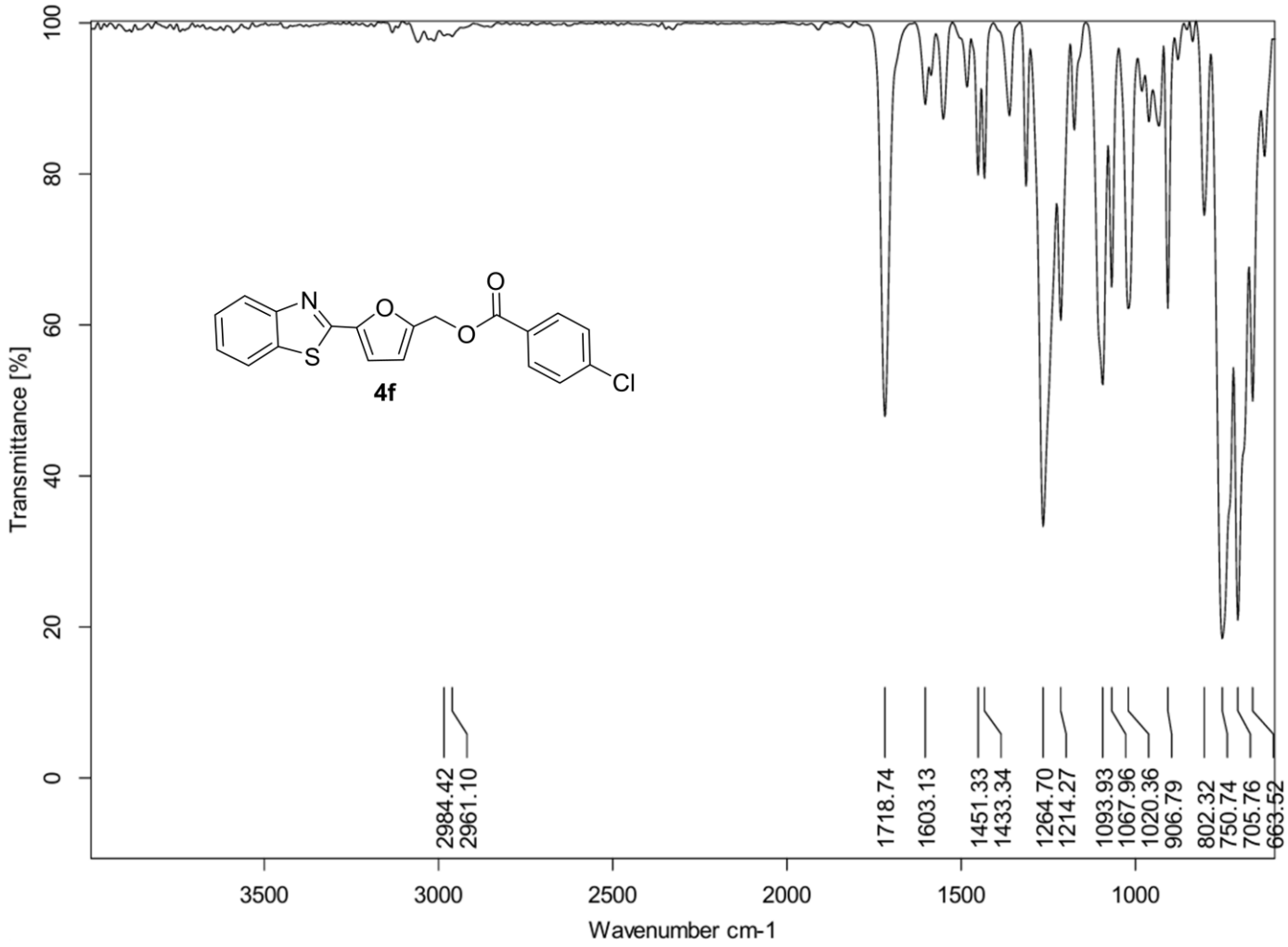

Figure S26. The FTIR spectrum of **4f.**

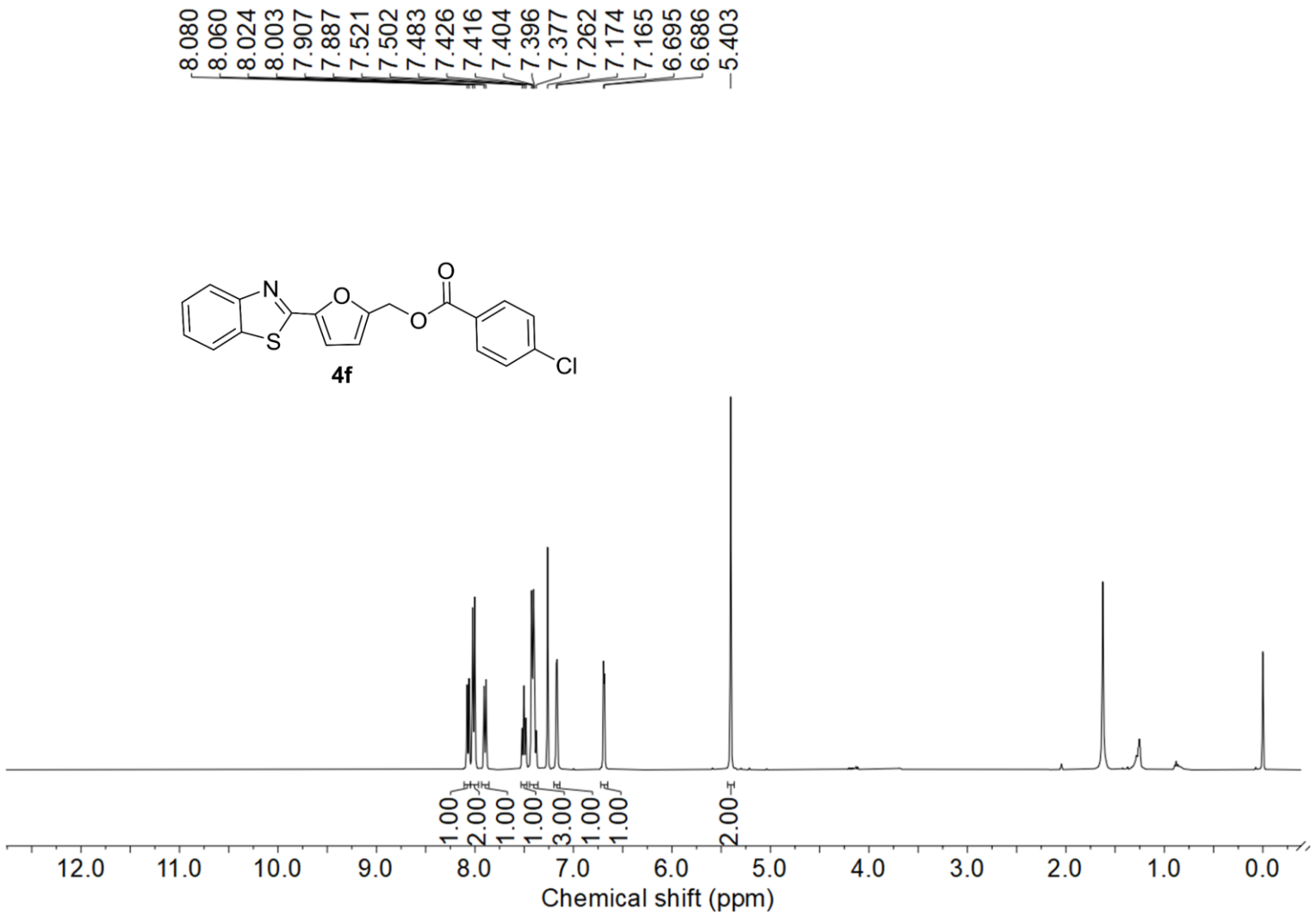

Figure S27. The ^{1}H-NMR spectrum of **4f**.

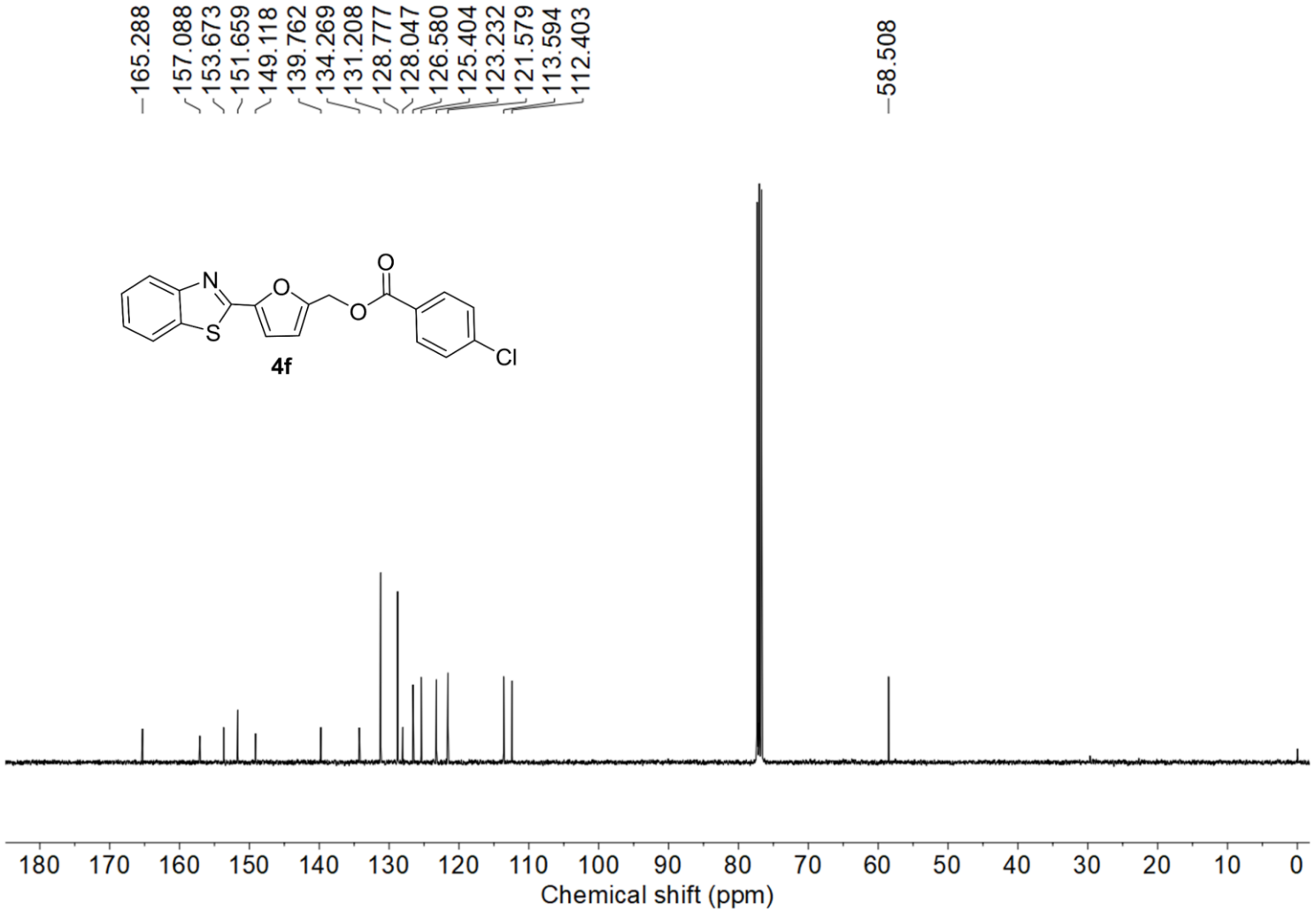

Figure S28. The ^{13}C-NMR spectrum of 4**f**.

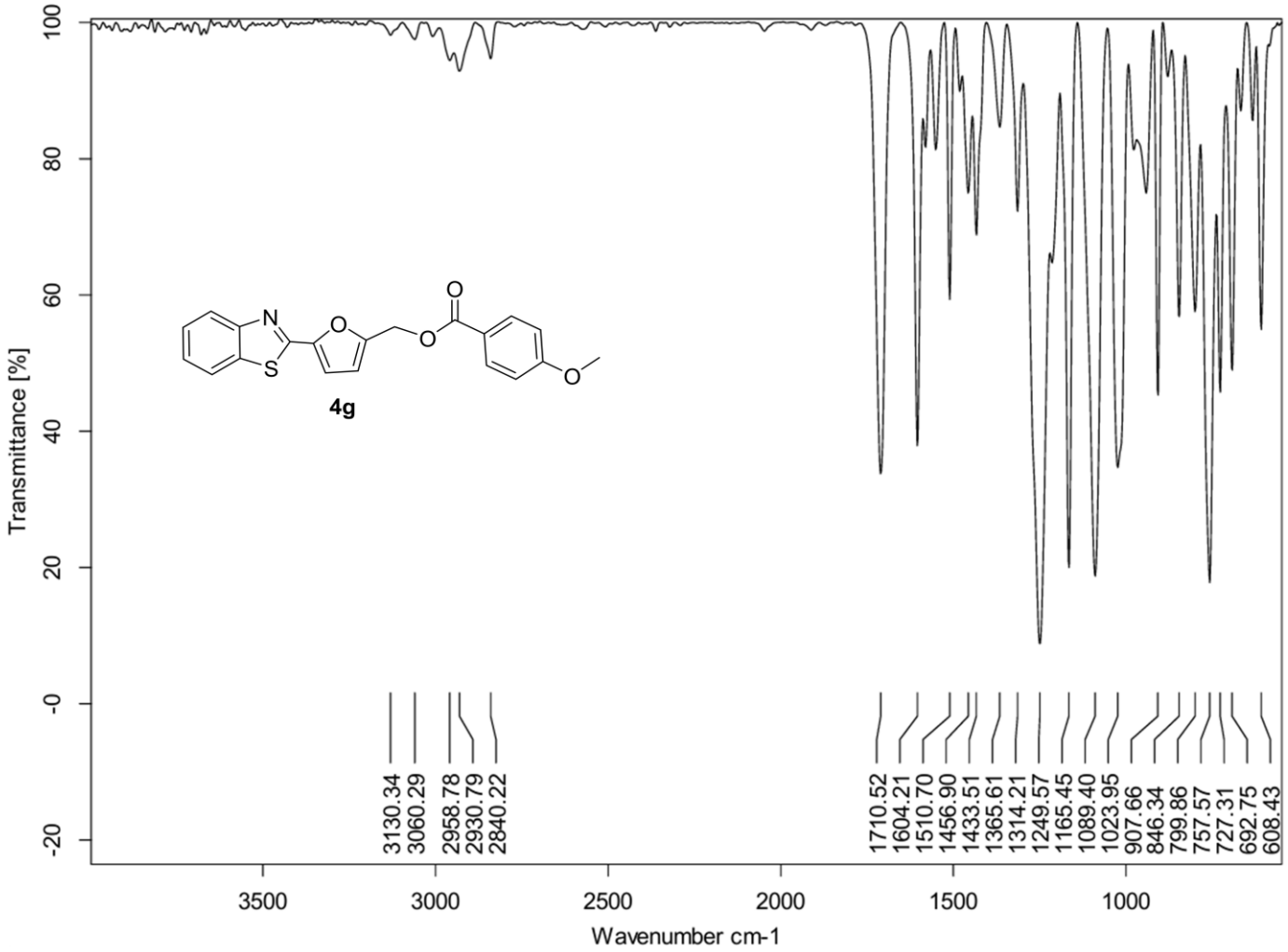

Figure S29. The FTIR spectrum of **4g**.

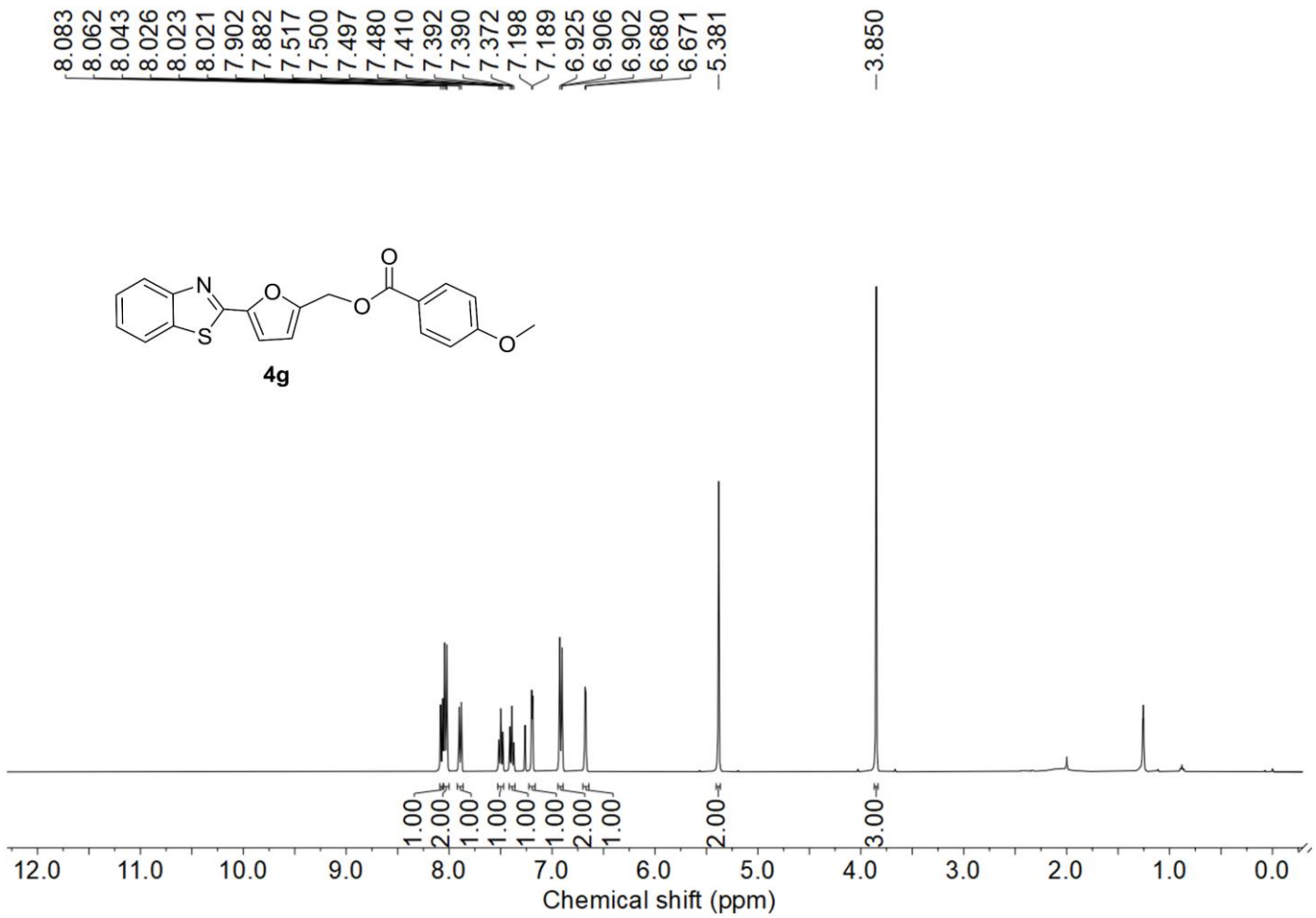

Figure S30. The ^{1}H-NMR spectrum of **4g**.

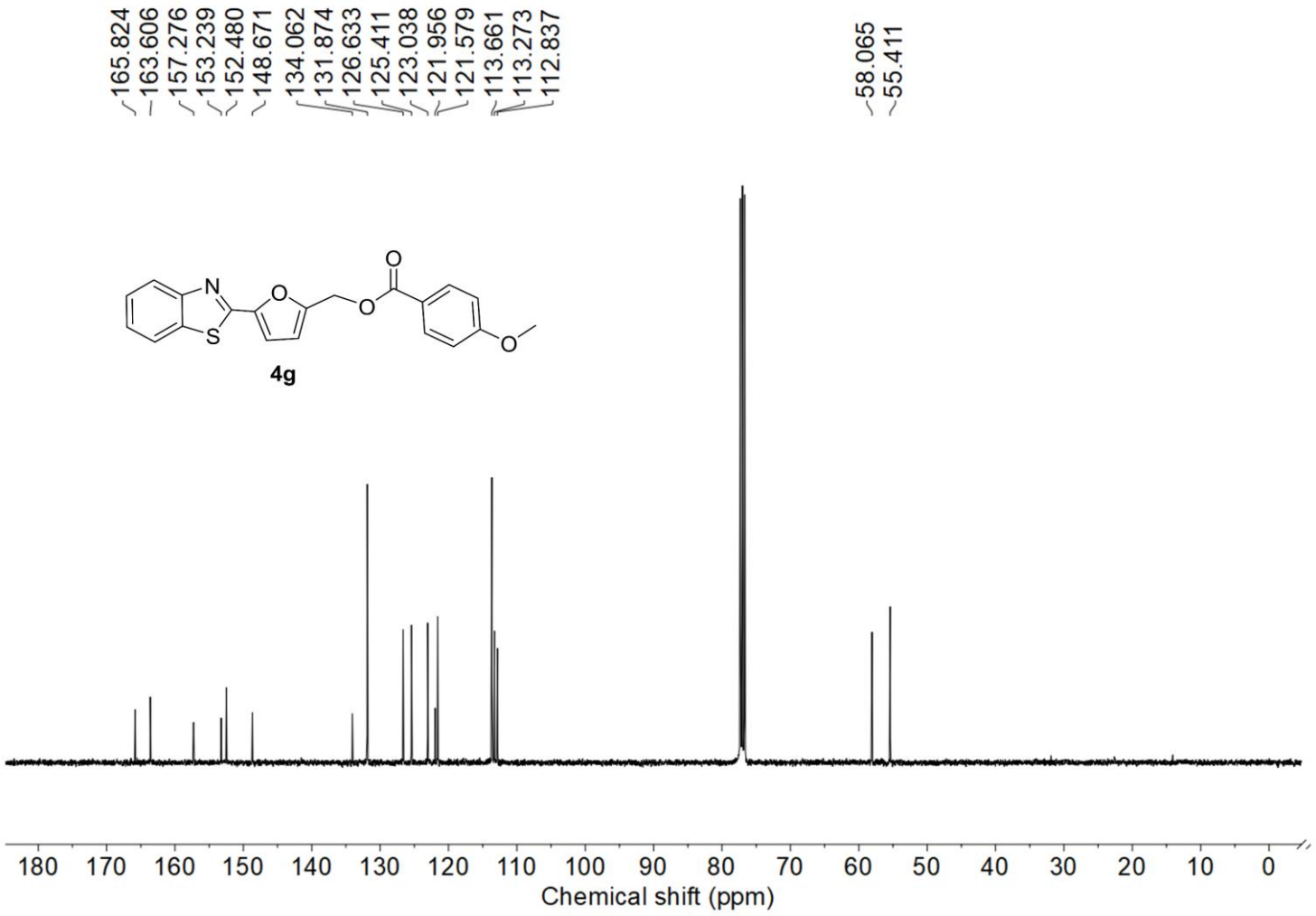

Figure S31. The ^{13}C-NMR spectrum of **4g**.

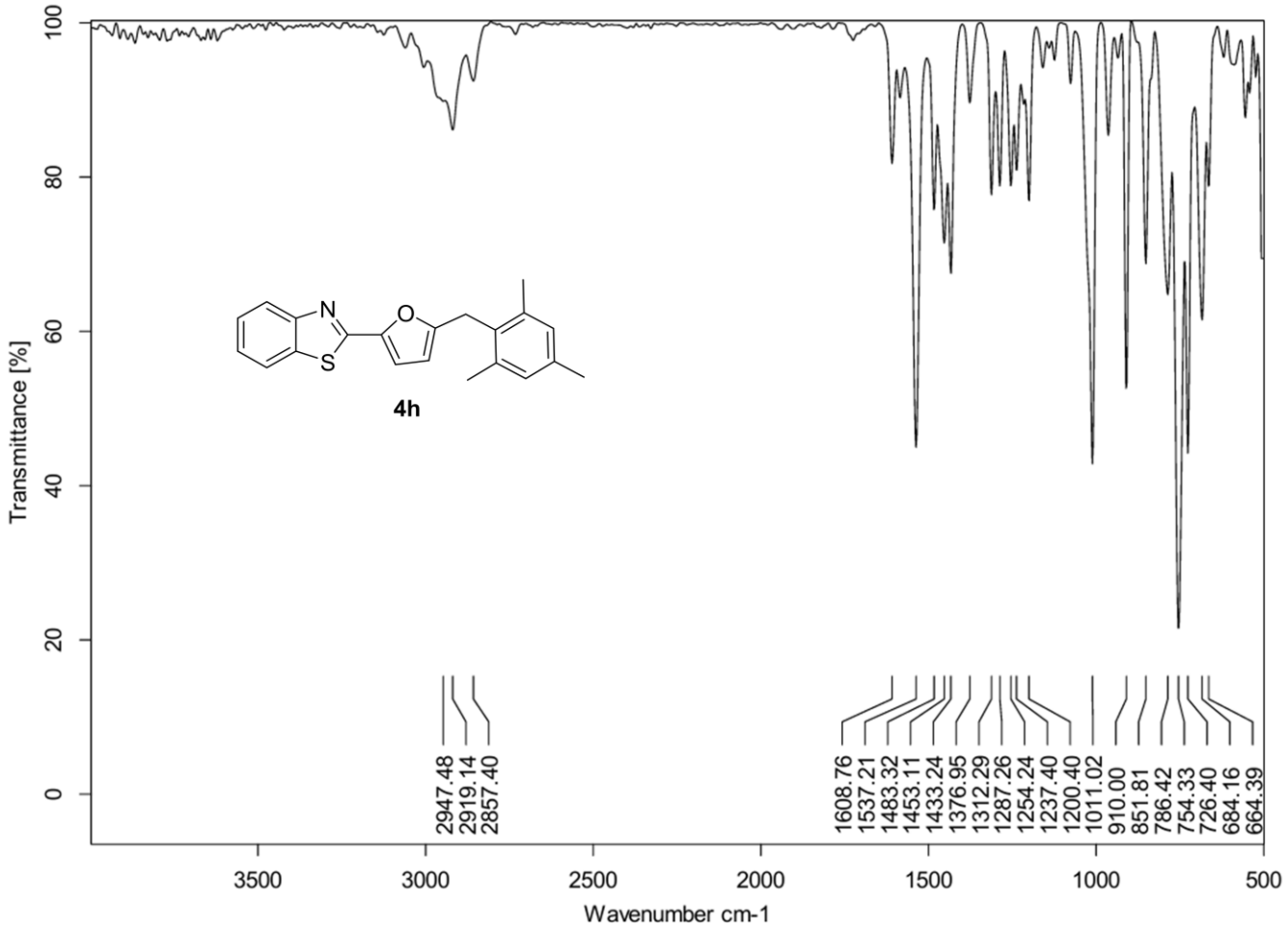

Figure S32. The FTIR spectrum of **4h**.

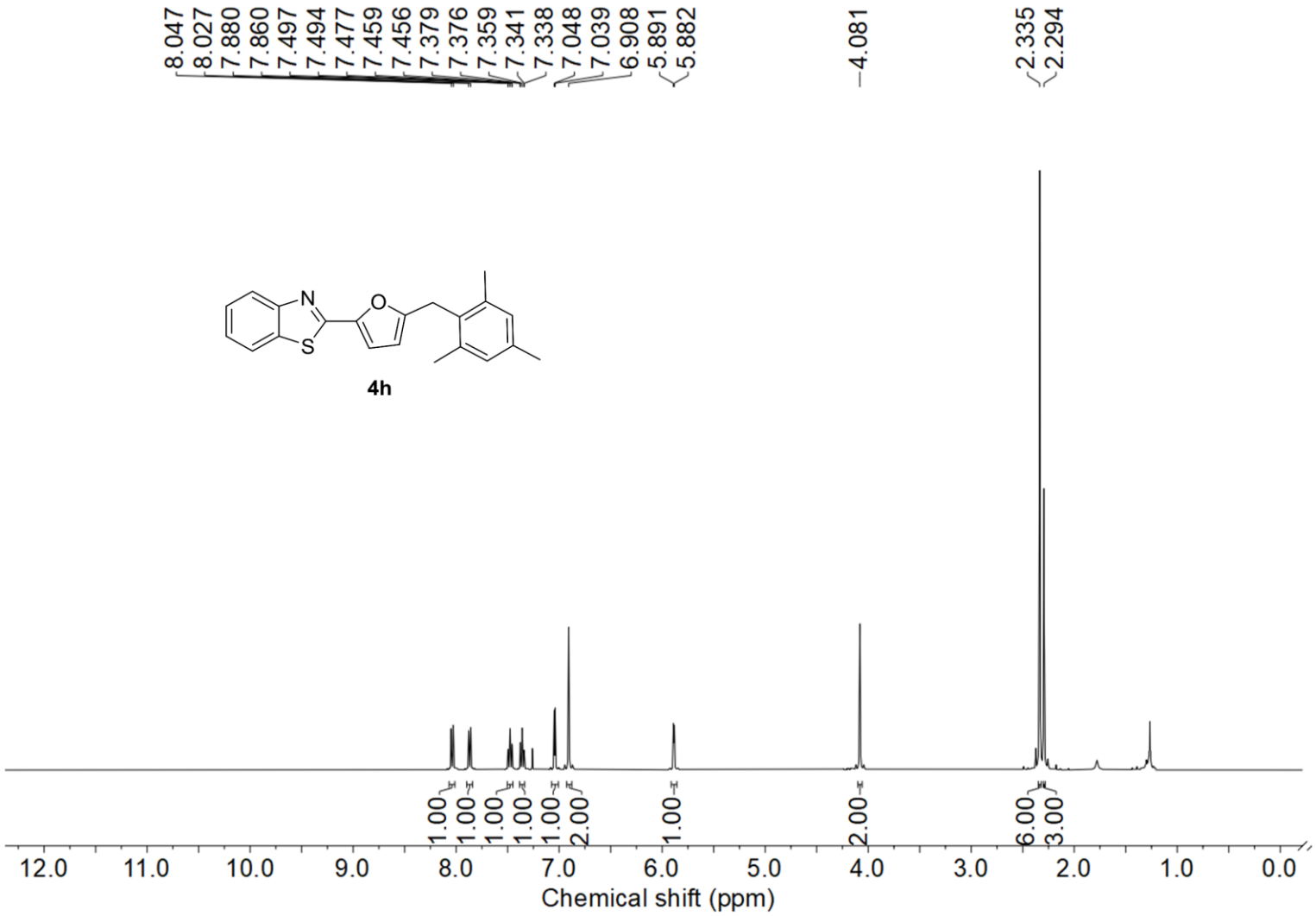

Figure S33. The ^{1}H-NMR spectrum of **4h**.

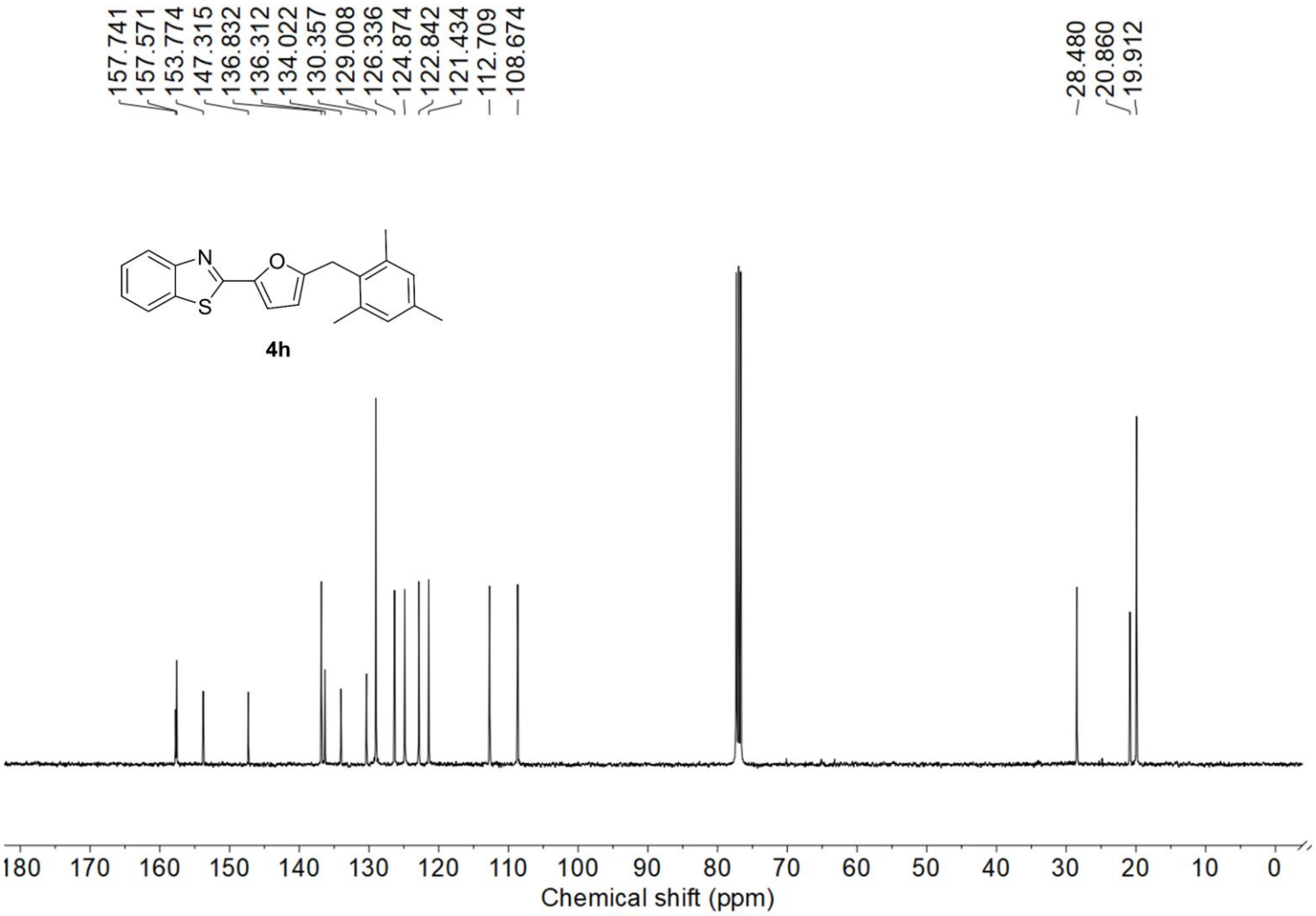

Figure S34. The ^{13}C-NMR spectrum of **4h.**

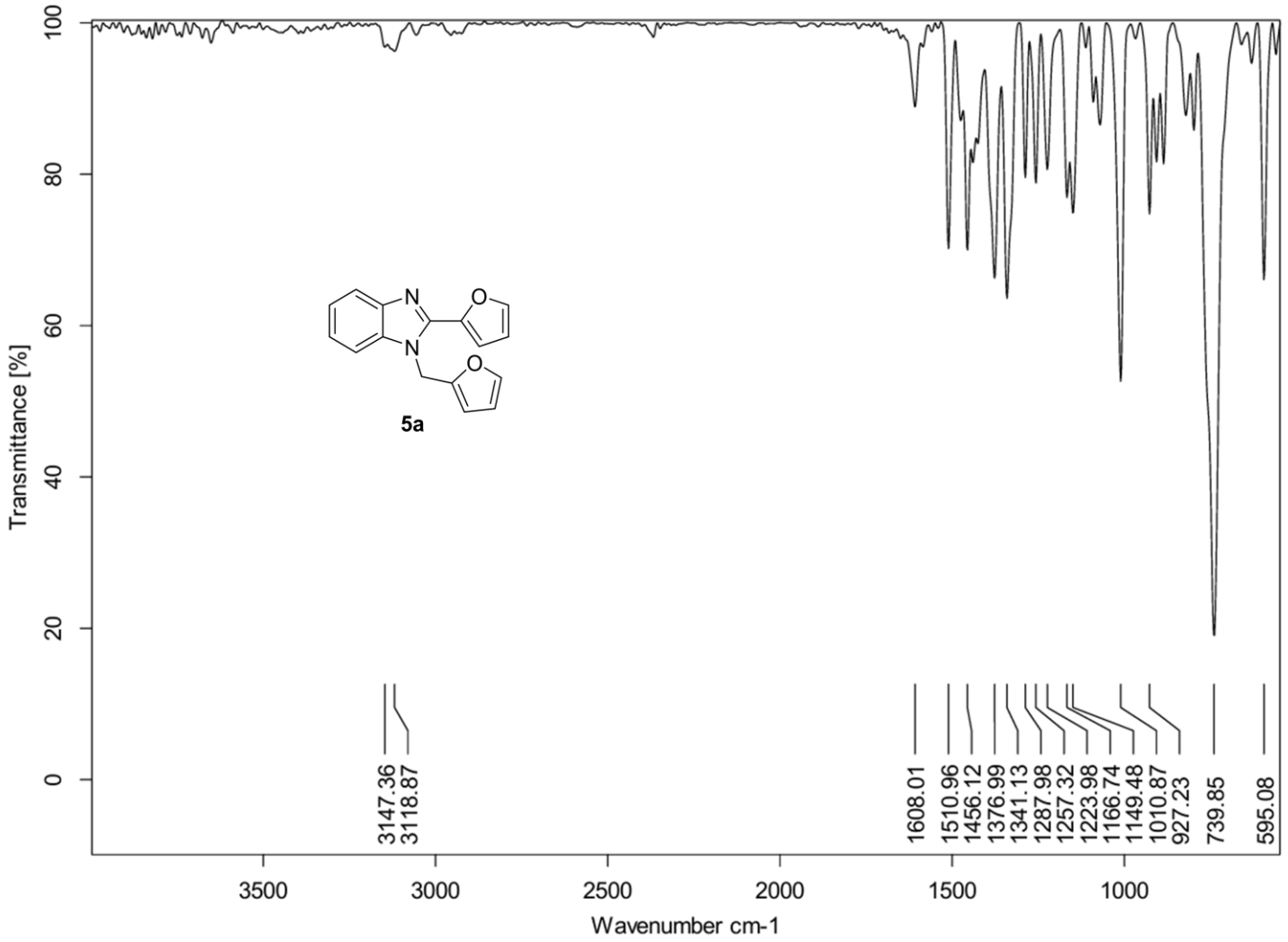

Figure S35. The FTIR spectrum of **5a**.

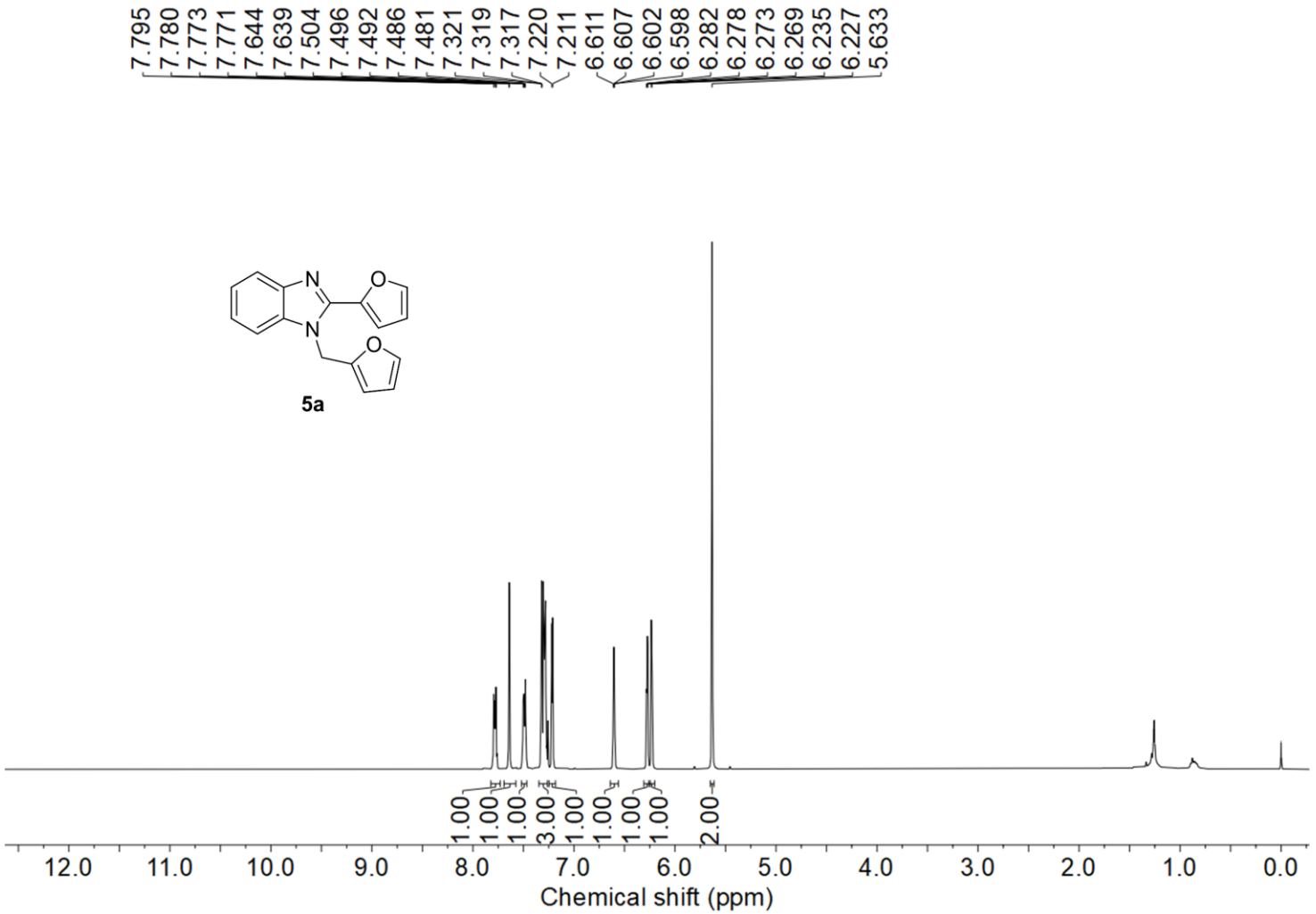

Figure S36. The ^{1}H-NMR spectrum of **5a**.

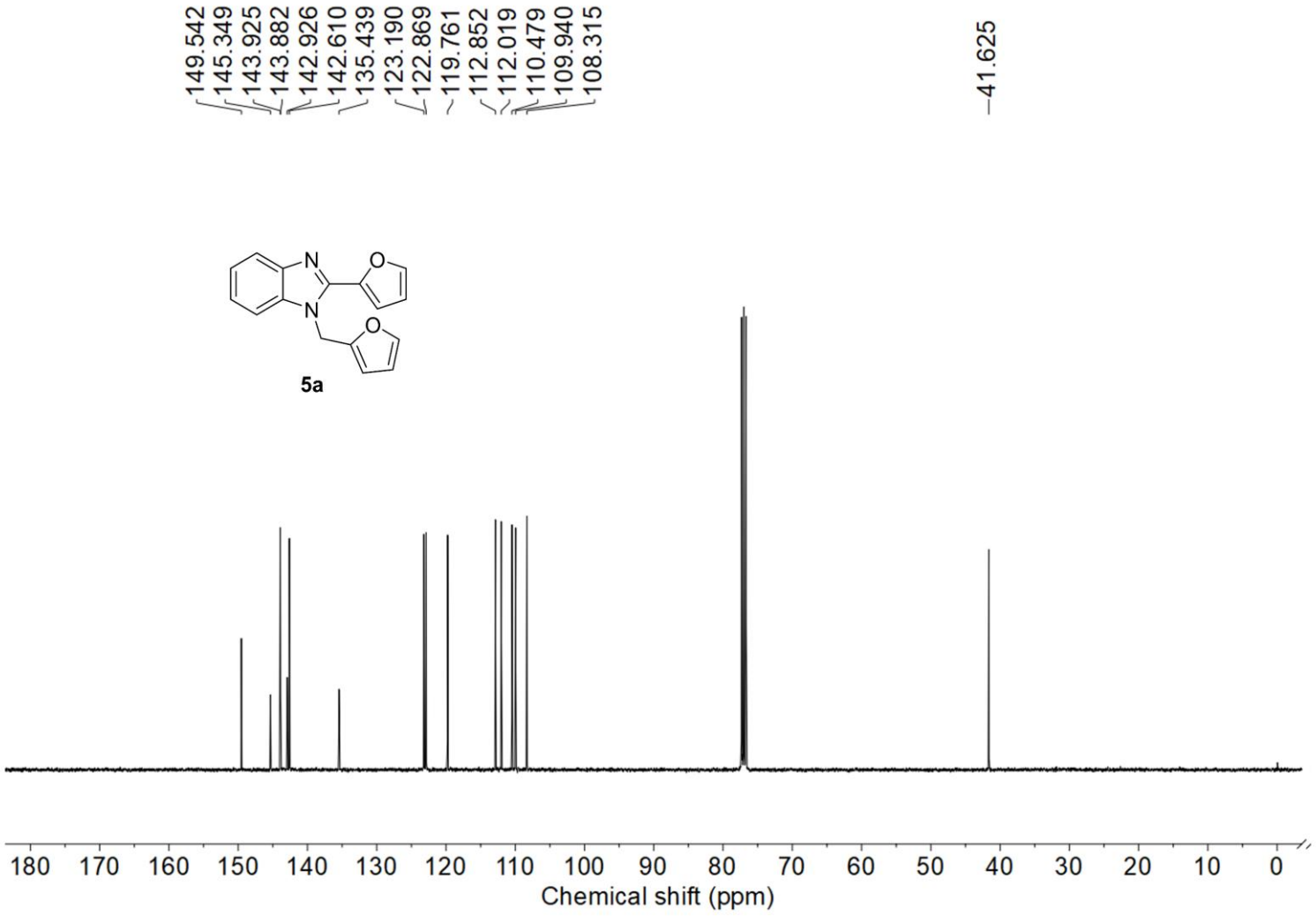

Figure S37. The ^{13}C-NMR spectrum of **5a**.

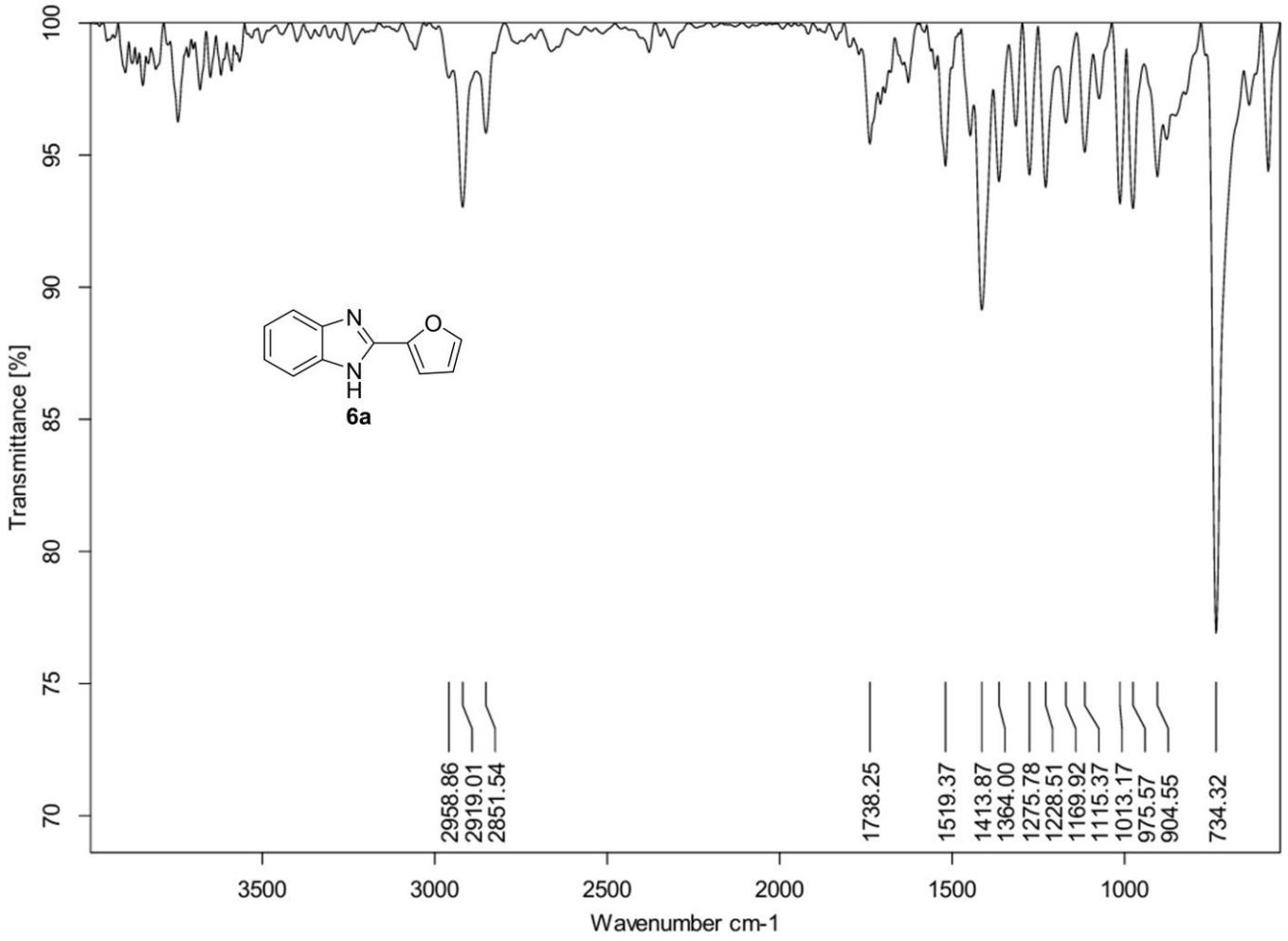

Figure S38. The FTIR spectrum of **6a**.

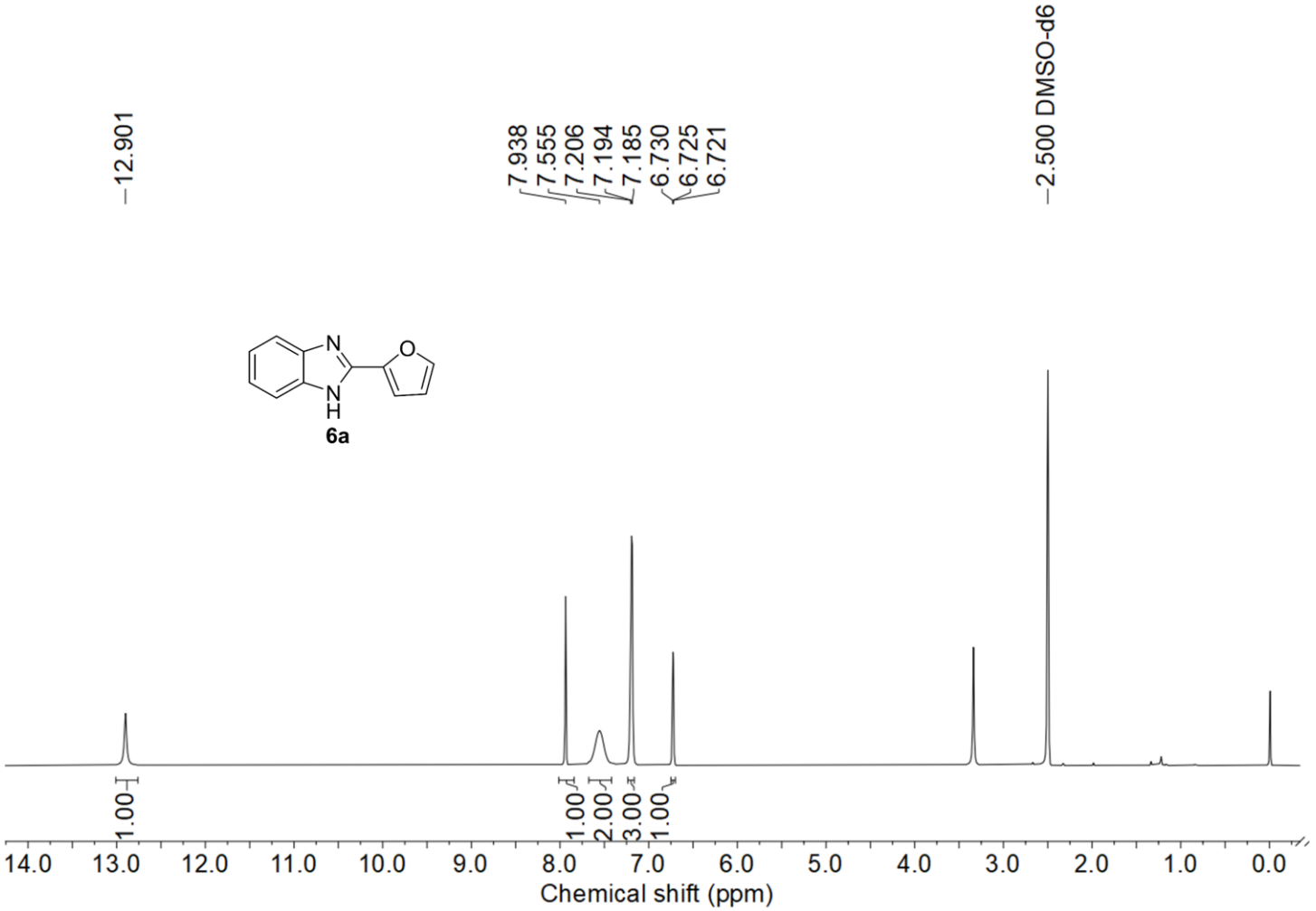

Figure S39. The ^{1}H-NMR spectrum of **6a**.

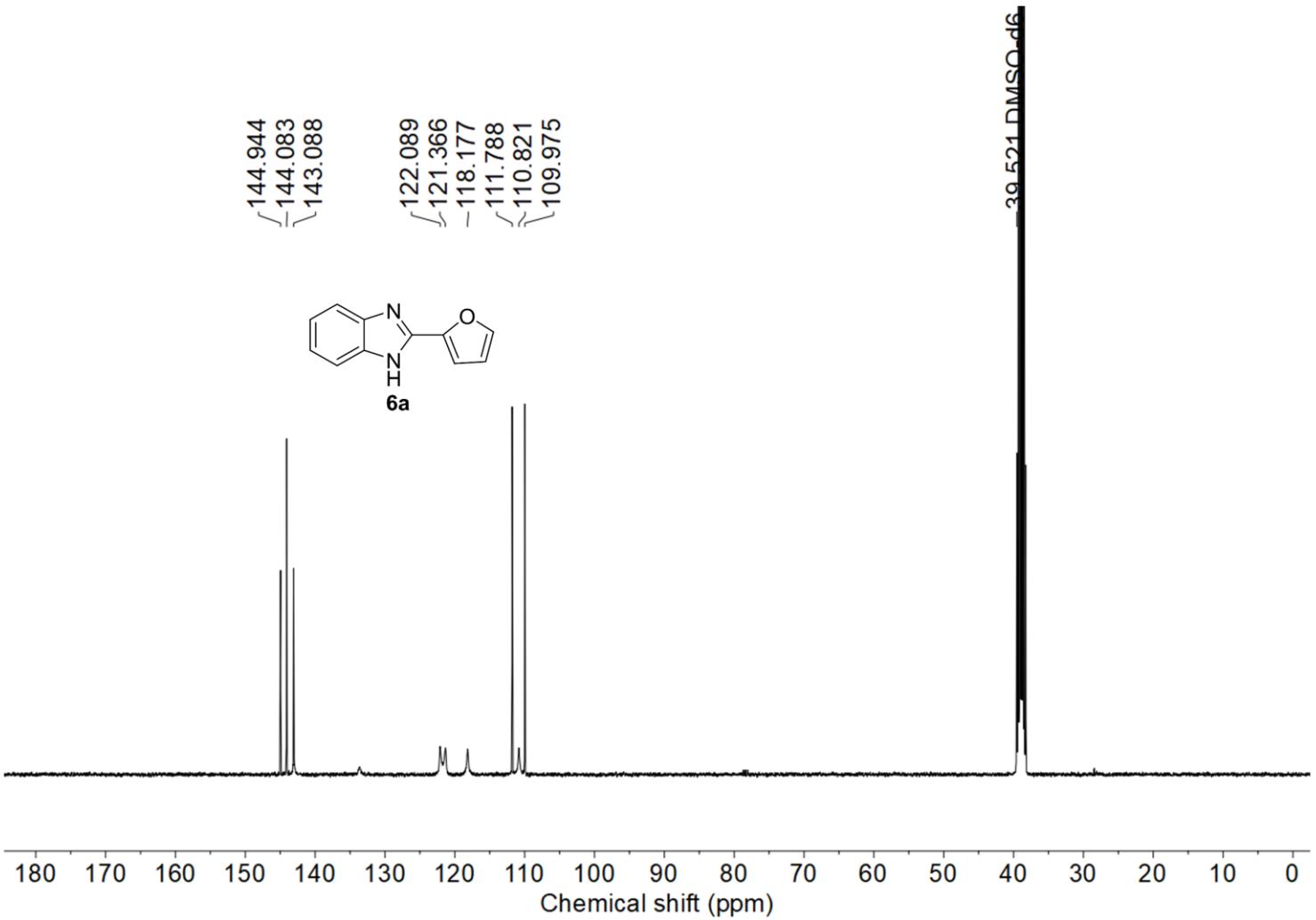

Figure S40. The ^{13}C-NMR spectrum of **6a**.

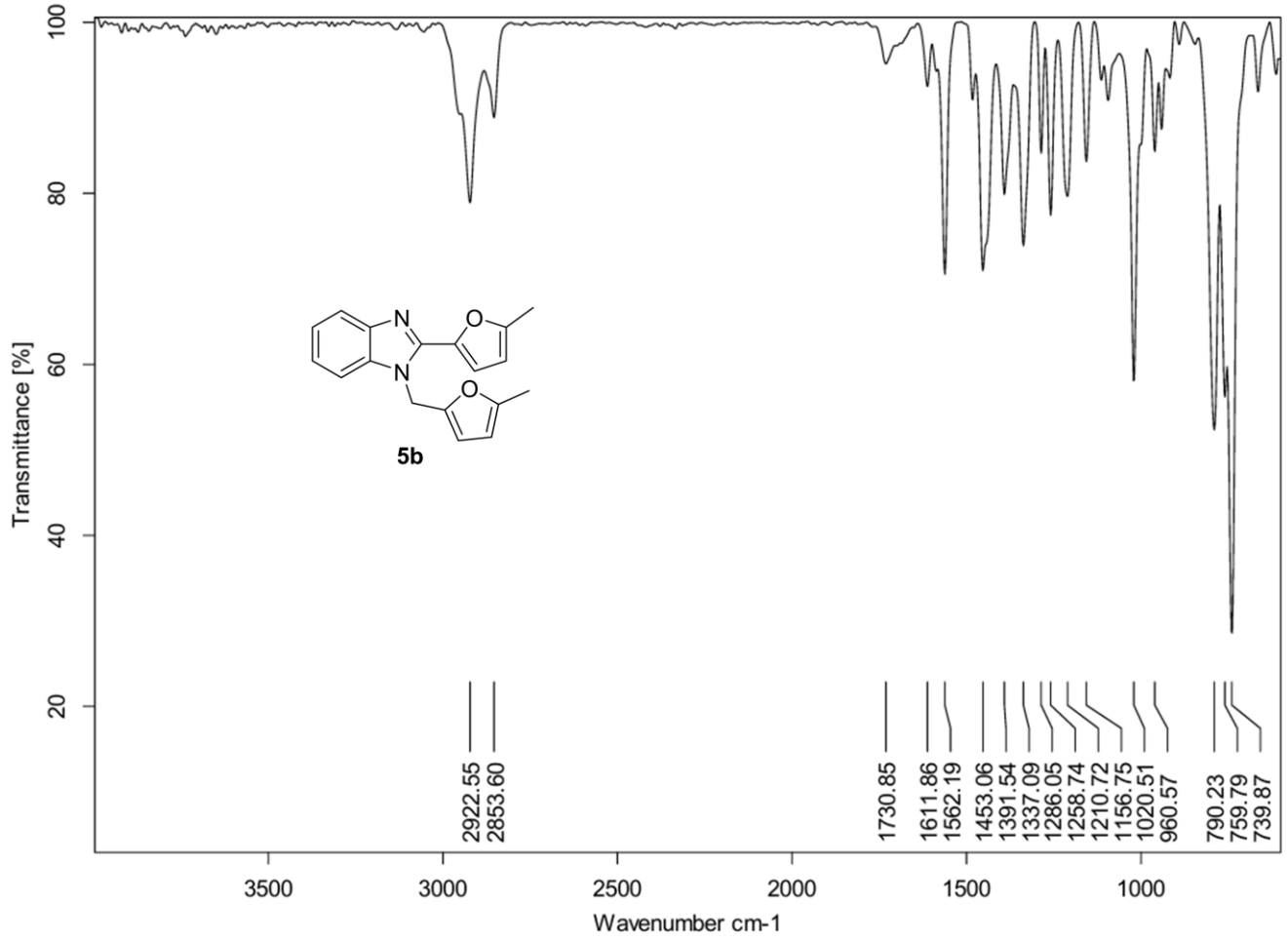

Figure S41. The FTIR spectrum of **5b**.

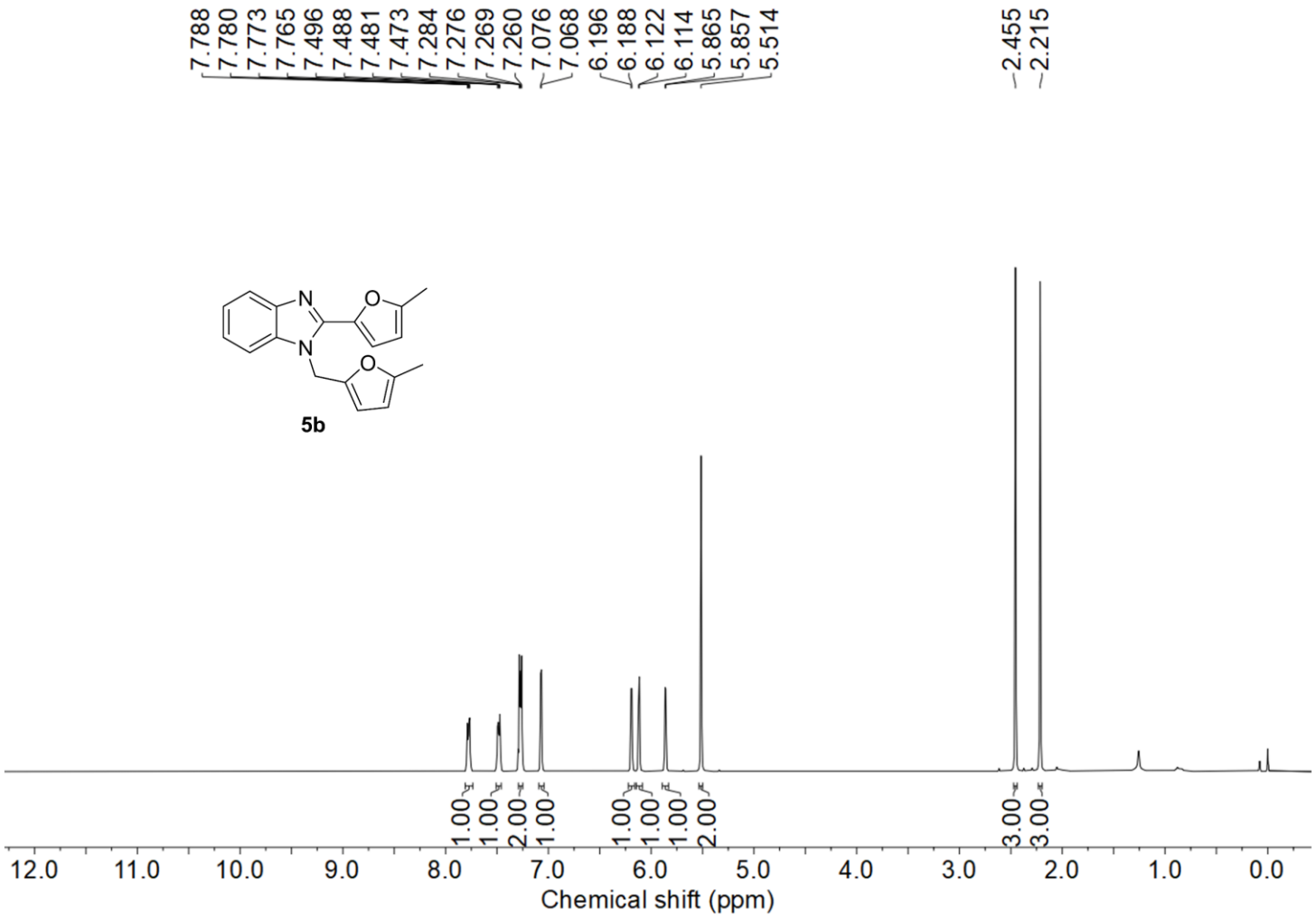

Figure S42. The ^{1}H-NMR spectrum of **5b**.

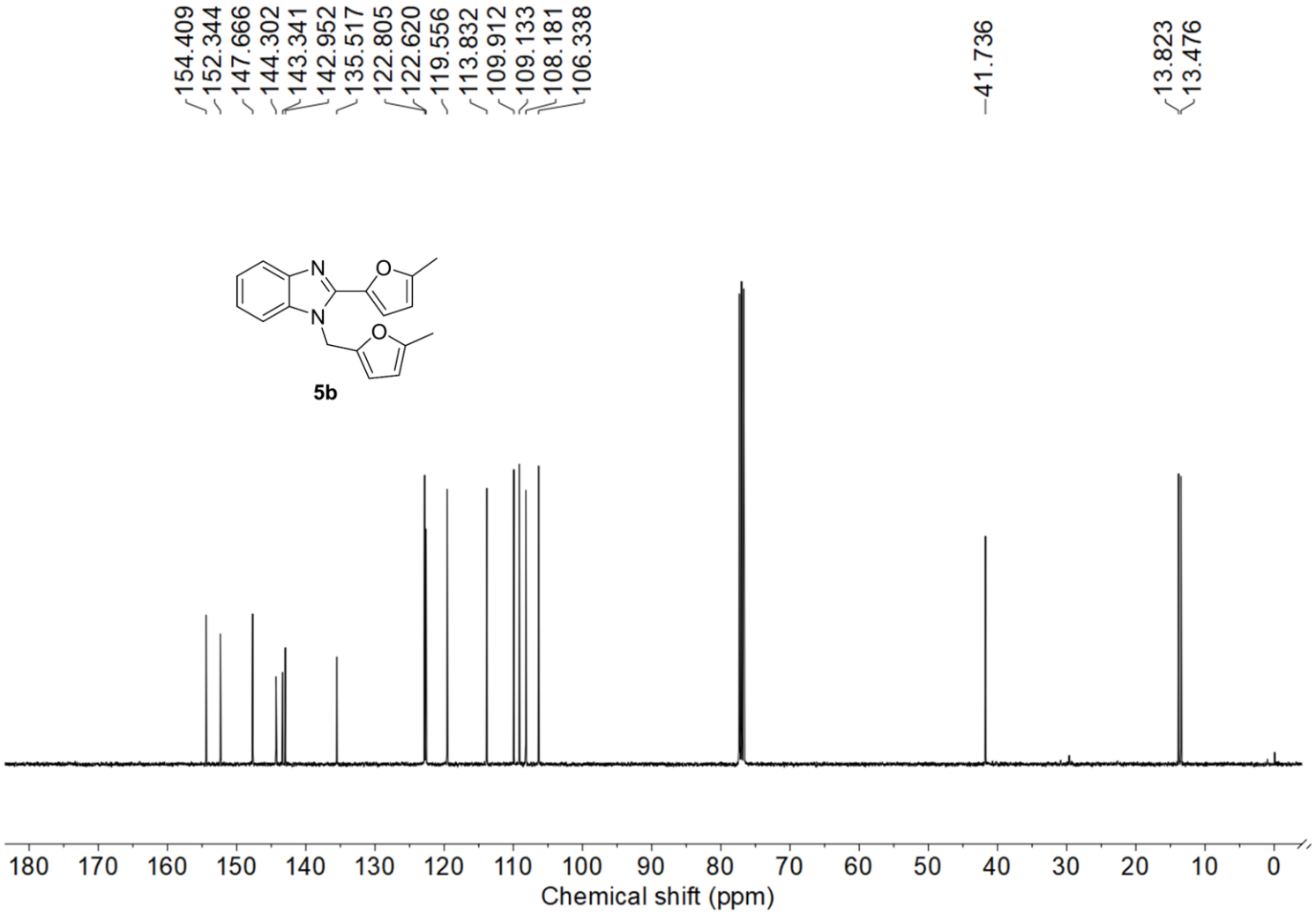

Figure S43. The ^{13}C-NMR spectrum of **5b**.

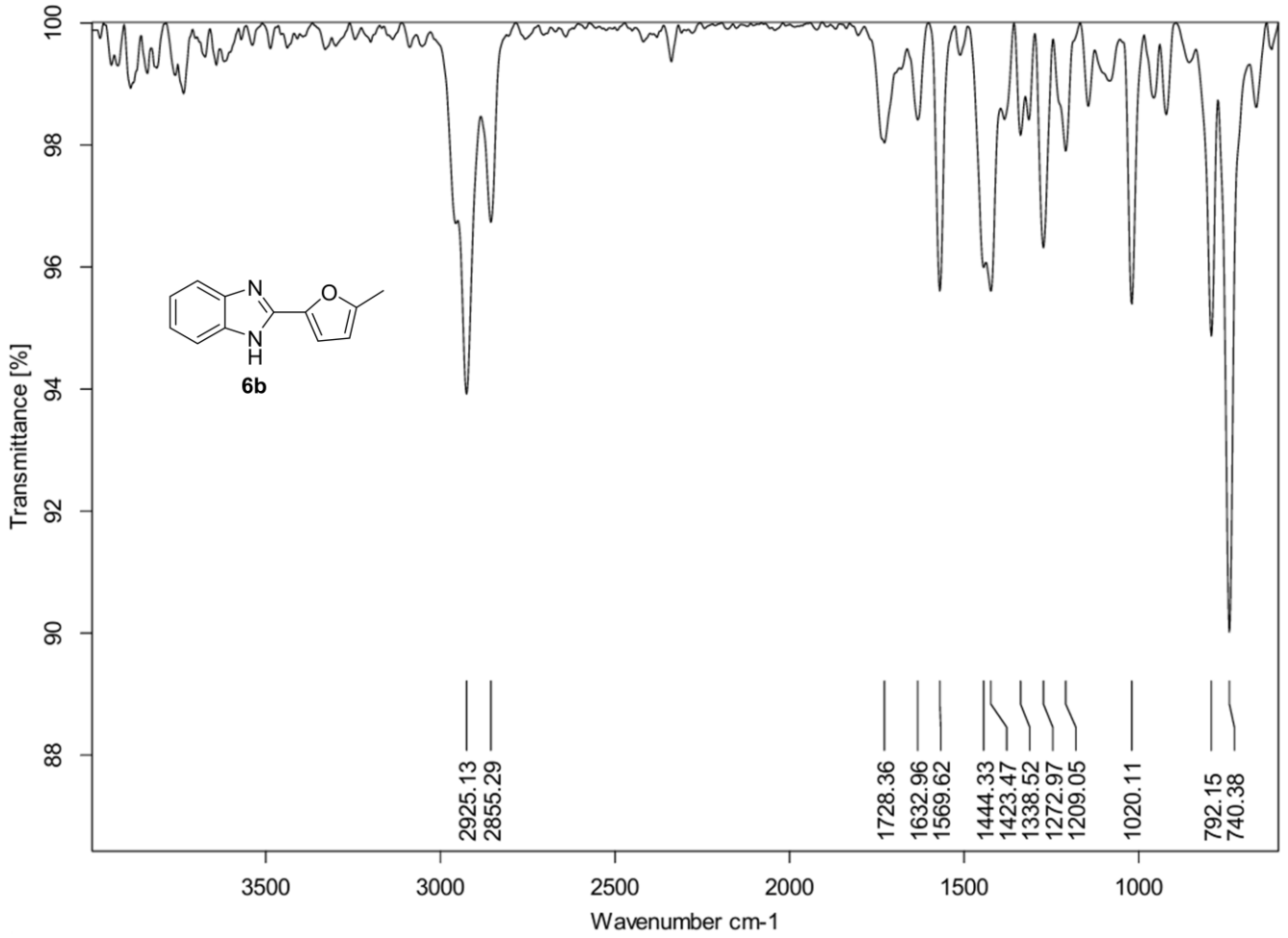

Figure S44. The FTIR spectrum of **6b**.

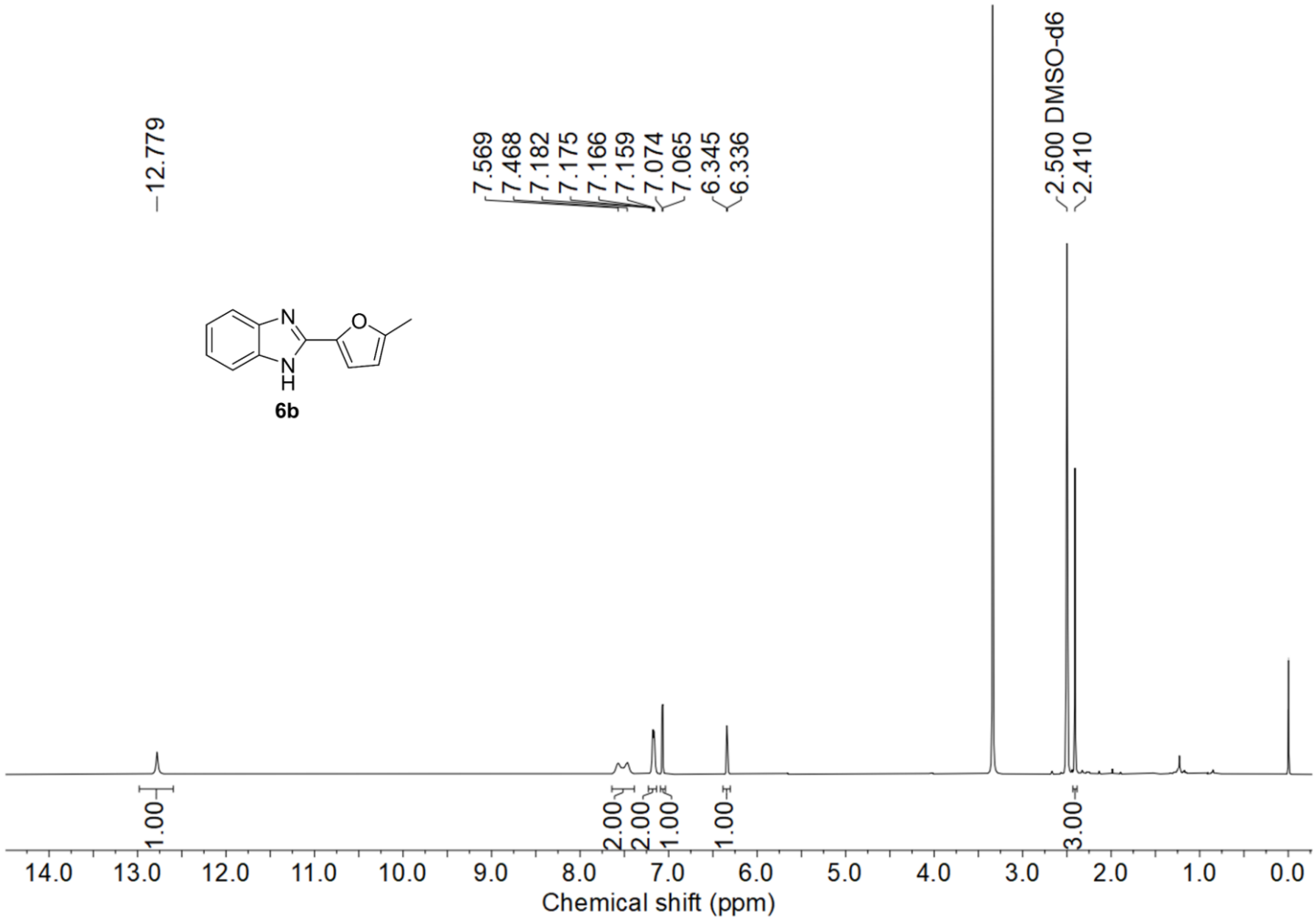

Figure S45. The ^{1}H-NMR spectrum of **6b**.

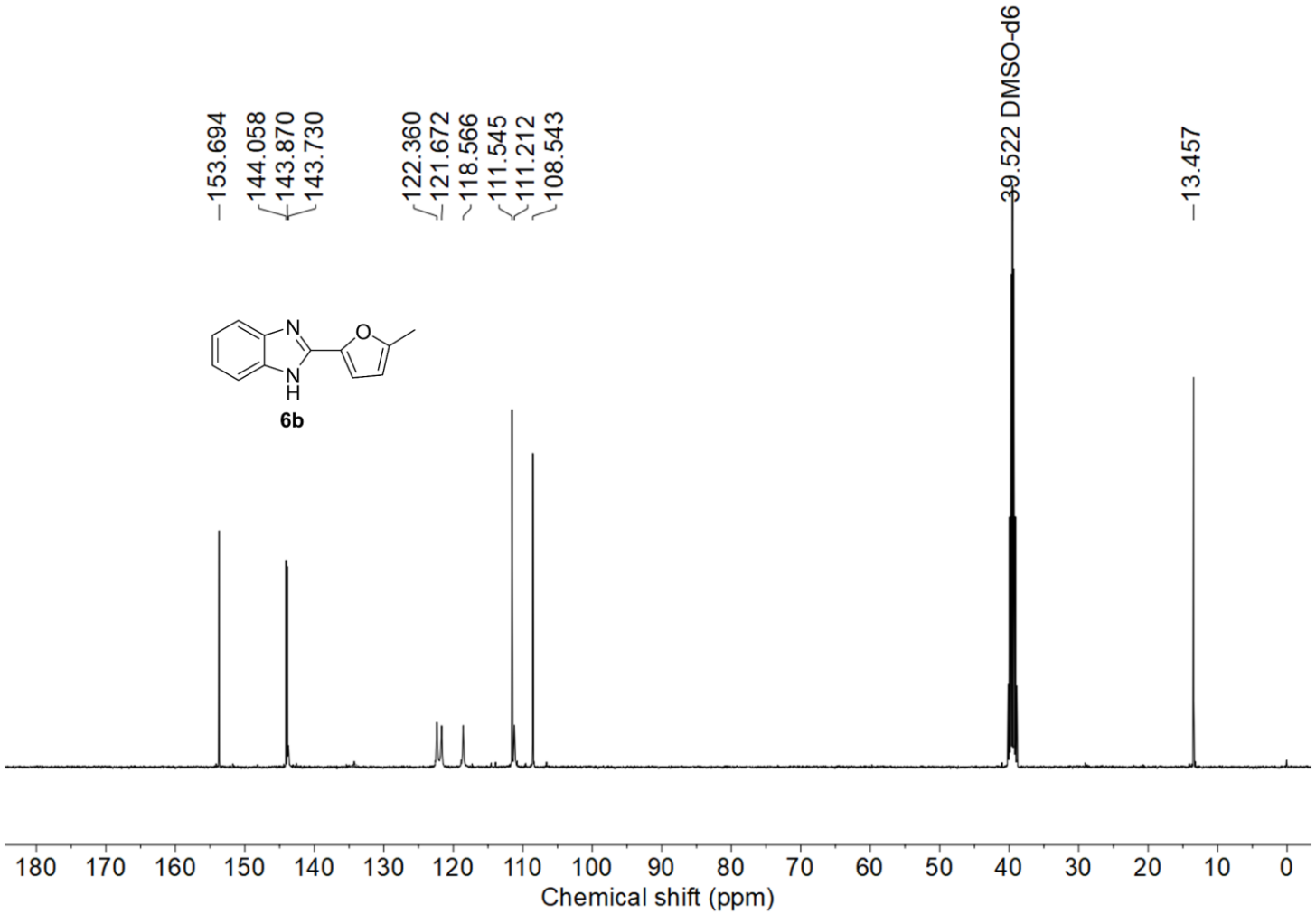

Figure S46. The ^{13}C-NMR spectrum of **6b**.

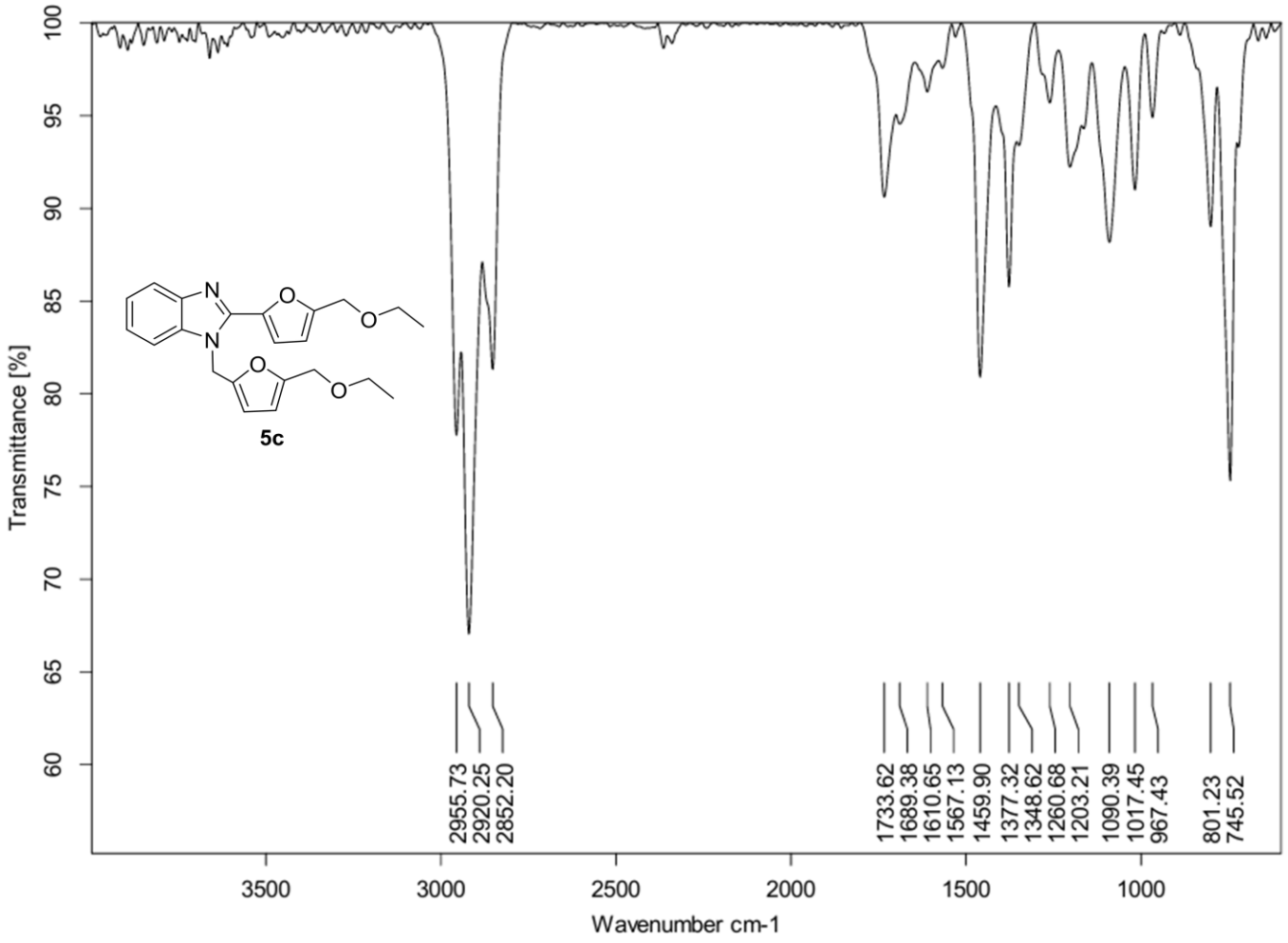

Figure S47. The FTIR spectrum of **5c**.

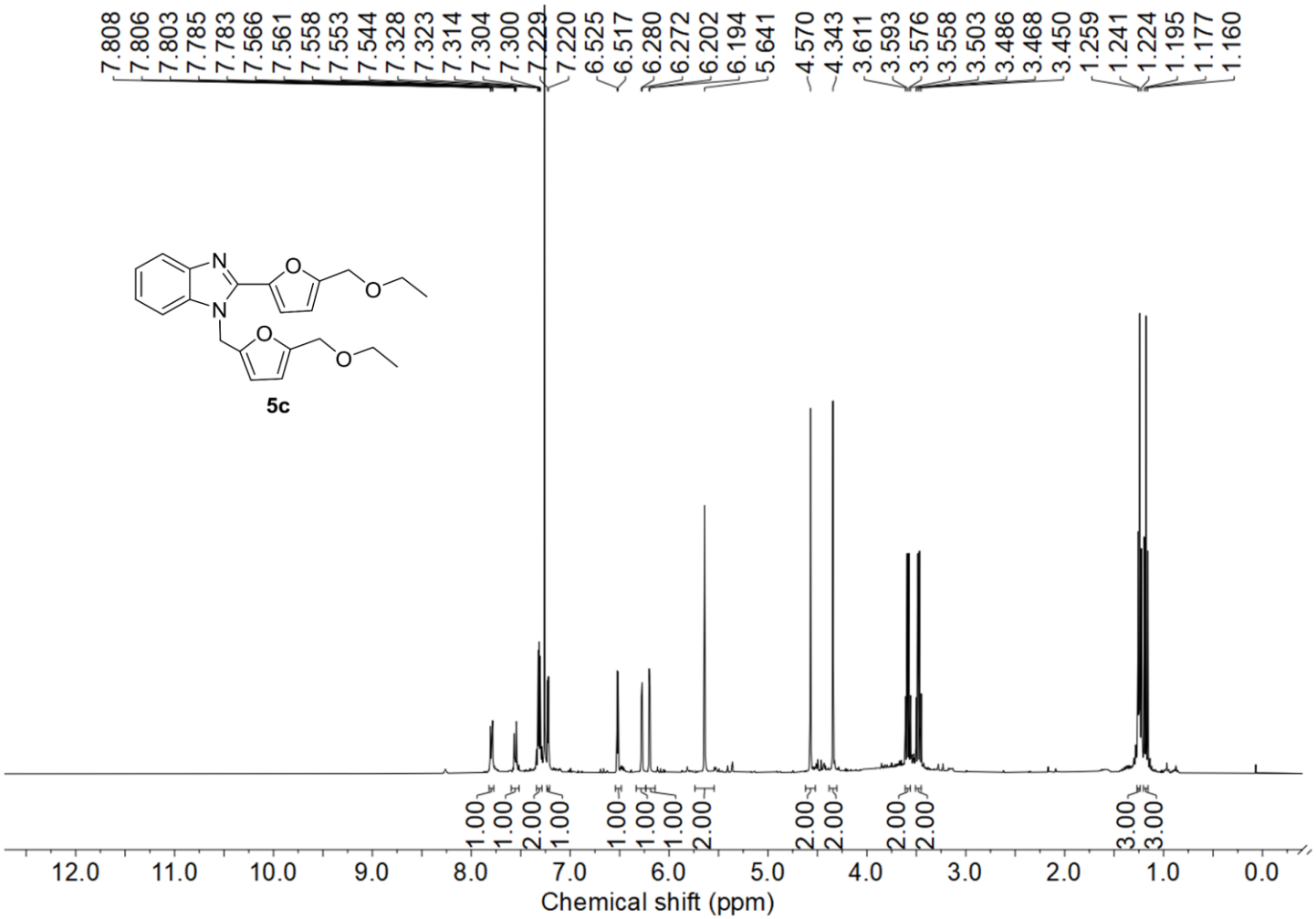

Figure S48. The ^{1}H-NMR spectrum of **5c**.

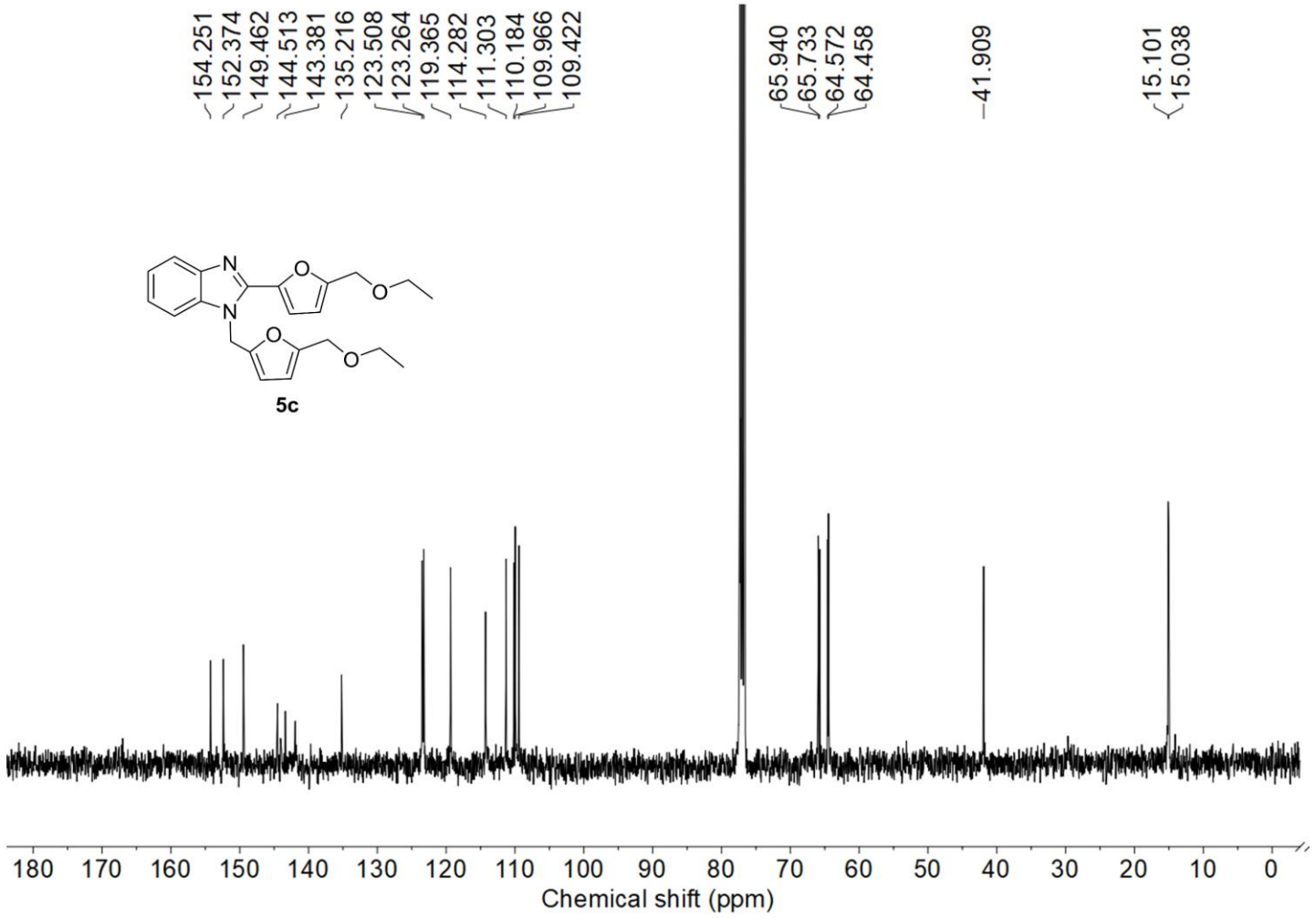

Figure S49. The ^{13}C-NMR spectrum of **5c**.

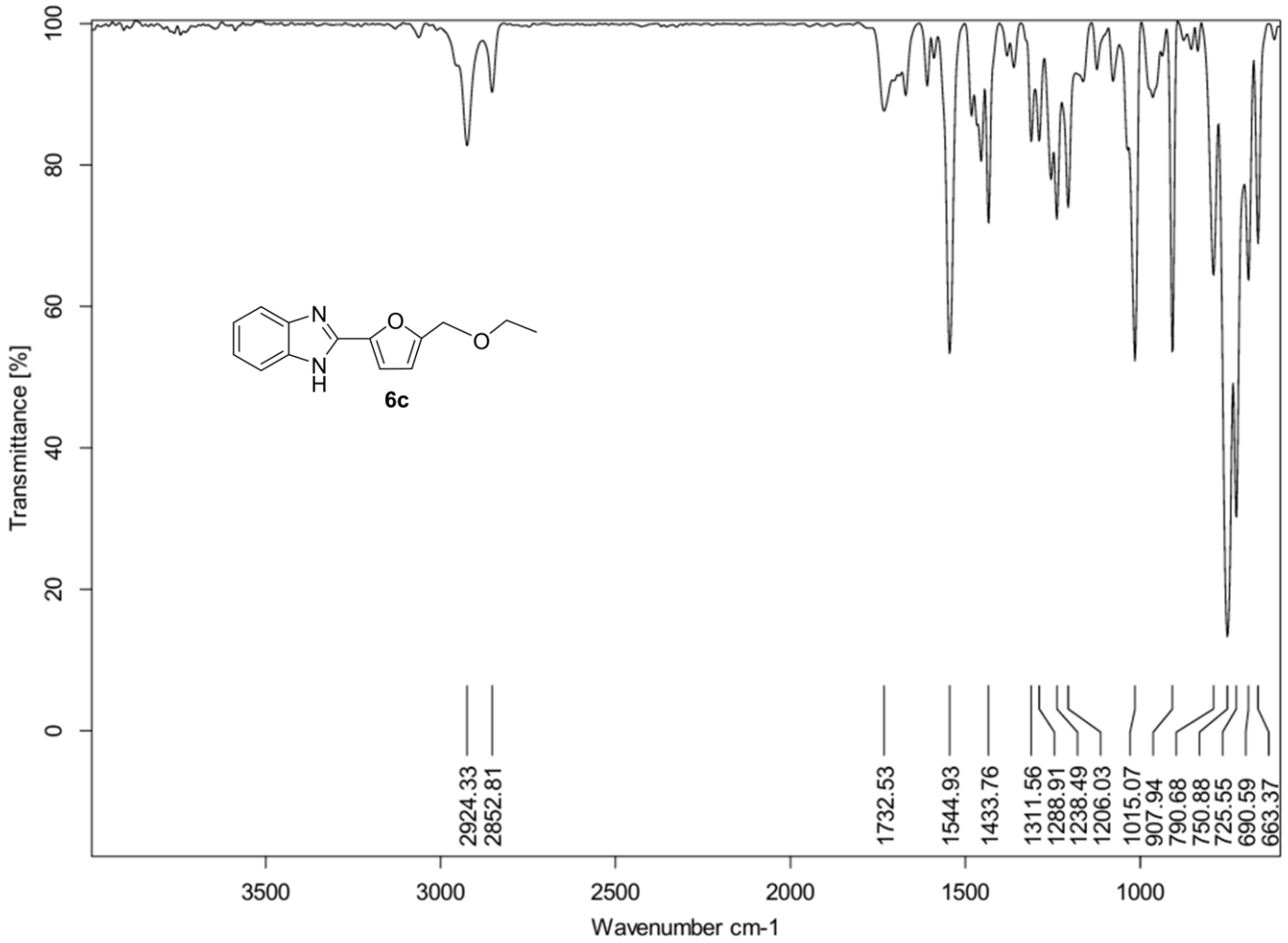

Figure S50. The FTIR spectrum of **6c**.

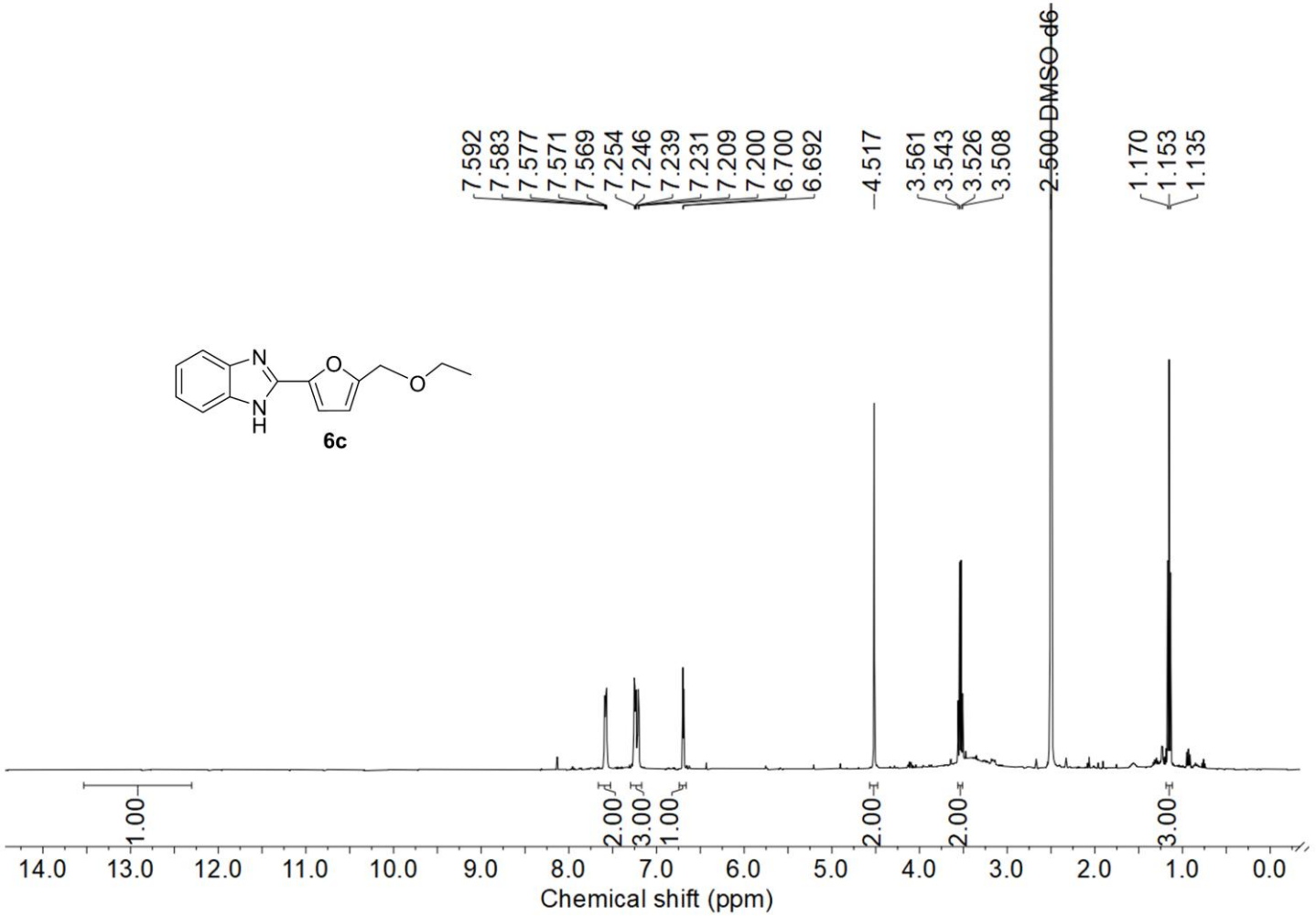

Figure S51. The ^{1}H-NMR spectrum of **6c**.

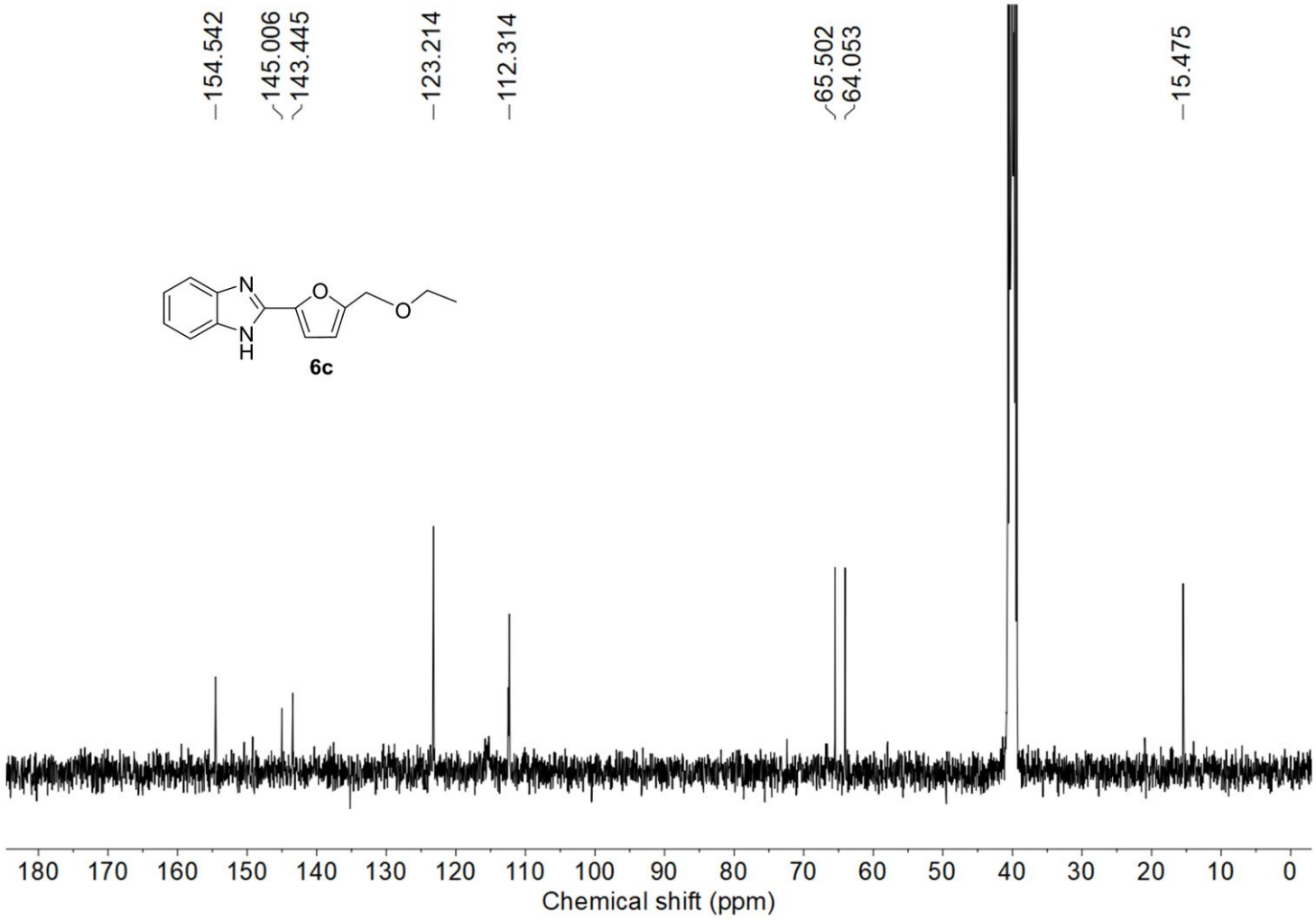

Figure S52. The ^{13}C-NMR spectrum of **6c**.

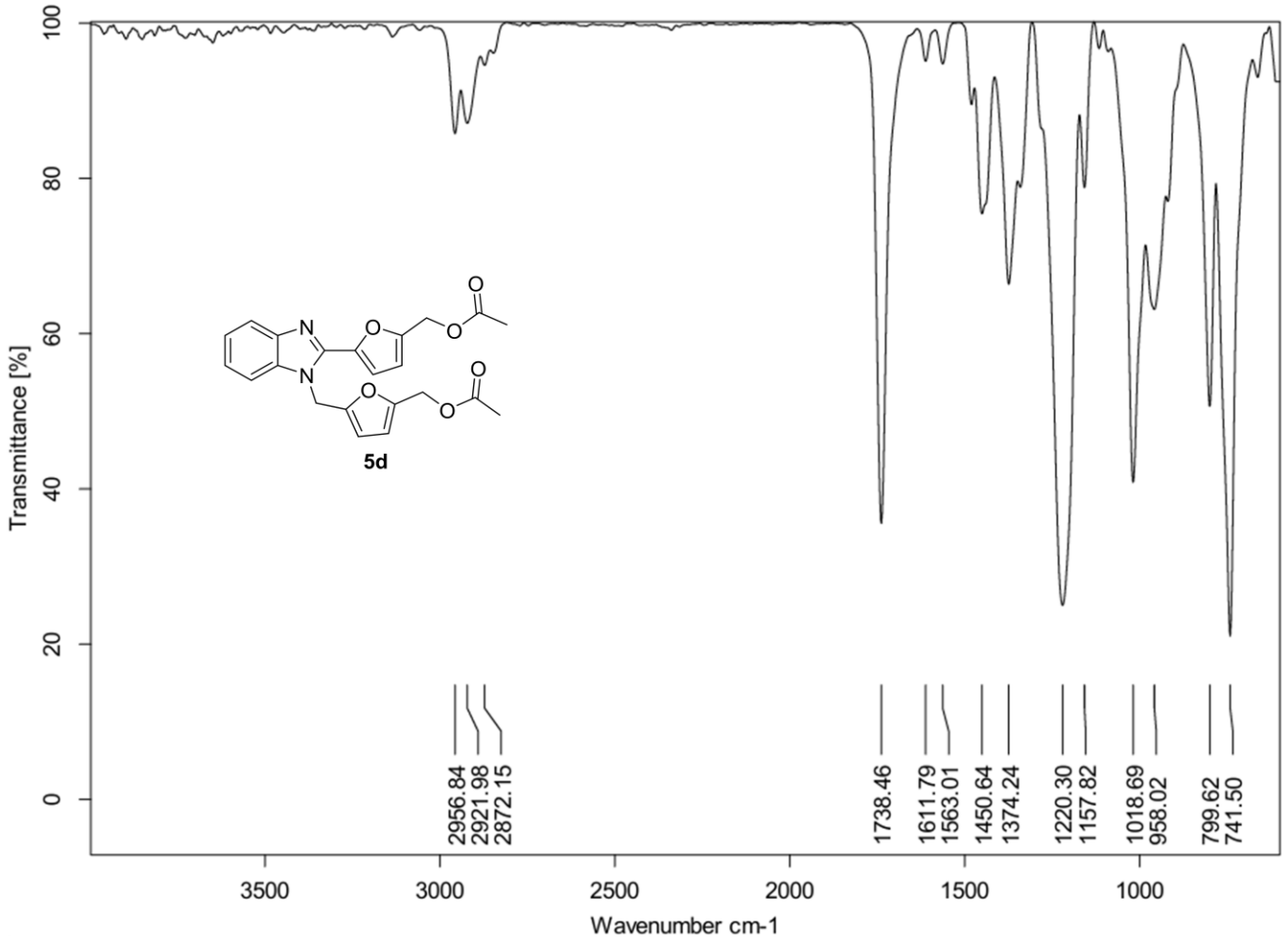

Figure S53. The FTIR spectrum of **5d**.

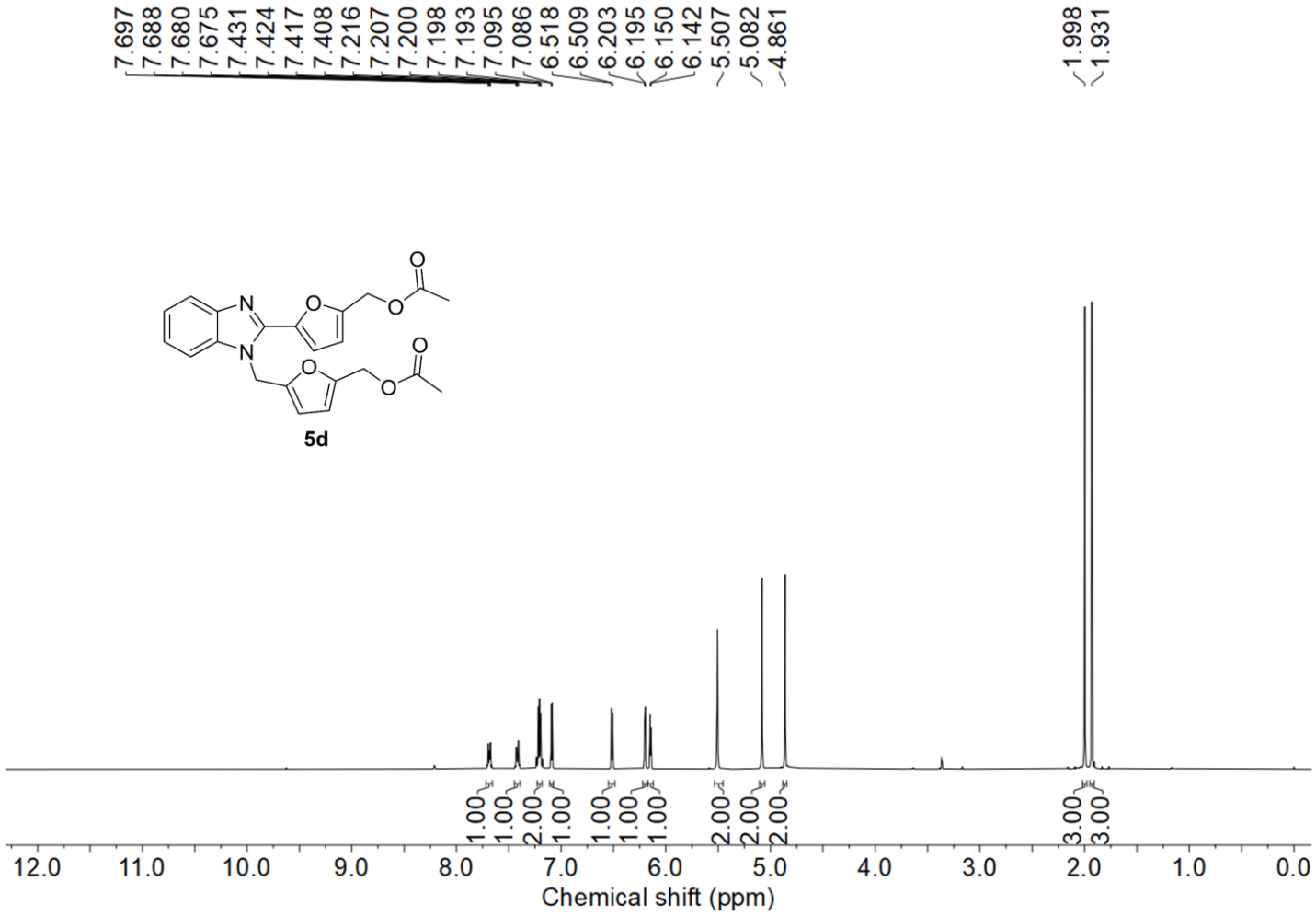

Figure S54. The ^{1}H-NMR spectrum of **5d**.

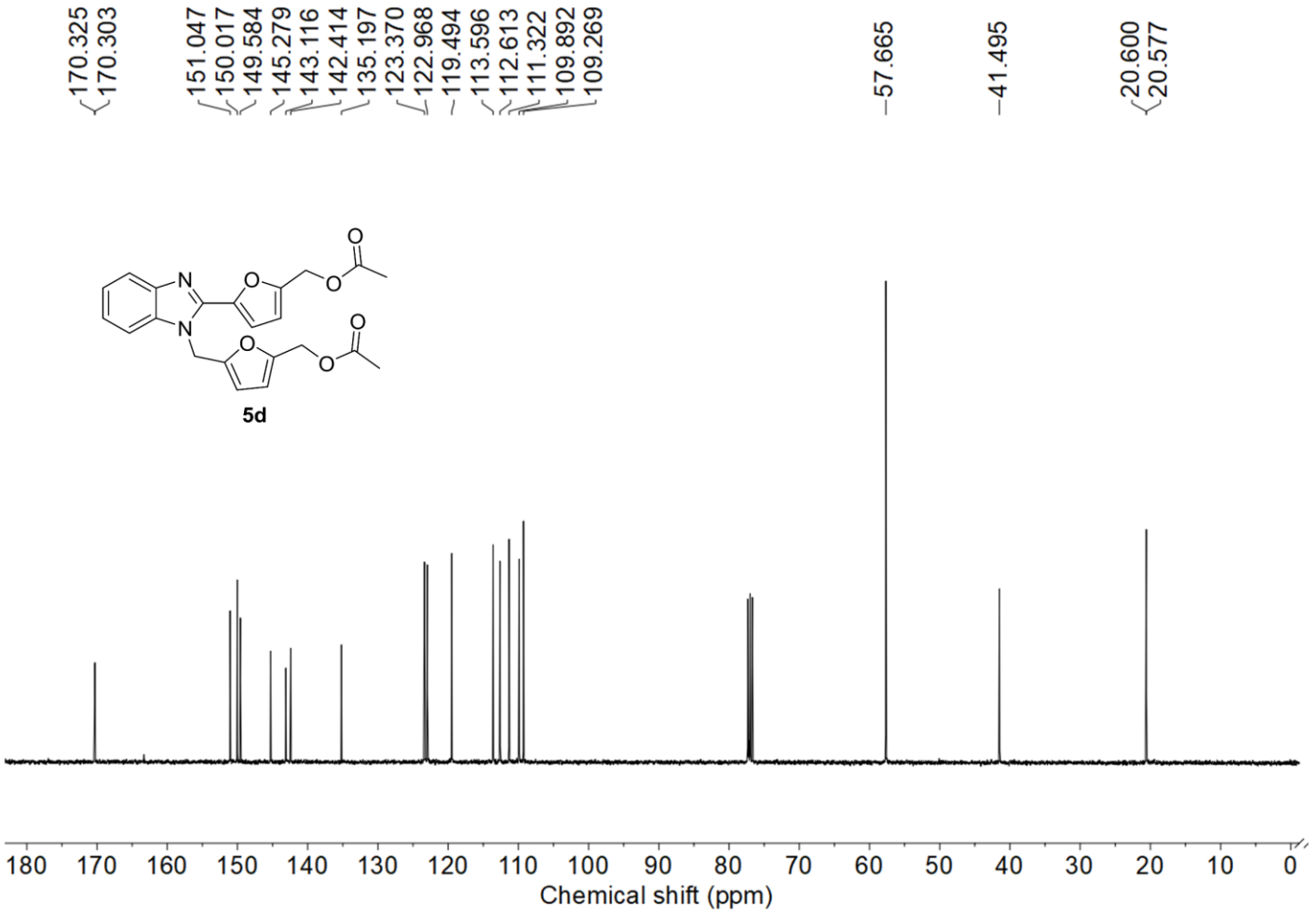

Figure S55. The ^{13}C-NMR spectrum of **5d**.

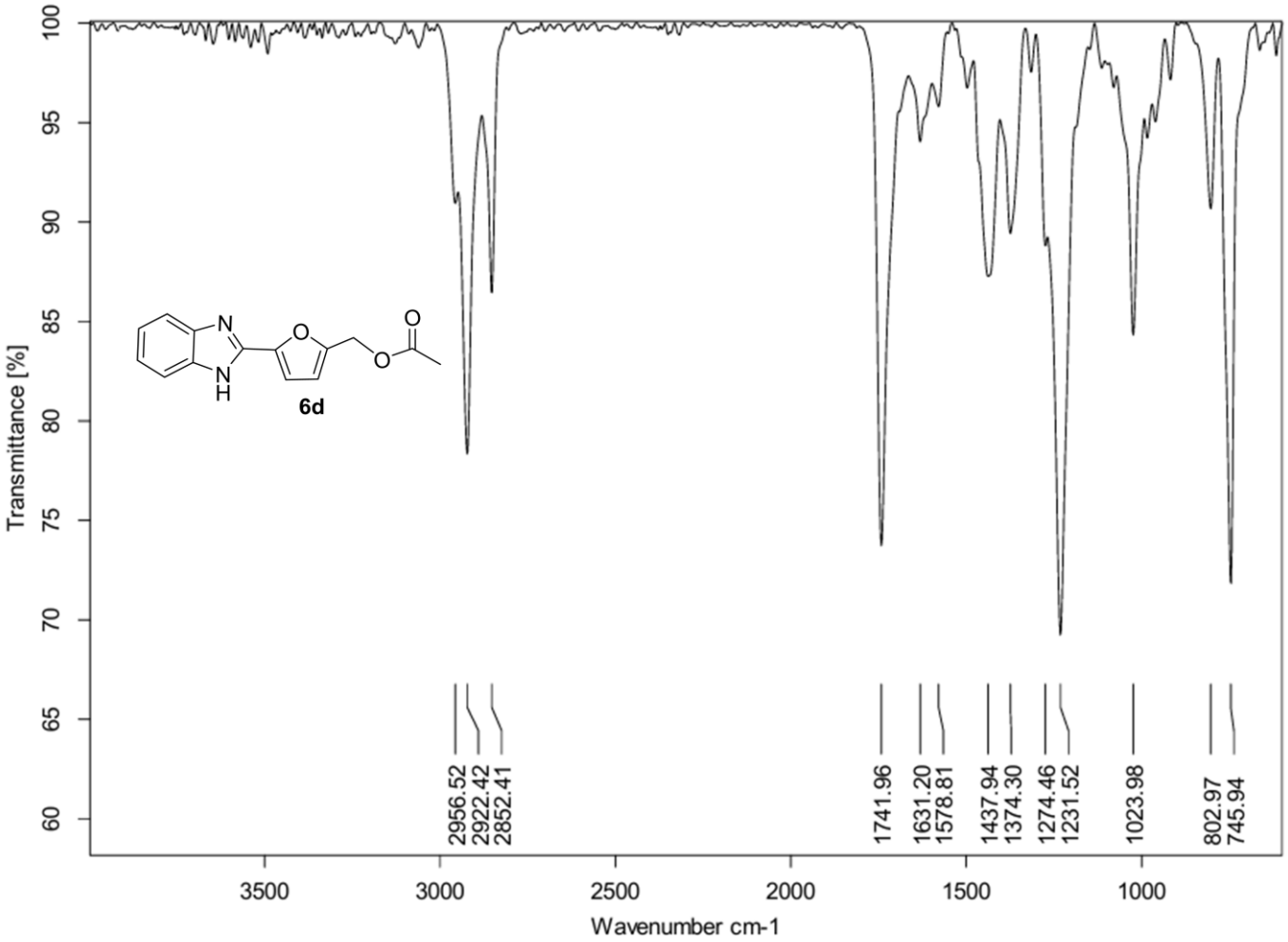

Figure S56. The FTIR spectrum of **6d**.

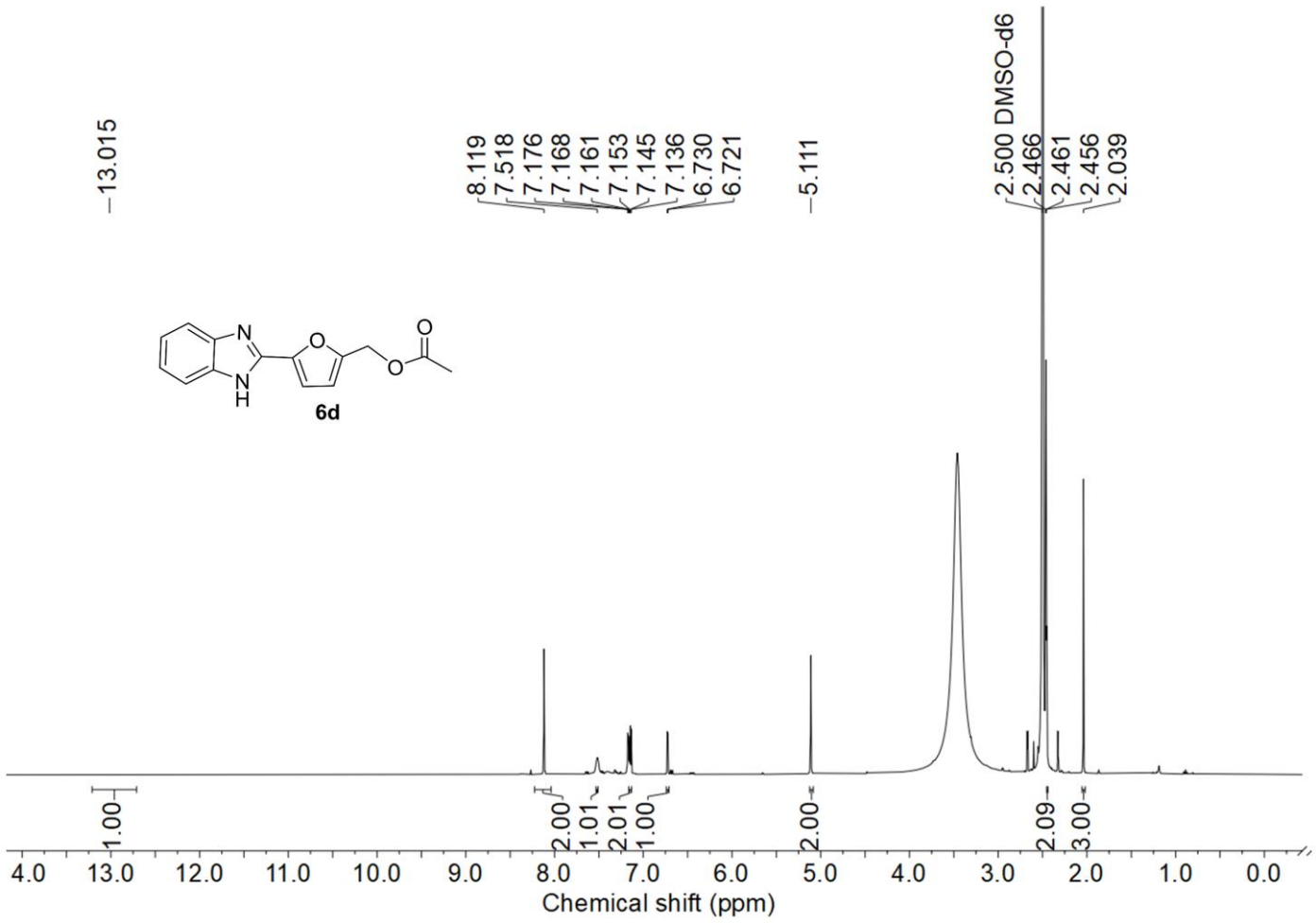

Figure S57. The ^{1}H-NMR spectrum of **6d**.

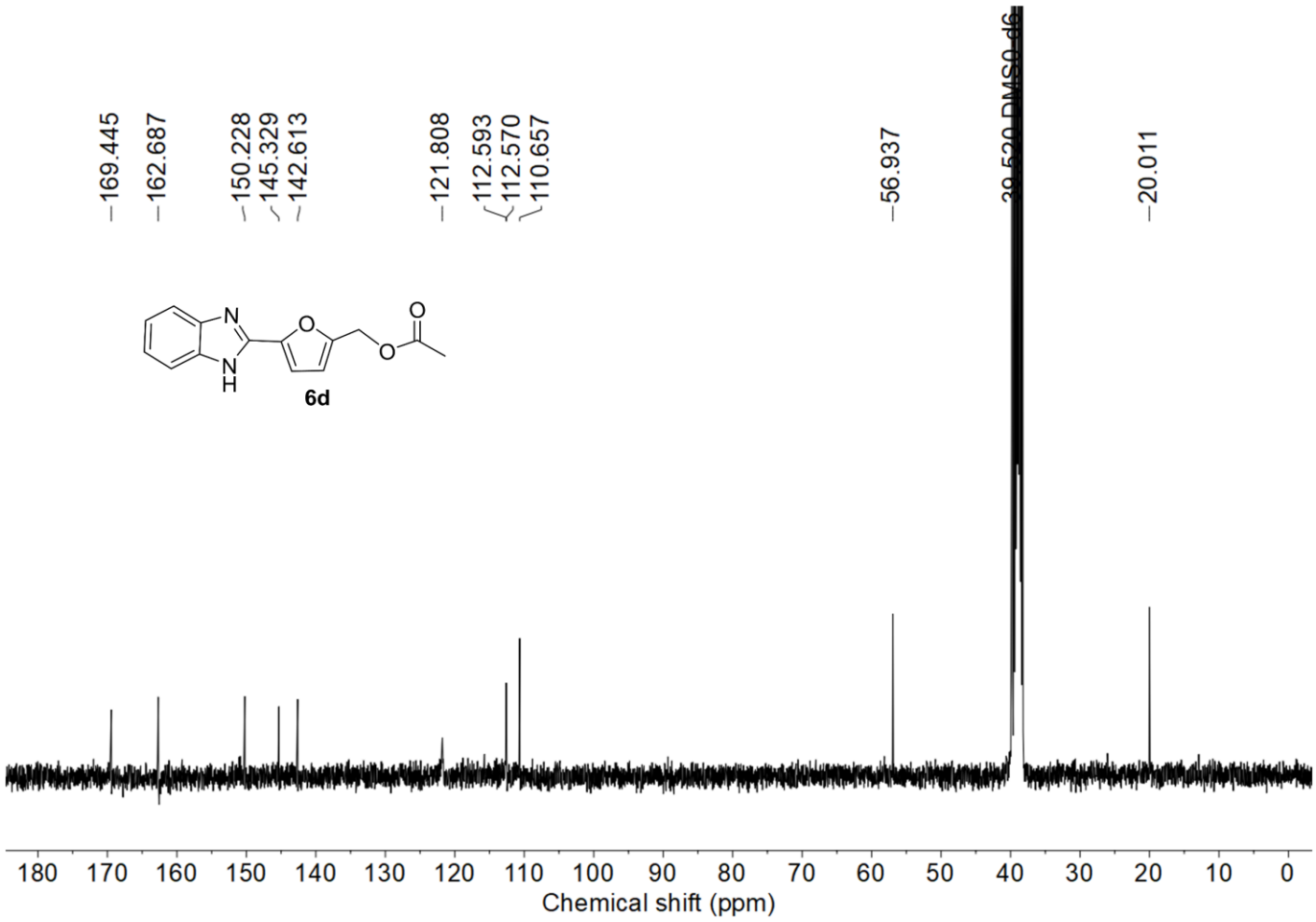

Figure S58. The ^{13}C-NMR spectrum of **6d**.

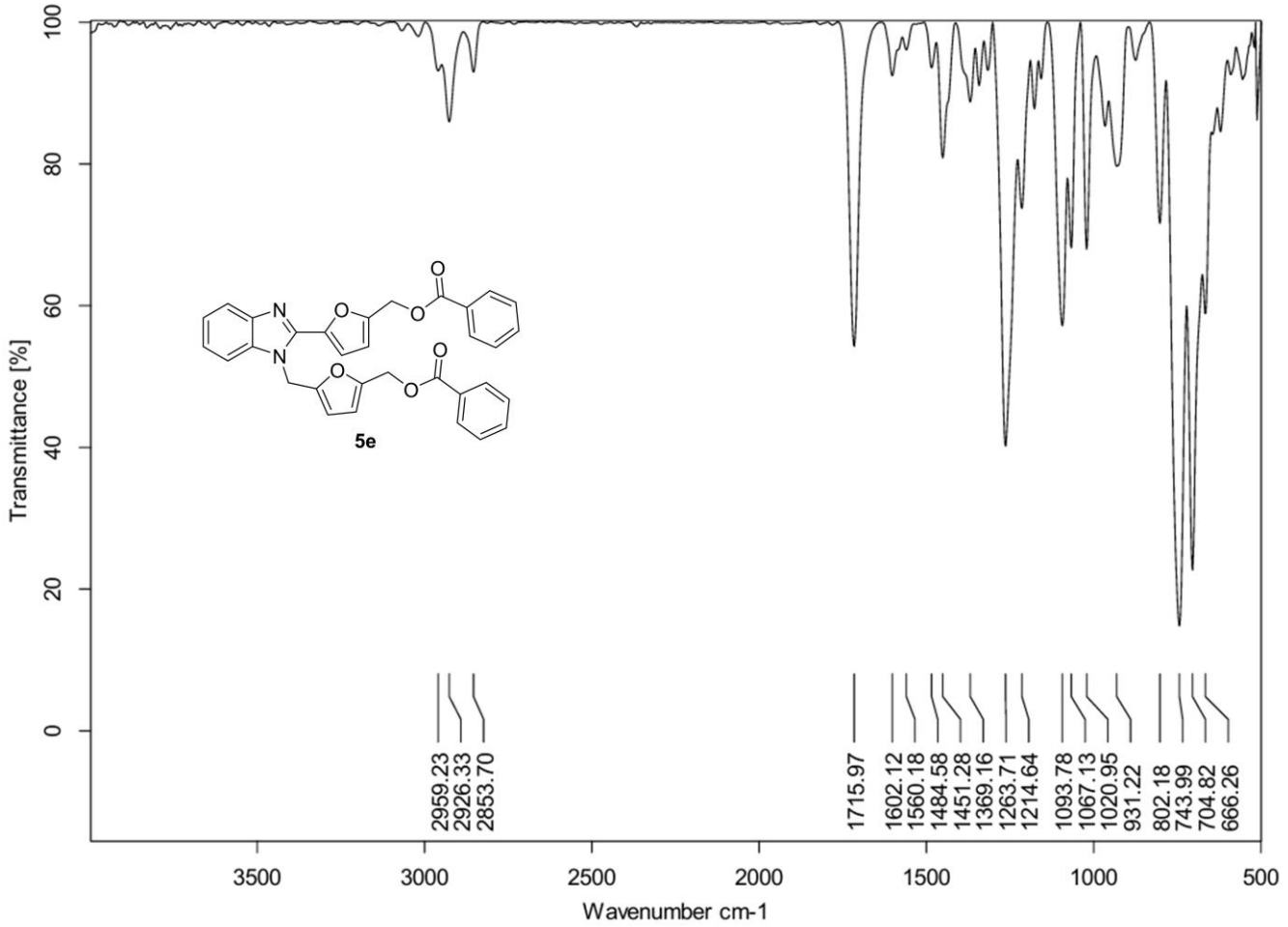

Figure S59. The FTIR spectrum of **5e**.

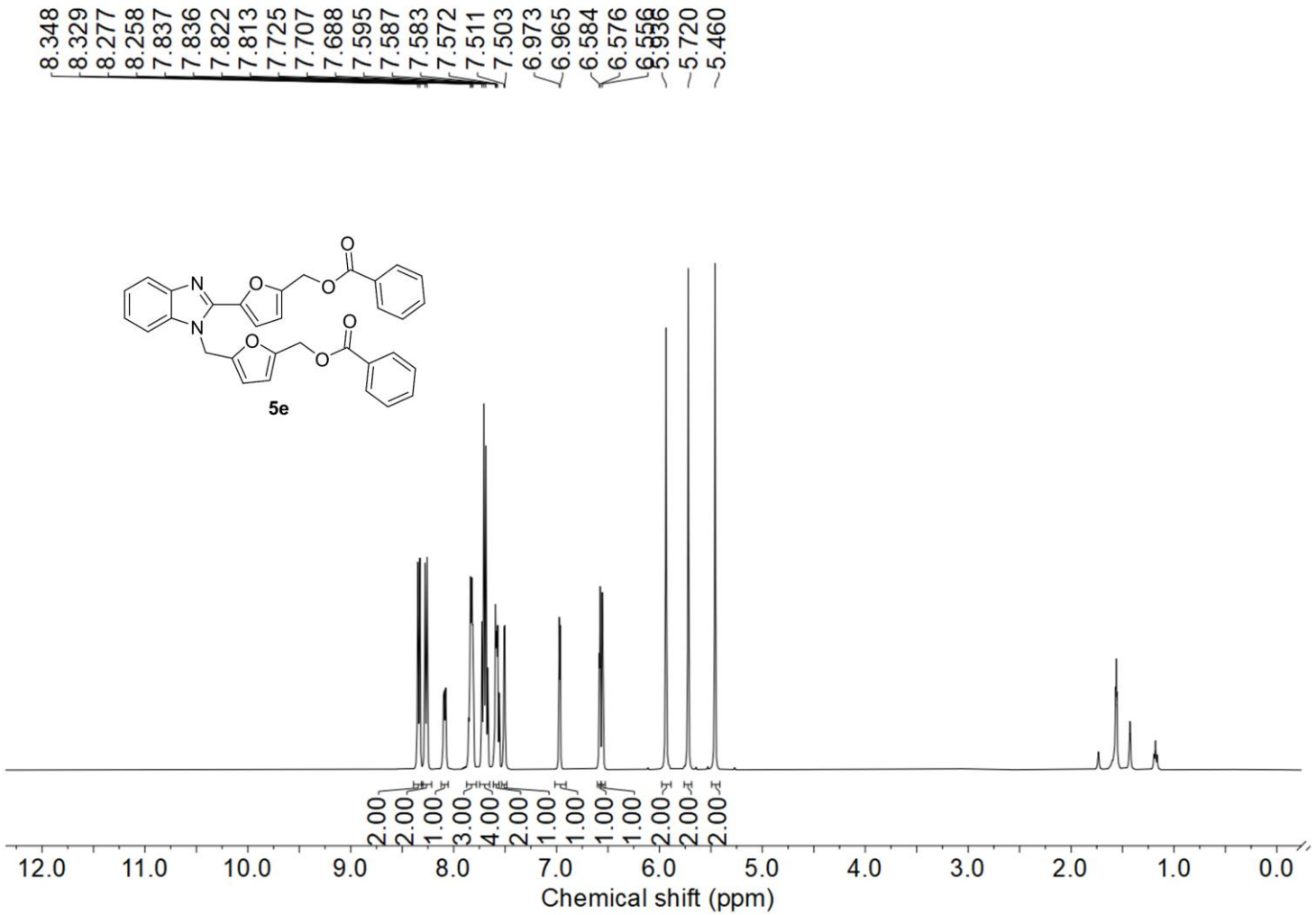

Figure S60. The ^{1}H-NMR spectrum of **5e**.

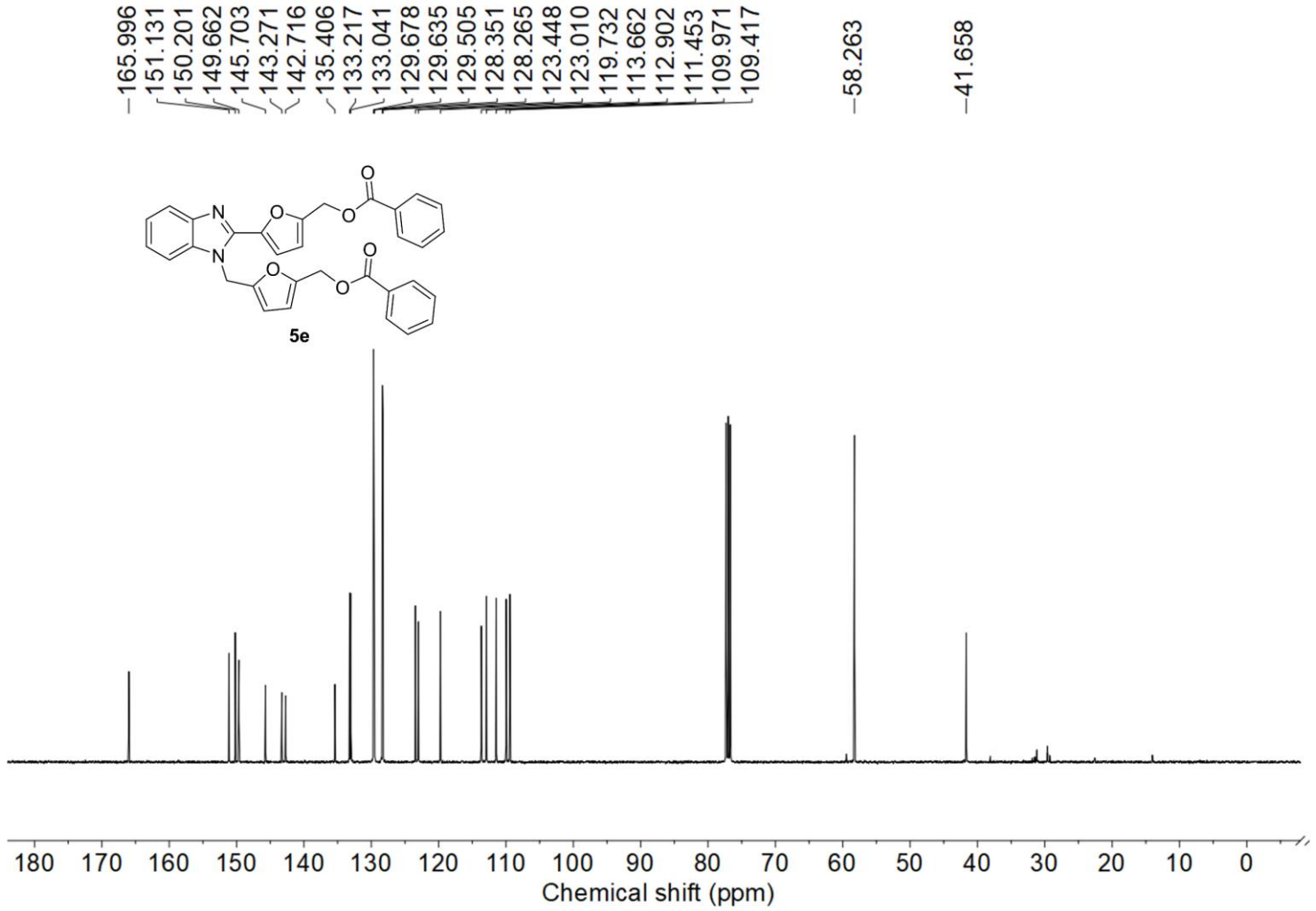

Figure S61. The ^{13}C-NMR spectrum of **5e**.

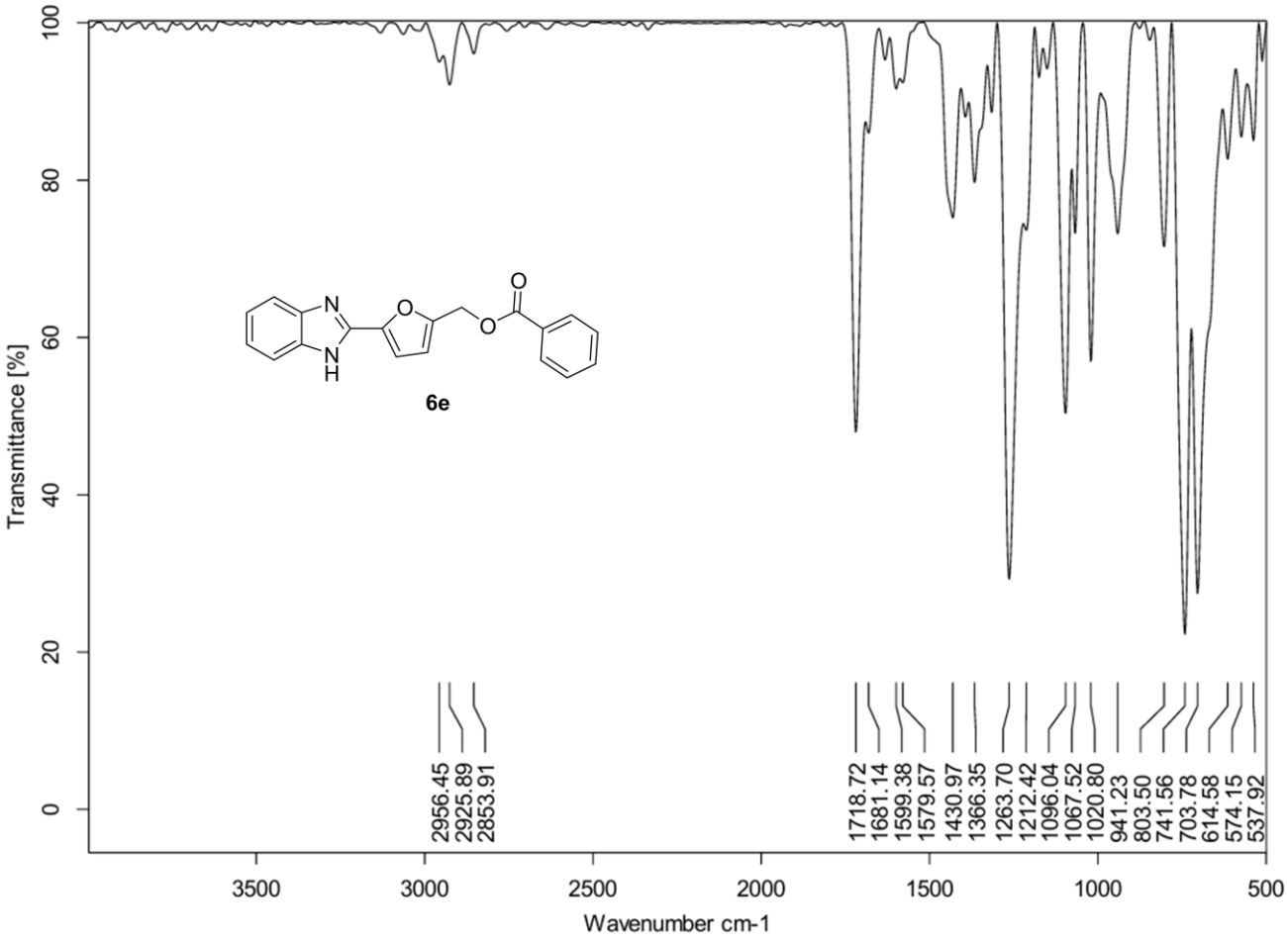

Figure S62. The FTIR spectrum of **6e**.

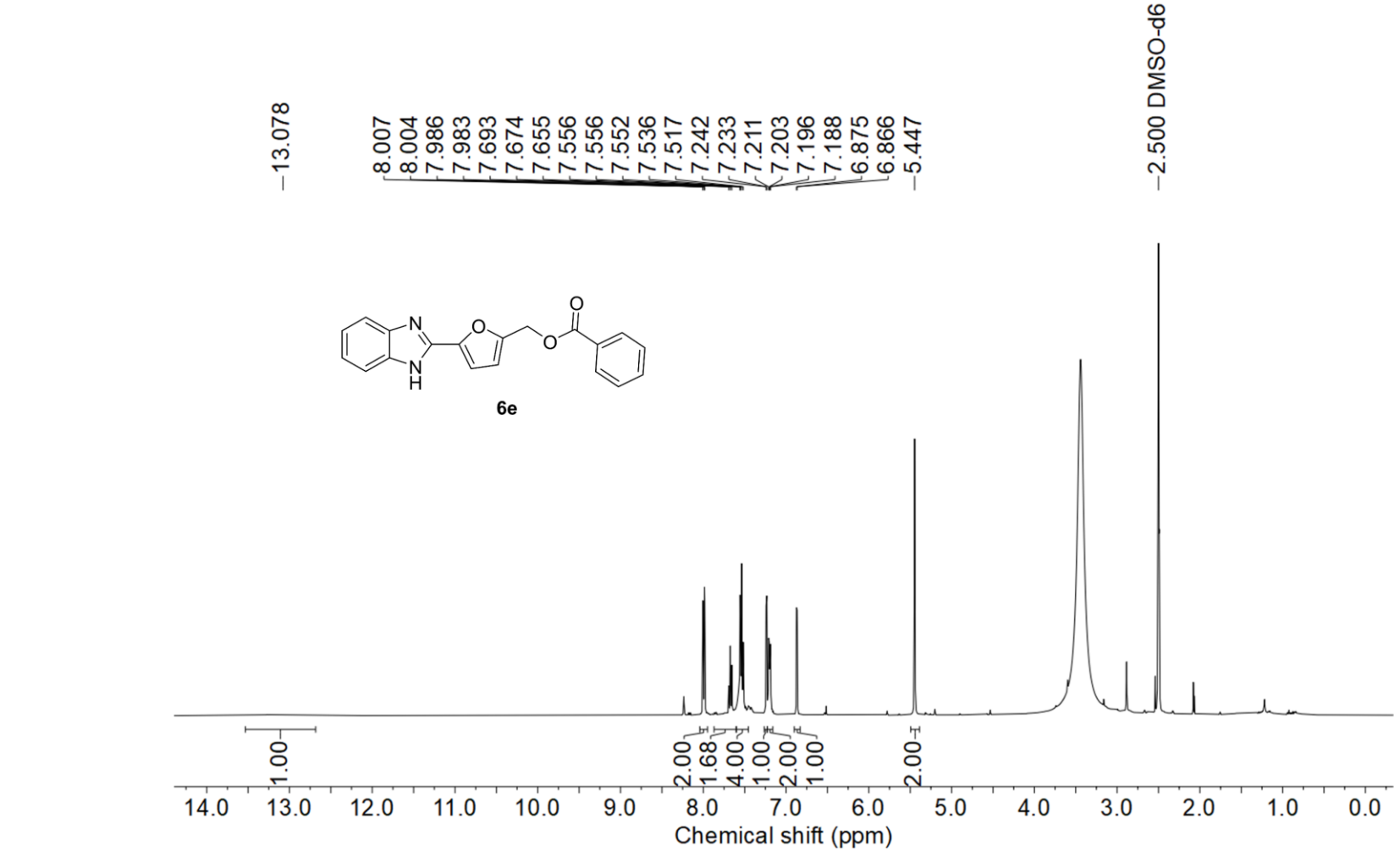

Figure S63. The ^{1}H-NMR spectrum of **6e**.

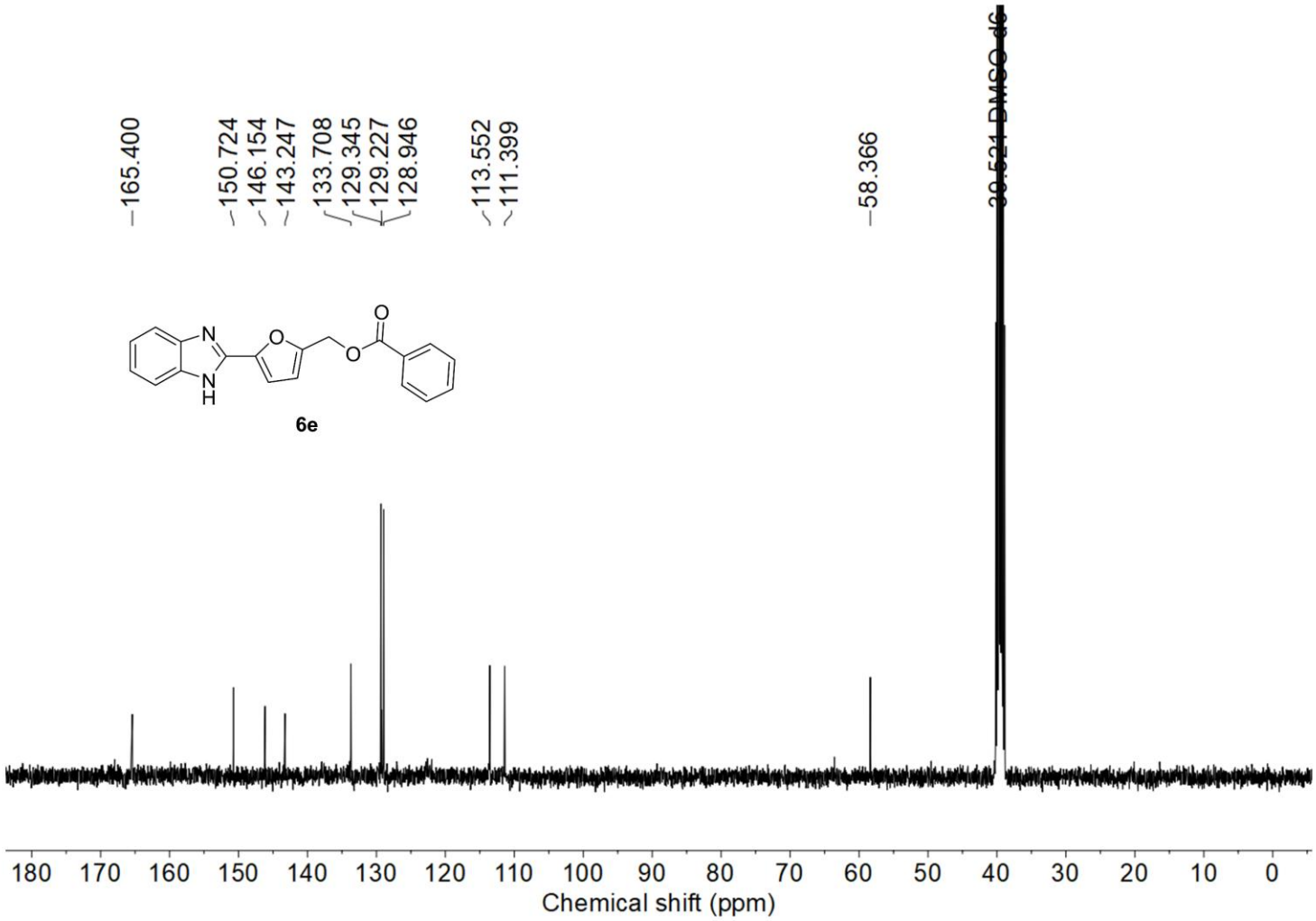

Figure S64. The ^{13}C-NMR spectrum of **6e**.

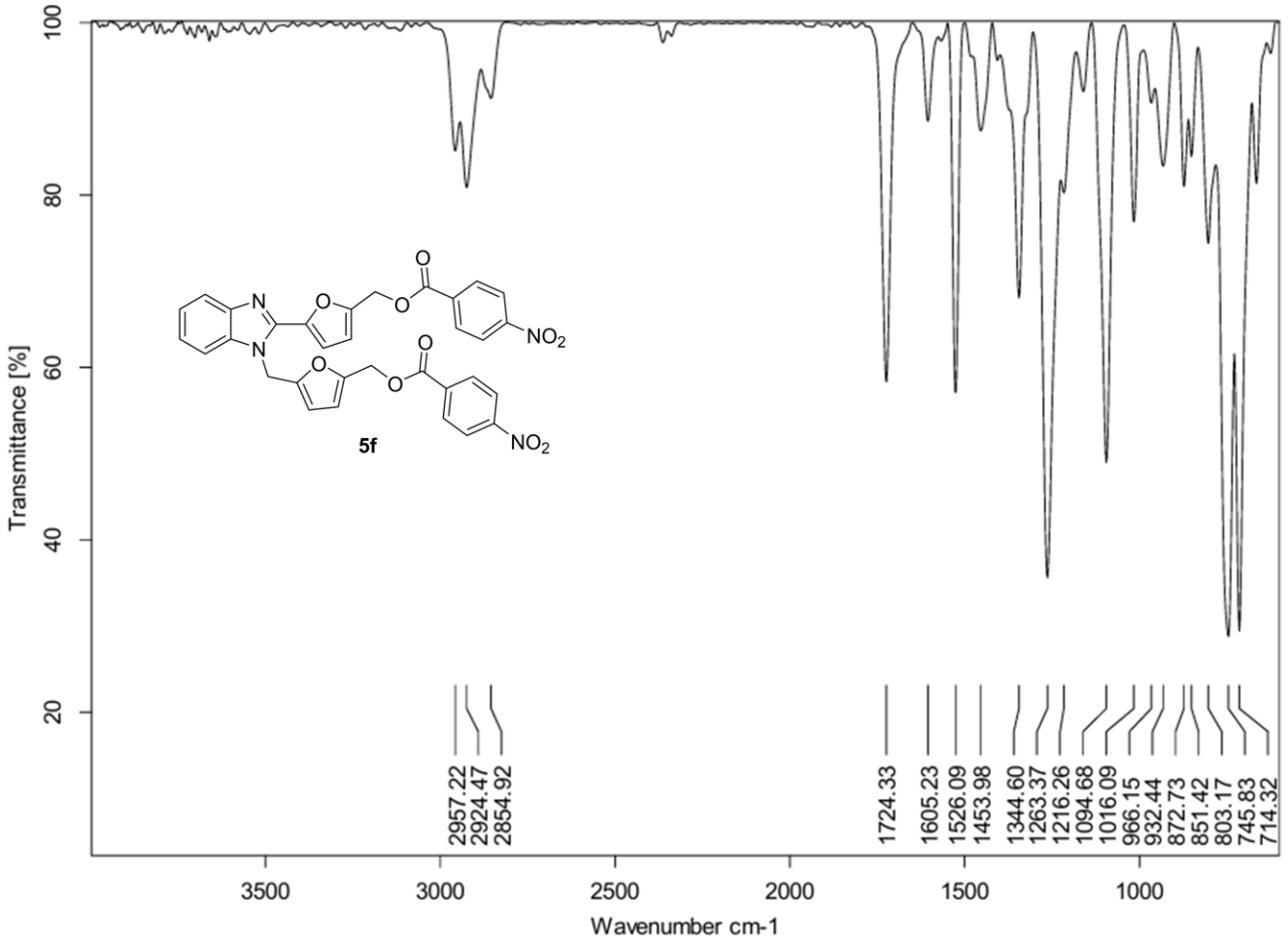

Figure S65. The FTIR spectrum of **5f**.

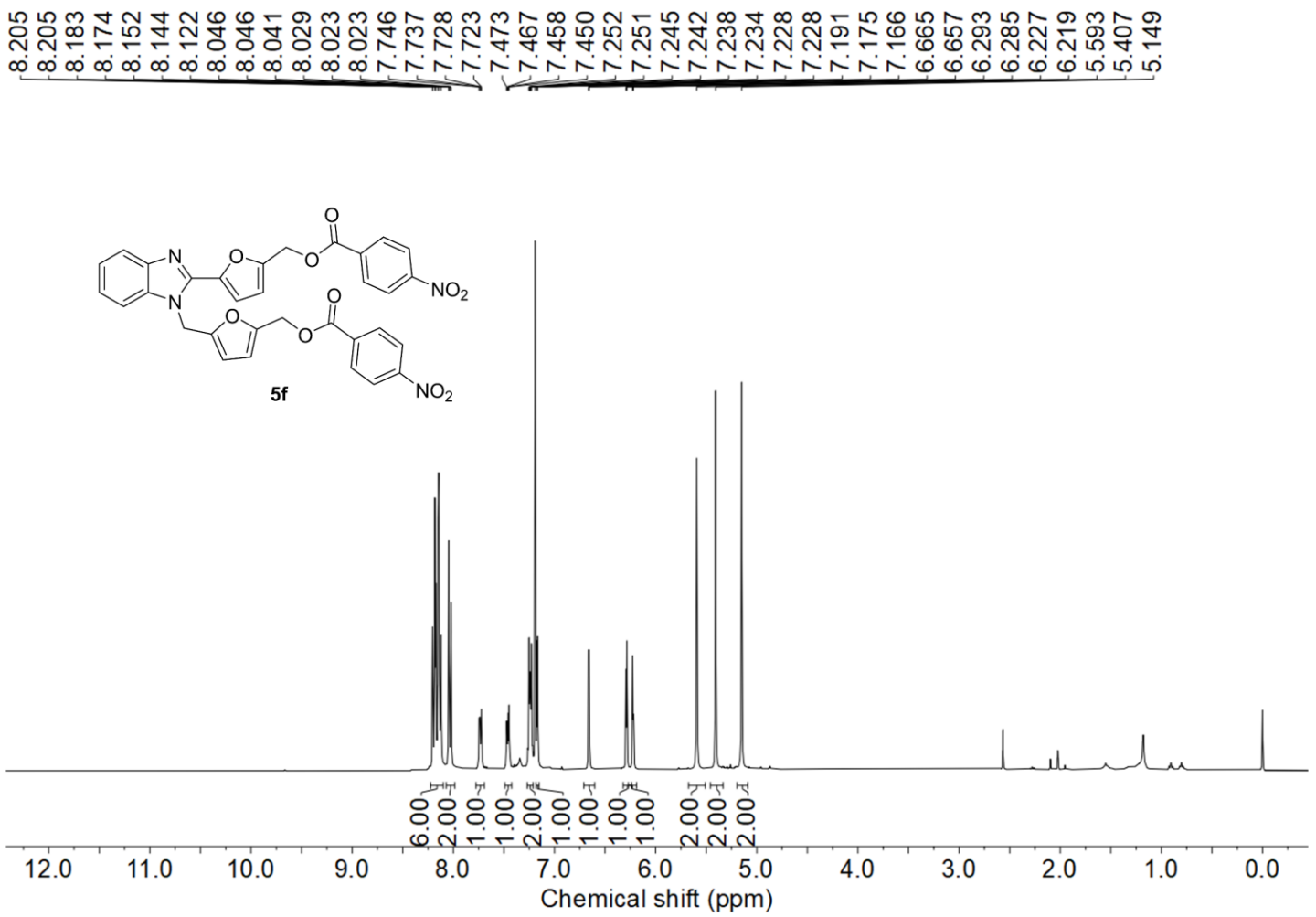

Figure S66. The ^{1}H-NMR spectrum of **5f**.

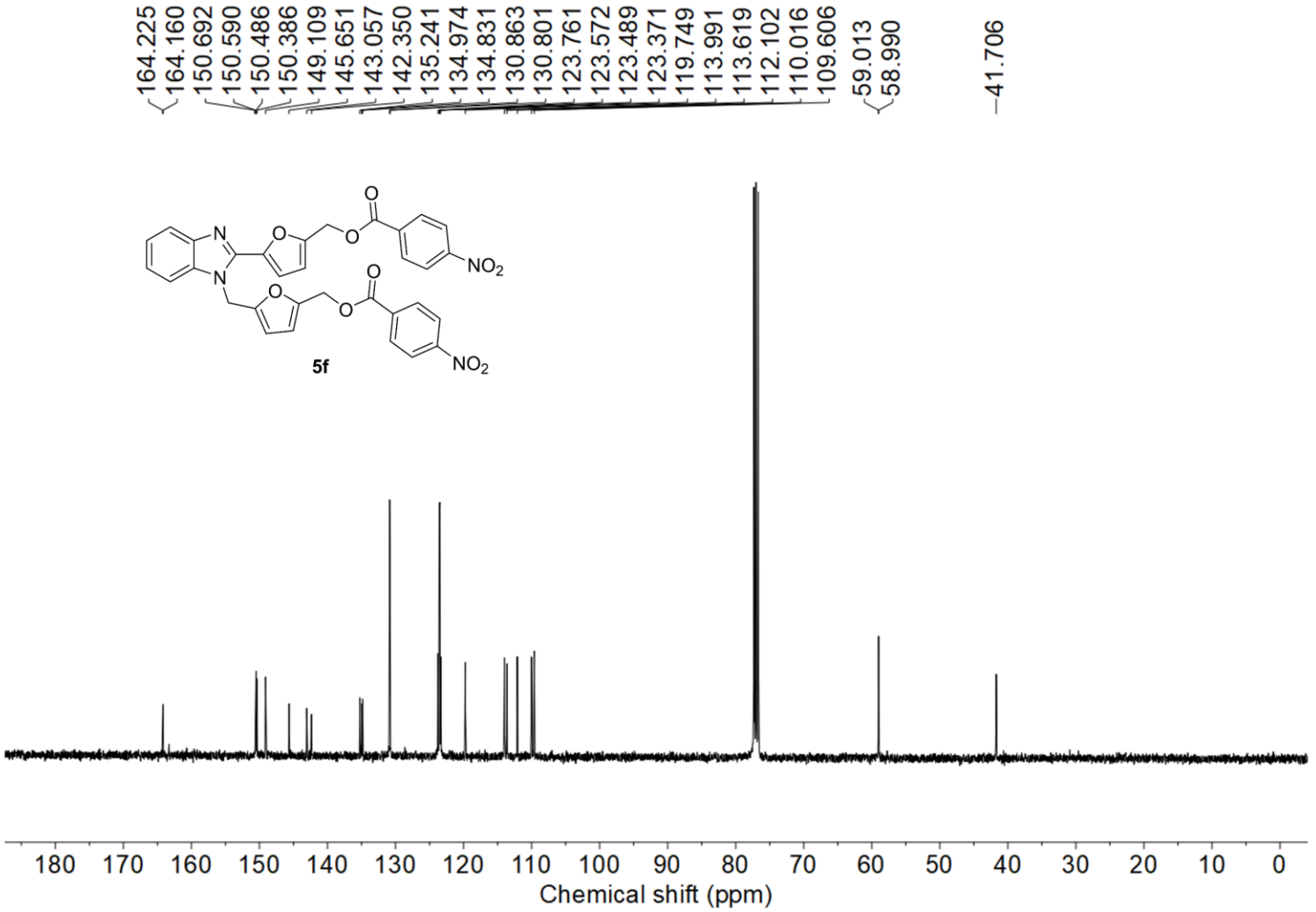

Figure S67. The ^{13}C-NMR spectrum of **5f**.

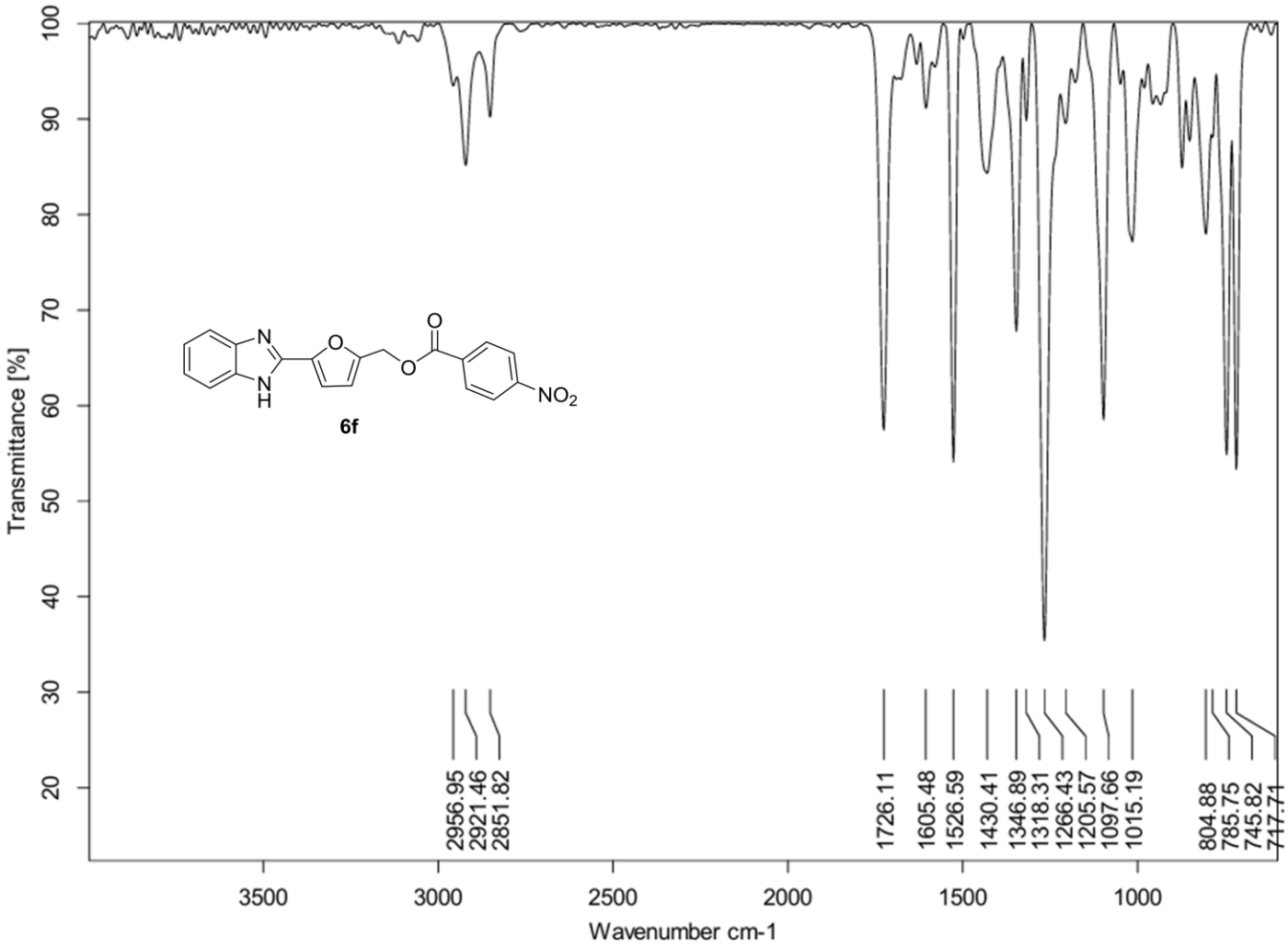

Figure S68. The FTIR spectrum of **6f**.

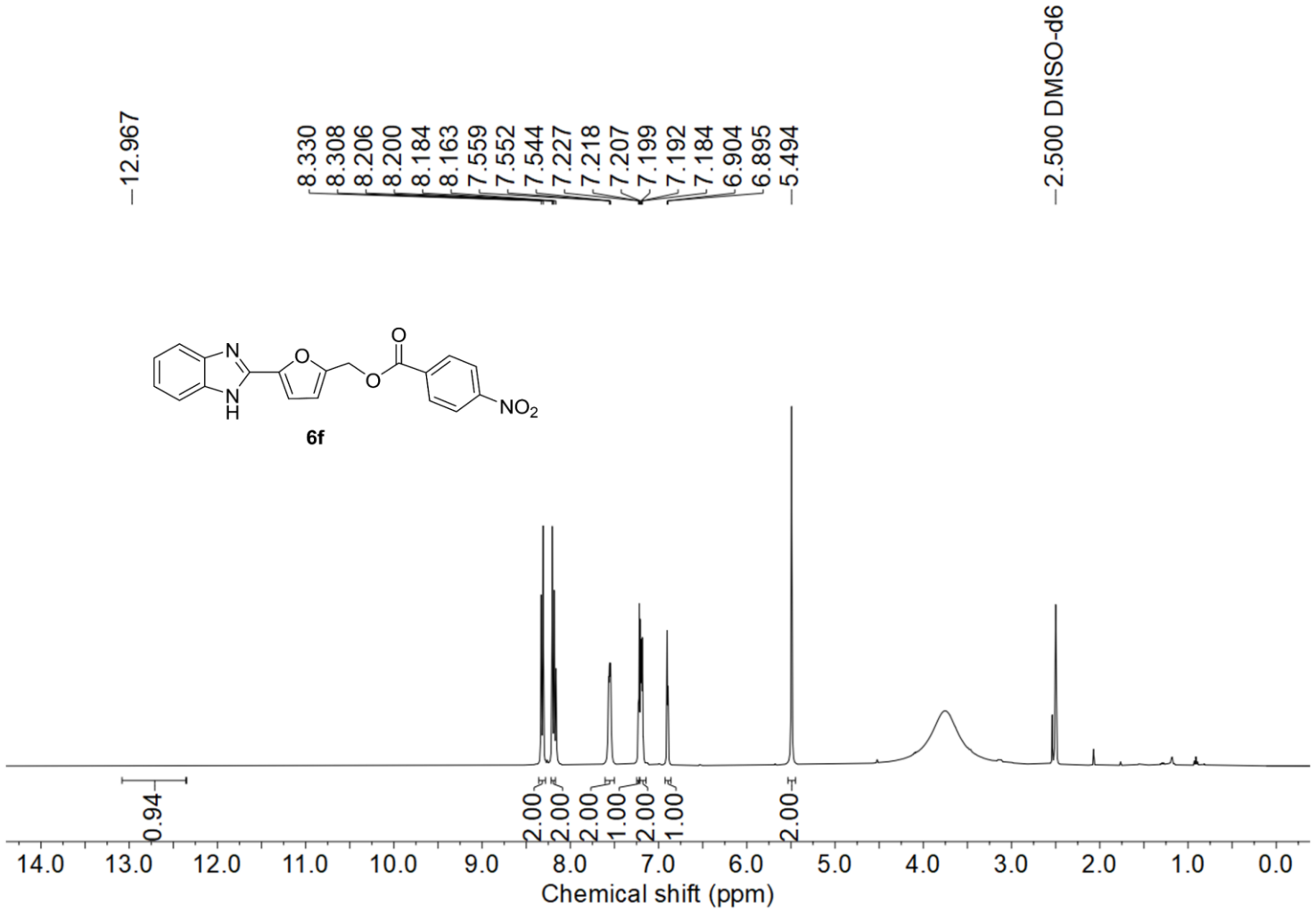

Figure S69. The ^{1}H-NMR spectrum of **6f**.

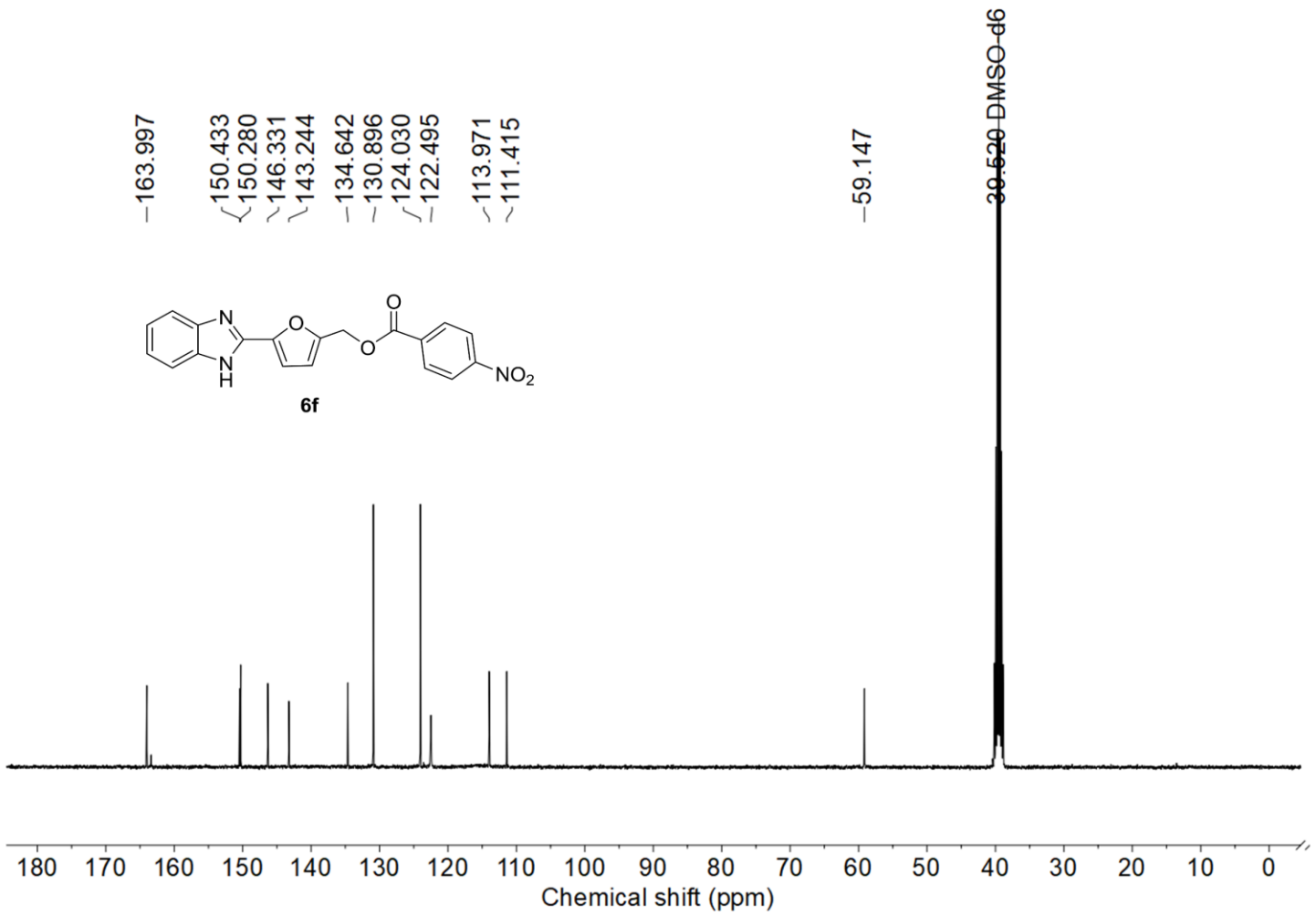

Figure S70. The ^{13}C-NMR spectrum of **6f**.

5. Petri plate images showing antimicrobial activity of synthesized compounds

Gram-positive strain- *Staphylococcus aureus* (***Sa***)

Gram-positive strain- *Escherichia coli* (***Ea***)

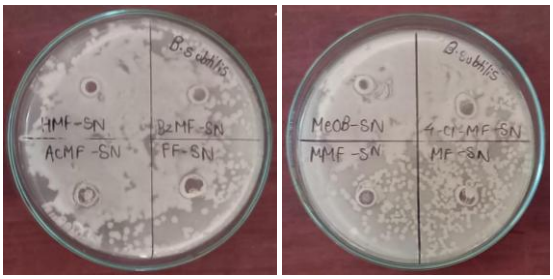

Gram-negative strain- *Bacillus subtilis* (***Bs***)

Gram-negative strain- *Pseudomonas aeruginosa* (***Ps***)

Figure S71. Photographic images of the Petri plates for studying antibacterial activities of Benzothiazoles (4a-4h) against the bacterial strains, Gram-positive (*Sa, Ea*), Gram-negative strains (*Bs, Ps*).

Gram-positive strain- *Staphylococcus aureus* (***Sa***)

Gram-positive strain- *Escherichia coli* (***Ea***)

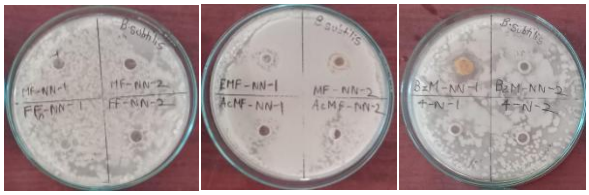

Gram-negative strain- *Bacillus subtilis* (***Bs***)

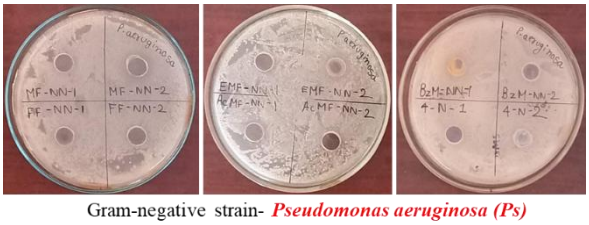

Gram-negative strain- *Pseudomonas aeruginosa* (***Ps***)

Figure S72. Photographic images of the Petri plates for studying antibacterial activities of 1,2-disubstituted benzimidazoles (5a-5f) and 2-substituted benzimidazoles (6a-6f) against the Gram-positive strains (*Sa, Ea*) and Gram-negative strains *(Bs, Ps*).

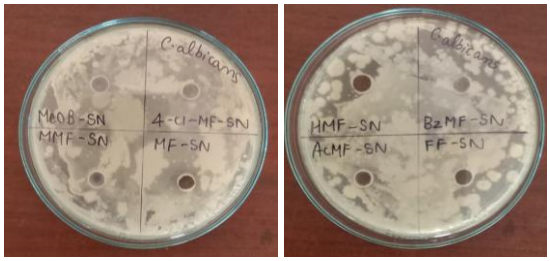

Candida albicans ***(Ca)***

Aspergillus niger ***(An)***

Figure S73. Photographic images of the Petri plates for studying antifungal activities of Benzothiazoles (4a-4h) against the fungal strains, *Candida albicans* (*Ca*), *Aspergillus niger* (*An*).

Aspergillus niger ***(An)***

Candida albicans ***(Ca)***

Figure S74. Photographic images of the Petri plates for studying antibacterial activities of 1,2-disubstituted benzimidazoles (5a-5f) and 2-substituted benzimidazoles (6a-6f) against the fungal strains, *Candida albicans* (*Ca*), *Aspergillus niger* (*An*).

6. References

1 N. S. Bhat, S. L. Hegde, S. Dutta and P. Sudarsanam, *ACS Sustainable Chem. Eng.*, 2022, **10**, 5803–5809.

2 N. S. Bhat, A. K. Yadav, M. Karmakar, A. Thakur, S. S. Mal and S. Dutta, *ACS Omega*, 2023, **8**, 8119–8124.

3 G. M. Sheldrick, *Acta Crystallogr., Sect. C: Struct. Chem.*, 2015, **71**, 3–8.

4 A. L. Spek, *J. Appl. Crystallogr.*, 2003, **36**, 7–13.

5 C. F. Macrae, I. Sovago, S. J. Cottrell, P. T. A. Galek, P. McCabe, E. Pidcock, M. Platings, G. P. Shields, J. S. Stevens, M. Towler and P. A. Wood, *J. Appl. Crystallogr.*, 2020, **53**, 226–235.

6 P. R. Spackman, M. J. Turner, J. J. McKinnon, S. K. Wolff, D. J. Grimwood, D. Jayatilaka and M. A. Spackman, *J. Appl. Crystallogr.*, 2021, **54**, 1006–1011.

7 Gaussian 16, Revision C.01, M. J. Frisch, G. W. Trucks, H. B. Schlegel, G. E. Scuseria, M. A. Robb, J. R. Cheeseman, G. Scalmani, V. Barone, G. A. Petersson, H. Nakatsuji, X. Li, M. Caricato, A. V. Marenich, J. Bloino, B. G. Janesko, R. Gomperts, B. Mennucci, H. P. Hratchian, J. V. Ortiz, A. F. Iz maylov, J. L. Sonnenberg, D. Williams-Young, F. Ding, F. Lipparini, F. Egidi, J. Goings, B. Peng, A. Petrone, T. Henderson, D. Ranasinghe, V. G. Zakrzewski, J. Gao, N. Rega, G. Zheng, W. Liang, M. Hada, M. Ehara, K. Toyota, R. Fukuda, J. Hasegawa, M. Ishida, T. Nakajima, Y. Honda, O. Kitao, H. Nakai, T. Vreven, K. Throssell, J. A. Montgomery Jr., J. E. Peralta, F. Ogliaro, M. J. Bearpark, J. J. Heyd, E. N. Brothers, K. N. Kudin, V. N. Staroverov, T. A. Keith, R. Kobayashi, J. Normand, K. Raghavachari, A. P. Rendell, J. C. Burant, S. S. Iyengar, J. Tomasi, M. Cossi, J. M. Millam, M. Klene, C. Adamo, R. Cammi, J. W. Ochterski, R. L. Martin, K. Morokuma, O. Farkas, J. B. Foresman and D. J. Fox, Gaussian, *Inc.*, *Wallingford, CT*, 2016.

8 GaussView, Version 5, R. Dennington, T. A. Keith and J. M. Millam, *Semichem Inc.*, Shawnee Mission, KS, 2016.

9 V. A. Truong, M. H. Tran, T. H. Nguyen and H. T. Nguyen, *RSC Adv.*, 2024, **14**, 39462–39471.

10 K. Shakeena, B. Srinivas, T. S. Sai Sriram, L. Prasad Chamanthula, K. Indukuri, M. M. Krishna Kumar and S. Kumar Alla, *Eur. J. Org. Chem.*, 2025, **28**, e202401043.

11 A. A. Wani, S. M. Bhujbal, D. Sherpa, D. Kathuria, S. S. Chourasiya, S. C. Sahoo and P. V. Bharatam, *Org. Biomol. Chem.*, 2025, **23**, 343–351.

12 J.-Y. Chen, K.-M. Li, Y.-X. Sun, Y. Xiao, F.-S. Guo, Y.-B. Huang and Q. Lu, *Green Chem.*, 2024, **26**, 4834–4843.

13 K. S. Singh, F. Joy and P. Devi, *Transition Met. Chem.*, 2021, **46**, 181–190.

14 V. Thönnißen, J. Westphäling, I. L. Atodiresei and F. W. Patureau, *Chem. - Eur. J.*, 2024, **30**, e202304378.